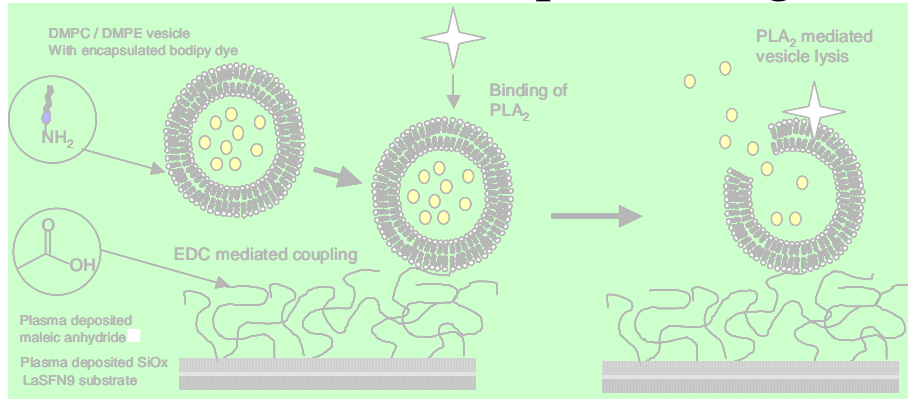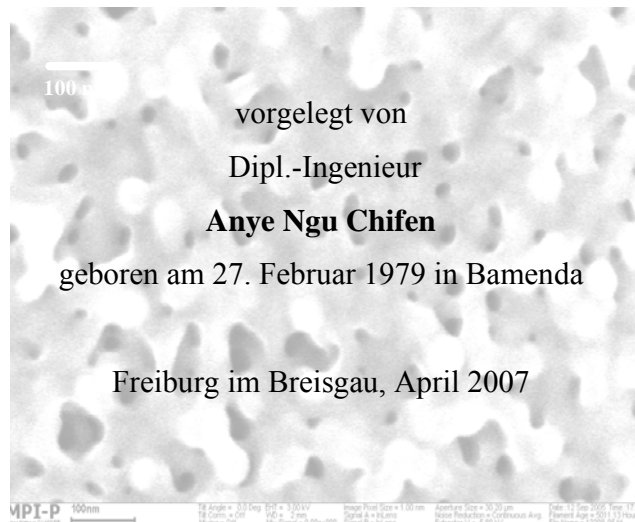# Plasma Polymerized
Biofunctional Multilayers based on
a SiO$_2$-like adhesion promoting film.

Dissertation zur Erlangung des Grades
„Doktor der Ingenieurwissenschaften"

der Fakultät für Angewandte Wissenschaften
der Albert-Ludwigs-Universität Freiburg im Breisgau

vorgelegt von

Dipl.-Ingenieur

Anye Ngu Chifen

geboren am 27. Februar 1979 in Bamenda

Freiburg im Breisgau, April 2007

Der Vorsitzende der Prüfungskommission:

Der Beisitzende der Prüfungskommission:

Erstgutachter: Prof. Dr. J. Rühe

Zweitgutachter: Prof. Dr. W. Knoll

Datum der Disputation: 30. April 2007

To my grandmother - Nimo Lum

Ich erkläre hiermit, dass ich die vorliegende Arbeit ohne zulässige Hilfe Dritter und ohne Benutzung anderer als der angegebenen Hilfsmittel angefertigt habe. Die aus anderen Quellen direct oder indirect übernommenen Daten und Konzepte sind unter Angabe der Quelle gekennzeichnet. Insbesondere habe ich hierfür nicht die entgeltliche Hilfe von Vermittlungs- oder Beratungsdiensten (Promotionsberaterinnen oder Promotionsberater) in Anspruch genommen. Niemand hat von mir unmittelbar oder mittelbar geldwerte Leistungen für Arbeiten erhalten, die im Zusammenhang mit dem Inhalt der vorgelegten Dissertation stehen. Die Arbeit wurde bisher weder im In- noch Ausland in gleicher oder ähnlicher Form einer anderen Prüfungsbehörde vorgelegt.”

Freiburg, den 30-04-2004

_____

Anye Ngu Chifen

Zielsetzung der Arbeit

Für die Anwendung von dünnen Polymerschichten auf kommerziellen Geräten, z.B. Sensoren, muß die Reaktionsfähigkeit der Dünnschichten heutzutage gezielt optimiert werden.

Häufig müssen die Oberflächenfilme mit deren Substraten mittels verschiedenen chemischen Reaktionsmethoden an die Grenzfläche gebunden werden, denn die chemische Zusammensetzung von diesen Oberflächenfilmen und Substraten ist stets unterschiedlich. Diese Optimierung der Grenzflächen von Substraten wird meist nass-chemisch durchgeführt, um die Leistungsfähigkeit des Films (und somit letztendlich die des Sensors) in verschiedenen Medien zu verbessern.

Beispielsweise sind Biosensoren, welche aus drei Bestandteilen bestehen, folgendermaßen aufgebaut: Bio-Film (Biomaterialen), Signalumwandler (elektrische Materialen) und Detektorelement. Dies bedeutet, dass die Effektivität der Biosensoren von der Stabilität oder Adhäsion zwischen den Biomaterialen und dem Signalumwandler abhängig ist.

Die Eigenschaften von synthetischen Biomaterialen spielen eine wesentliche Rolle für die Konzeptionierung eines Biosensors, z.B. in der Gewebetechnik- und Bioelektronikindustrie. Die Reaktionsprozesse an den Grenzflächen zwischen den synthetischen Biomaterialien und biologischen Medien kommen heutzutage sehr häufig im interdisziplinären Bereich zum Einsatz. Trotzdem gibt es eine Reihe von Bio-Filmen, die durch verschiedene Methoden hergestellt worden sind und nicht zum Einsatz kommen können da sie mangelnde Adhäsionseigenschaften auf Substraten in natürlichen extrazellularen Medien aufweisen.

In diesem Sinne ist für die Anwendung von Bio-Filmen in einem Biosensor die Optimierung der Adhäsion zwischen dem Bio-Film und einem Subtrat notwendig, um die funktionellen Eigenschaften in Lösungen beizubehalten.

In dieser Arbeit sollten stabile plasma polymerisierte Schichtsysteme (Engl. Multilayer), welche die Adhäsion zwischen einer elektrischen Grenzfläche und einer biofunktionellen Dünnschicht (Film) optimieren, entwickelt werden. Weiterhin sollen die entwickelten Multilayer stabile und bio-funktionelle Eigenschaften besitzen, um eventuell biologische Moleküle anzubinden.

Um diese Multilayer zu entwickeln, wurde der Zusammenhang zwischen den Plasma Prozessparametern und den Eigenschaften von abgeschiedenen SiO_2 -artigen Filmen untersucht, wobei die dünnen SiO_2 Filme als eine Adhäsionsschicht zwischen einem bio-funktionellen Film und

einem Substrat (z.B. Signalumwandler) dienten. Die Adhäsionseigenschaft der SiO_2 –artigen Filme wurde durch O_2 Plasma optimiert, somit konnten die bio-funktionellen Filme angebunden werden.

Im zweiten Teil dieser Arbeit wurden Stabilität und Alterung SiO_2 –artiger Filme und Multilayer im wässrigen Medium untersucht. Diese Untersuchungen begründen sich aus der Zielsetzung dieser Arbeit, stabile Multilayer zu entwickeln, die die Anbindung von biologischen Molekülen im wässrigen Medium verbessern sollten.

Eine Anwendungsmöglichkeit der angebundenen Biomoleküle oder biologisch relevanten Molekülen (z.B. Vesikel) auf die plasma polymerisierten Multilayer wurde untersucht, indem Fluorophormoleküle in die Vesikel eingekapselt wurden. Die Auflösung der Vesikel, um die Fluorophormoleküle freizusetzen, erfolgte ausschließlich durch enzymatische Reaktion und wurde fluoreszenz-spektroskopisch verfolgt.

Dieser Abschnitt der Arbeit basiert auf einem Biosensor, welcher für die robuste Bestimmung membranauflösender Toxine verwendet werden könnte.

Zum Schluss wurden nano-poröse SiO_2 –artige Filme hergestellt, die als mögliche Materialen für biologischen Zwecken eingesetzt werden könnten.

Teile dieser Arbeit wurden bereits auf der Konferenz „*17th International Symposium on Plasma Chemistry*" in Kanada und der Tagung „*Gordon Research Conference (Plasma Processing Science)*", in Boston, USA präsentiert. Diese Arbeit ist in über 4 verschiedenen wissenschaftlichen Zeitschriften publiziert bzw. eingereicht worden (siehe Publikationsliste Seite. 129).

1 Contents

Chapter 1

1 Plasma, Plasma Polymerization, Multilayer films

1.1 Introduction

The term 'plasma' has a long history. It comes from the ancient Greek language and meant 'what is formed'.[1] The history of plasma is interwoven with many disciplines. Three basic fields of study made unique and early contributions to the development of plasma physics as a discipline: electric discharges, magneto-hydrodynamics (in which a conducting fluid such as mercury is studied), and kinetic theory.[2-6] Interest in electric-discharge phenomena may be traced back to the beginning of the 19th century, with three English physicists – Michael Faraday in the 1830's and Joseph John Thomson and John S. Edward Townsend at the turn of the 19th century. They laid the foundations of the present understanding of the phenomena.

Irving Langmuir introduced the term "plasma" in 1923 while investigating electric discharges. In 1929, he and Lewi Tonks, another physicist working in the United States, used the term to designate those regions of a discharge in which certain periodic variations of the negatively charged electrons could occur. They called these variations plasma oscillations, their behaviour suggested that of a jelly-like substance. It was not until 1952, when two other American physicists, David Bohm and David Pines, first considered the collective behaviour of electrons in metals as distinct from that in ionized gases, was the general applicability of the concept of a plasma fully appreciated.[3]

Plasma has been described as an electrically conducting medium in which there are roughly equal numbers of positively and negatively charged particles, produced when the gas atoms become ionized. It is also referred to as the fourth state of matter, distinct from the solid, liquid, and gaseous states. This ionized gas state is also known as "glow discharge". This state can be partially ionized or completely ionized. In the case of complete ionization, the state would consist solely of electrons and protons (e.g. hydrogen nuclei).[3, 7]

Plasma may be produced in the laboratory by heating a gas to an extremely high temperature, which causes such vigorous collisions between its atoms and molecules that electrons are ripped free, yielding the requisite electrons and ions. A similar process occurs inside stars.

A practical application of plasma involves the glow discharge that occurs between two electrodes at pressures close to 1 bar. Such glow discharges are responsible for the light given off by neon tubes and other light sources such as fluorescent lamps, which operate by virtue of

the plasmas produced in electric discharge. The degree of ionization in such plasmas is usually low. The electrons responsible for current flow are produced by ionization in a region near the cathode, with most of the potential difference between the two electrodes occurring there. This region does not contain plasma, but the region between it and the anode (i.e., the positive electrode) does.

The first potential application of plasma can be traced as far back as 1874 appearing in the reports of DeWilde and Thenard. Separately, they observed solid deposits generated in plasma by some kind of electrical discharge. Little attention was paid to these deposits, which were then known as by-products. At that time, there was not much development or attention focused on polymers, and this process was not recognized as plasma polymerization. In the early 1960's the formation of materials in plasma was recognized as a means of synthesizing polymers.[3] This method of polymerization, which is based on radicals has been exploited over the last 3 decades to form new materials or modify surfaces of other materials.

Plasma polymerization refers to the formation of polymeric material under the influence of plasma. The term 'glow discharge polymerization' has also been used, which is synonymous with plasma polymerization. The most practical means of carrying out plasma polymerization involves the use of an electric glow discharge in a vacuum. Chemical reactions that occur under plasma conditions are generally very complex and consequently, non-specific in nature. Such reactions are of merit when special excited states of molecules are required as intermediate states and cannot be achieved, or can be achieved only with great difficulty by conventional chemical reactions. Thus, plasma polymerization should be recognized as a special means of preparing unique polymers that cannot be made by other methods – rather than as a special way of polymerizing monomers.

The material obtained from this well-recognized concept of polymerization has numerous advantages over other conventional polymers. Pinhole free thin films (> 10 nm) can be deposited on most substrates, which yield better adhesion, chemical, mechanical properties and thermal stability. On one hand, unique surface modifications (up to 10 μm thickness), without changing the bulk properties of the material, has been achieved due to the photons and active species present in the plasma.[8-10] Although, this method of polymerization is expensive due to of the vacuum system, from the standpoint of environmental protection, plasma technologies seem to be a very promising modern technique.[11-14]

Plasma polymers possess a rather disordered structure that is dependent on the intensity and energy of the species bombarding the growing film. Chains of plasma polymers are shorter and in addition they are randomly branched and terminated with a high degree of cross-linking than

in conventional polymerization method. In most cases, a large number of free radicals are trapped within the network. These radicals cannot recombine rapidly and therefore when the plasma polymer is exposed to the atmosphere they react with the oxygen and water vapour. This often leads to observed aging in plasma polymers.

Although a great number of studies has been done to make this process more understandable, it is still a complex and exotic form to fabricate new materials. A wide variety of parameters can directly affect the chemical and physical characteristics of a plasma. Subsequently, these parameters affect the surface of the newly formed polymer. Some examples of these parameters are: gas types, treatment power, treatment time and operating pressure, which can be varied by the operator. System parameters such as electrode location, reactor design, gas inlet and vacuum, are set by the design of the plasma equipment.[2, 13, 15, 16] Multilayers films are obtained by deposition of two or more thin layers (organic, inorganic) onto a substrate by different physical and chemical methods. These multilayer films have also been deposited by plasma polymerization far back in the 60's for numerous applications, e.g. for food packaging, integrated optics, semiconductors and protection layers.[17-20] These layers have been constantly modified to improve the initial drawbacks, such as poor inter-layer adhesion, film stress, and inhomogeneity. Nowadays, well established processes are used for the fabrication of mostly inorganic multilayers for diverse applications, e.g. optics, surface protection and painting.[21-26]

Recently, the development of multilayers (< 100nm) via plasma polymerization has become a topic of interest to combine the well established Si-technology with biology.[27] From a materials science point of view, the bio-application of most materials strongly depends on the nature of its surface, while physical and mechanical properties depend mostly on its bulk. Although, the chemical composition, roughness and topological organization of the topmost layers of biomaterials are crucial in the interaction with biological systems, these layers must be adhered to suitable substrates. In general, plasma-polymerized films adhere well to many substrates, but this also depends on the chemical composition of the flm. Thus, designing multilayers with functional bio-surfaces seem to be a promising method to stabilized functional surfaces under different environmental conditions. Most of the wet-chemical methods employed for the fabrication of bio-functional multilayers also face the problem of instability after a certain period of time. To improve the stability, certain relevant plasma aided modifications will create covalent bonds at the inter-layers of a multilayer.[28-30]

1.2 "State of Art" in Plasma Polymerization

It is well known that deposition of material occurs on a surface, if the surface is exposed to an electrical discharge operated in a gaseous atmosphere containing organic vapors or gases. In the early 19th century, the deposits found after an electrical discharge were investigated,[1] leading to the explanation of electric discharge and the 'plasma' state as described by S. E. Townsend, I. Langmuir and L. Tonks.

Until 1952, König and co-workers prepared carbonaceous films in a glow discharge in benzene vapors using a parallel plate electrode arrangement powered by a single 50 Hz voltage.[31] The chemical characterization by infrared spectroscopy absorption spectra showed not only a hydrocarbon plasma polymer, but also a hard polymer and a material similar to amorphous hydrogenated carbon (a-C:H) was formed. This was then reported by Schmellenmeier how to prepare a-C:H films.[32] Schmellenmeier's report was extensively studied by many researchers, but it was not until 1960 when Goodman reported the real application of plasma polymerized styrene as a dielectric separating film.[33] Since the 60's, the intensively studied plasma polymerization has been recognized as a developing field. Much credit for this development goes to the work of M. Schen, A. T. Bell, H. Yasuda, N. Inagaki, R. d'Agostino and many others.[34-36] Since the earliest systematic research during the 1960s, this field has undergone an enormous expansion. Plasma has been used both in laboratories and industries principally for etching, surface modification and deposition of films, particularly diamond-like carbon for the semi-conductor industry.

In the 1970's, organic polymers were treated in plasma with non-polymerizable gases. Yasuda and co-workers used nitrogen and argon plasma to modify the surfaces of organic polymers.[35, 37-39] This surface modification was carried out to improve the polymer properties such as printability, chemical inertness and introduce surface cross-linking. Several reviews and journal articles related to polymer surface modification and polymerization has been reported by R. d'Agostino, B. Ratner, M. Wertheimer, J. Behnisch and many others.[40-48] The plasma polymerization conditions were classified as "harsh" or "mild". The fabrication under "harsh" conditions was carried out under high input power and above room temperature. On the contrary, the "mild" conditions described the deposition under low input power and below room temperature. O. Takai and Y. Hisamatsu have investigated these conditions by fabricating coatings for semiconductor industry using plasma polymerization.[49] These conditions were used to prepare hard coatings from acrylic acid, tetramethoxysilane or a

mixture of both monomers and oxygen.[50-53] Related to these harsh conditions, polymerization processes that used ion beam were restricted to laboratory scale until 1976, when L. Holland showed how the film hardness increases with ion energy by using a dc negative self bias on a radio frequency (rf) powered electrode.[36, 54] This further increased the interest of hard coatings fabricated using different monomers. The most prominent gas used was CF_4 to produce fluorocarbon films, which have been investigated by J. Nebdal, L. Holland, J. Biederman and R. d'Agostino.[55-57] All these researchers worked on the fabrication of amorphous fluorinated carbon (a-C:F) from CF_4, CF_3Cl, C_2F_3Cl monomers. Furthermore, hard coatings were fabricated using different monomers. M. Wertheimer, M. J. Vasile with other authors investigated the chemical and electrical properties of the plasma polymerized organosilicon films, which were deposited with and without ion bombardment. Rf input power between 50 – 300 W and a total flow rate for $HMDSO/O_2$ of 20 sccm was used. It was shown that carbon-free films can be obtained by highly diluting the monomer in oxygen at high input power, while mild conditions lead to a high carbon content in the polymer. These two conditions represent the optimized criterion to obtain excellent barrier films, which was later used for food packaging applications by Tetrapak in the late 70's. [31, 34, 58-61]

In the last decades, new insights and several diagnostic techniques have been introduced and developed to understand the microscopic mechanisms during film deposition. It has been explained by F. Normand, C. Vallee and A. Granier[62-67] that the plasma environment changes drastically upon co-polymerization, e.g. hexamethyl disiloxane (monomer) and oxygen. Some related works published by these authors and others have analyzed the oxygen positive ions produced during the fabrication of SiO_2 films from tetraethoxysilane and oxygen gas. The complex nature of the plasma polymerization process, due to the plasma variables (ion energy, substrate temperature, monomer concentration, input power, etc.), were investigated using mass spectrometry and Langmuir probes.

Much of the research on "soft" polymers in the past few years has been carried out by B. Ratner and co-workers, mainly for application in the biomedical industry.[46, 68, 69] The deposition of anti-fouling (PEO-like) and bacterial resistant (Ag/PEO-like) coatings produced using rf plasma were reported by R. d'Agostino. These PEO-like films were plasma polymerized under mild conditions, so the plasma polymer retained more of the molecular structure of the precursor. The mild conditions were controlled by pulsing the input power for numerous monomers.[70-72]

A great deal of work performed by many researchers in this field of plasma processing has produced two major important results: (i) the utilization of this technology for many

applications has increased and (ii) the understanding the microscopic mechanisms of interactions, particularly for the film deposition processes has improved.[7, 73-75] The utilization of this technology for different sectors has encouraged researchers to work with a variety of monomers and different kinds of plasma systems so as to meet the demands in many industrial sectors.

A recent report by Förch and co-workers examines the challenges in surface science, whereby plasma polymerization has been used to synthesize reproducibly defined surfaces from hard coatings to bio-functional films.[76] The report showed that the applications of plasma polymers continuously increase in the domain of surface science, from SiO_2-like films to biological surfaces. Some of these biological surfaces are presently applied in medical implants, tissue engineering, bioelectronics and biosensors.[27, 77, 78] The demand of defined polymer surfaces in the biosensor industry has an extremely rapid development with an estimated market annual growth for labchips / biochips of 40 % and 60 % in 2002 and 2005 respectively.[27, 79] Most of its impact is technologically based on structuring of the materials, which can be improved using plasma polymers.

Despite the amount of work done in plasma polymerization during the last decades, more challenges are still to be expected, e.g. thermal, mechanical, optical and electrical instabilities. Most often the chemical non-uniformity, aging effects and instability of biopolymers in the native, liquid state hinders broader applications. However new procedures, as demanded by the current state of the art for the improvement of film stability and uniformity, are needed. Several candidates that may also remarkably improve the adhesion could be short time post-deposition irradiations by an energetic source.

So far, the films deposited are highly adherent, single layer coatings with novel chemistries and physical properties are stable under ambient conditions. In the case of subjecting single "soft" or biopolymer films in aqueous medium, their adhesion on various substrates deteriorates, which makes it unfavorable for further application. The adhesion of single thin films on substrates was addressed in the last decade by W. Unger, C. Oehr and R. d'Agostino.[80-82] However, adhesion has been improved for single films and multilayer, in which they proposed the substrate modification and gradient layer fabrication to improve the substrate-film, or interlayer bonding. Thus for the use of these multilayer (μm scale) has been implemented in painting, corrosion and surface protection purposes.[83] This method of improving the adhesion can be miniaturized, i.e. application of thin multilayer films (nm scale) to improve adhesion of functional biopolymers on different substrates. This would help in the

pursuit of application of such films in various sectors auch as biosensor, biomaterial, and biomedical implant technology and so on. [84, 85]

Another critical point is to scale-up procedure of the deposition technique for large area and especially large volume 3D objects, which is still a major challenge, but has been improved over the last few years.[86]

Despite the amount of work to be accomplished in plasma polymerization, the amount of waste is several orders of magnitude lower and less dangerous than conventional chemical wet processes used for the same purpose. Bearing in mind that plasma polymerization occurs without solvents in a reduced pressure vessel, which is self-contained and thereby optimizes waste management. Thus, in the future, the market of plasma polymers will not be endangered from this perspective.[87]

1.3   Aim of this thesis:

The aim of this thesis is to design stable plasma polymerized (pp) multilayer, which will improve the adhesion between an electrical interface and a bio-functional film.

Nowadays, the reactivity of a film on a sensor device or model system needs to be optimized. More often, these films have a different chemical composition than their substrates, which lead to poor device efficiency. Specifically, biosensor devices consist of three components namely; bio-material, transducer (connects both components) and detector element. Thus, the crucial step for developing an array platform is a stable adhesion between the electrical surface and the functional bio-material.

Bio-materials play an essential role for the fabrication of a biosensor platform, tissue engineering and bioelectronics. These materials have been used nowadays in broad inter-disciplinary area where properties and processes at interfaces between synthetic materials and biological environments have been investigated. So far, these materials have been obtained by various fabrication methods and were not suitable for specific applications, due to some major problems such as adhesion, mechanical degradation and bio-incompatibility of the films when subjected to the natural extra-cellular environment. From this point of view, it is important to design a new bio-material platform that will address some of these drawbacks mentioned herein.

The aim of this work was to design a multilayer using plasma enhanced chemical vapor deposition (PECVD), whereby, the inter-layer adhesion is to be optimized between an electrical insulator material and the bio-functional film. Furthermore, the possible application of the designed multilayer system was to be implemented in a biological medium.

Firstly, the correlation between the plasma parameters and the film properties of deposited pp organosilicon films was investigated. Whereby, ultra thin SiO_2 –like films were deposited and would serve as an adhesion interlayer between a functional organic layer and an electrical substrate. The adhesion properties of the SiO_2 –like layer was optimized for the subsequent pp of a bio-material film via a plasma modification process.

Secondly, the aging in air and stability in aqueous medium of the multilayer were also investigated.

Finally, a possible application of the biofunctional multilayer was achieved by attaching fluorophore-encapsulated vesicles on the plasma polymerized multilayer. The fluorophore release was initiated enzymatically and then monitored by fluorescence spectroscopy, which could be implemented as a biosensor.

1.4   Reference

1.   Arzimovich, L. A., Elementary Plasma Physics 1965 (originally published in Russian, 1963).

2.   Chen, F. F., Introduction to Plasma Physics and Controlled Fusion, vol. 1, Plasma Physics. 1984.

3.   Yasuda, H., Plasma Polymerization. Academic Press: 1985.

4.   Kelley, M. C.; Heelis, R. A., The Earth's Ionosphere: Plasma Physics and Electrodynamics. Academic Press: 1989.

5.   Eliezer, Y.; Eliezer, S., The Fourth State of Matter: An Introduction to the Physics of Plasma. 1989

6.   Howes, R.; (eds.), A. F., The Energy Sourcebook , A Guide to Technology, Resources, and Policy. New York: American Institute of Physics: 1991.

7.   D'Agostino, R.; Cramarossa, F.; Fracassi, F.; Illuzzi, F., Plasma Deposition, Treatment, and Etching of Polymers. Academic Press, San Diego, CA,: 1990.

8.   Chan, C.-M.; Ko, T.-M.; Hiraoka, H., Polymer surface modification by plasmas and photons. Surface Science Reports 1996, 24, 24.

9.   Mittal, K. L., Polymer Surface Modification: Relevance to Adhesion. VSP BV, The Netherlands, : Utrecht, 1996.

10.   Sarmadi, M.; Denes, F., Surface modification of polymers under cold plasma conditions. Tappi Journal 1996, 79, (8), 189-204.

11.   Fozza, A. C.; Roch, J.; KlembergSapieha, J. E.; Kruse, A.; Hollander, A.; Wertheimer, M. R., Oxidation and ablation of polymers by vacuum UV radiation from low pressure plasmas. Nuclear Instruments & Methods in Physics Research Section B-Beam Interactions with Materials and Atoms 1997, 131, (1-4), 205-210.

12.   Whitaker, A. F.; Jang, B. Z., Oxygen Plasma Environment - Its Effect on Polymers. Sampe Journal 1994, 30, (2), 30-41.

13.   Wang, Y.; Zhang, J.; Shen, X. Y., Surface structures tailoring of hexamethyldisiloxane films by pulse rf plasma polymerization. Materials Chemistry and Physics 2006, 96, (2-3), 498-505.

14.   Casserly, T. B.; Gleason, K. K., Effect of substrate temperature on the plasma polymerization of poly(methyl methacrylate). Chemical Vapor Deposition 2006, 12, (1), 59-66.

15.   Grüniger, A.; Bieder, A.; Sonnenfeld, A.; von Rohr, P. R.; Muller, U.; Hauert, R., Influence of film structure and composition on diffusion barrier performance of SiOx thin films deposited by PECVD. Surface and Coatings Technology 2006, 200, (14-15), 4564-4571.

16.   Yasuda, H.; Hirotsu, T., Critical Evaluation of Conditions of Plasma Journal of Polymer Science: Polymer Chemistry Edition 1978, 16, 17.

17.   Sun, F. Q.; Cai, W. P.; Li, Y.; Jia, L. C.; Lu, F., Direct growth of mono- and multilayer nanostructured porous films on curved surfaces and their application as gas sensors. Advanced Materials 2005, 17, (23), 2872-+.

18.   Sangaletti, T.; Depero, L. E.; Dieguez, A.; Marca, G.; Morante, J. R.; Romano-Rodriguez, A.; Sberveglieri, G., Microstructure and morphology of tin dioxide multilayer thin film gas sensors. Sensors and Actuators B-Chemical 1997, 44, (1-3), 268-274.

19.   Petty, M. C., Application of Multilayer Films to Molecular Sensors - Some Examples of Bioengineering at the Molecular-Level. Journal of Biomedical Engineering 1991, 13, (3), 209-214.

20. Ray, M. A.; Greene, J. E.; Polack, A. J.; Welsh, L. B., Rf-Sputter-Deposited Multilayer Thin-Film Oxygen Sensors. Journal of Vacuum Science & Technology a-Vacuum Surfaces and Films 1983, 1, (2), 322-322.

21. Martinu, L.; Poltras, D., Plasma deposition of optical films and coatings: A review [Review]. Journal of Vacuum Science & Technology A-Vacuum Surfaces & Films 2000, 18, (6), 2619-2645.

22. Knight, J. C.; Page, T. F., Interfacial Phases and the Adhesion of Amorphous Hydrogenated Carbon-Films Deposited by Rf Chemical Vapor-Deposition onto (100) Silicon. Surface & Coatings Technology 1992, 53, (2), 121-128.

23. Sahli, S.; Segui, Y.; Ramdani, S.; Takkouk, Z., R.f. plasma deposition from hexamethyldisiloxane-oxygen mixtures. Thin Solid Films 1994, 250, (1-2), 206-212.

24. Grundmeier, G.; Stratmann, M., Influence of oxygen and argon plasma treatments on the chemical structure and redox state of oxide covered iron. Applied Surface Science 1999, 141, (1-2), 43-56.

25. Kurosawa, S.; Aizawa, H.; Miyake, J.; Yoshimoto, M.; Hilborn, J.; Talib, Z. A., Detection of deposition rate of plasma-polymerized silicon-containing films by quartz crystal microbalance. Thin Solid Films 2002, 407, (1-2), 1-6.

26. Grundmeier, G.; Thiemann, P.; Carpentier, J.; Barranco, V., Tailored thin plasma polymers for the corrosion protection of metals. Surface & Coatings Technology 2003, 174, 996-1001.

27. Kasemo, B., Biological surface science. Surface Science 2002, 500, (1-3), 656-677.

28. Muir, B. W.; McArthur, S. L.; Thissen, H.; Simon, G. P.; Griesser, H. J.; Castner, D. G., Effects of oxygen plasma treatment on the surface of bisphenol A polycarbonate: a study using SIMS, principal component analysis, ellipsometry, XPS and AFM nanoindentation. Surface and Interface Analysis 2006, 38, (8), 1186-1197.

29. Angelini, E.; Grassini, S.; Rosalbino, F.; Fracassi, F.; Laera, S.; Palumbo, F., PECVD coatings: analysis of the interface with the metallic substrate. Surface and Interface Analysis 2006, 38, (4), 248-251.

30. Wavhal, D. S.; Zhang, J. M.; Steen, M. L.; Fisher, E. R., Investigation of gas phase species and deposition of SiO2 Films from HMDSO/O-2 plasmas. Plasma Processes & Polymers 2006, 3, (3), 276-287.

31. Klembergsapieha, J. E.; Sapieha, S.; Wertheimer, M. R.; Yelon, A., Charge Trapping in Plasma-Polymerized Thin-Films. Applied Physics Letters 1980, 37, (1), 104-105.

32. Schmellenmeier, H., Traversable gas-meltdown machine. Zeitschrift Des Vereines Deutscher Ingenieure 1944, 88, 298-299.

33. Tkachuk, B. V.; V. V. Bushin, V. V.; Kolotyrkim, V. M.; Smetankina, V. M., Polym. Sci. USSR 1967, 9, 2018.

34. Vasile, M. J.; Smolinsk.G, Organosilicon Films Formed by an Rf Plasma Polymerization Process. Journal of the Electrochemical Society 1972, 119, (4), 451-&.

35. Yasuda, H., Plasma for Modification of Polymers. Abstracts of Papers of the American Chemical Society 1975, (169), 21-21.

36. Holland, L., A Review of Plasma Process Studies. Surface Technology 1980, 11, (3), 145-169.

37. Yasuda, H., Plasma for Modification of Polymers. Journal of Macromolecular Science-Chemistry 1976, A 10, (3), 383-420.

38. Yasuda, H.; Bumgarner, M. O.; Marsh, H. C.; Morosoff, N., Plasma Polymerization of Some Organic Compounds and Properties of Polymers. Journal of Polymer Science Part a-Polymer Chemistry 1976, 14, (1), 195-224.

39. Yasuda, H.; Marsh, H. C.; Brandt, E. S.; Reilley, C. N., Reactions of Nitrogen and Argon Plasma with Organic Polymers. Abstracts of Papers of the American Chemical Society 1975, 170, (Aug24), 34-34.

40. Liston, E. M.; Martinu, L.; Wertheimer, M. R., Plasma Surface Modification of Polymers for Improved Adhesion - a Critical-Review. Journal of Adhesion Science and Technology 1993, 7, (10), 1091-1127.

41. Hollander, A.; Klembergsapieha, J. E.; Wertheimer, M. R., Vacuum-Ultraviolet-Induced Oxidation of Polyethylene. Macromolecules 1994, 27, (10), 2893-2895.

42. Behnisch, J.; Zimmermann, H., Topokinetics of the Polyene Formation in Poly(Vinyl Chloride) Films during Treatment with Nonoxidative Plasma. International Journal of Polymeric Materials 1992, 16, (1-4), 139-142.

43. Behnisch, J.; Friedrich, J.; Zimmermann, H., Topokinetics of the Polyene Formation in Pvc Films during Treatment with Nonoxidative Plasma. Acta Polymerica 1991, 42, (1), 51-52.

44. Johnston, E. E.; Ratner, B. D., Surface characterization of plasma deposited organic thin films. Journal of Electron Spectroscopy and Related Phenomena 1996, 81, (3), 303-317.

45. Ratner, B. D., Plasma Deposition of Organic Thin-Films - Control of Film Chemistry. Abstracts of Papers of the American Chemical Society 1993, 205, 110-POLY.

46. Ratner, B. D., Plasma Deposition for Biomedical Applications - a Brief Review. Journal of Biomaterials Science-Polymer Edition 1992, 4, (1), 3-11.

47. Lamendola, R.; dAgostino, R., RF plasma deposition of barrier thin films from hexamethyldisilazane and hexamethyldisiloxane containing feeds. Abstracts of Papers of the American Chemical Society 1997, 213, 499-POLY.

48. Yasuda, H.; Hirotsu, T., Polymerization of Organic-Compounds in an Electrodeless Glow-Discharge .9. Flow-Rate Dependence of Properties of Plasma Polymers of Acetylene and Acrylonitrile. Journal of Applied Polymer Science 1977, 21, (11), 3167-3177.

49. Takai, O.; Hisamatsu, Y., Sio2 Coating and Plasma Anodization of Metals and Semiconductors. Thin Solid Films 1981, 84, (4), 369-378.

50. Cho, D. L.; Claesson, P. M.; Golander, C. G.; Johansson, K., Structure and Surface-Properties of Plasma Polymerized Acrylic-Acid Layers. Journal of Applied Polymer Science 1990, 41, (7-8), 1373-1390.

51. Cho, D. L.; Claesson, P. M.; Golander, C. G.; Johansson, K. S., Structure and Surface-Properties of Plasma Polymerized Acrylic-Acid Layers. Abstracts of Papers of the American Chemical Society 1990, 199, 28-Pmse.

52. Ohkubo, J.; Inagaki, N., Influences of the System Pressure and the Substrate-Temperature on Plasma Polymers. Journal of Applied Polymer Science 1990, 41, (1-2), 349-359.

53. Inagaki, N.; Ohishi, K., Preparation of Amino Group-Containing Polymers by Plasma Polymerization. Journal of Polymer Science Part a-Polymer Chemistry 1985, 23, (5), 1445-1454.

54. Mnatsakanyan, A. K., Elementary Process Kinetics in a Plasma of Inert-Gases, Molecules, and Alkali-Metal Vapors (Review). High Temperature 1974, 12, (4), 745-762.

55. Yasuda, H.; Bumgarner, M. O.; Hillman, J. J., J. Appl. Polym Sci. 1975, 19, (531).

56. Martinu, L.; Biederman, H.; Zemek, J., Metal Doped Polymer-Films Prepared by Simultaneous Plasma Polymerization of Tetrafluoromethane and Evaporation of Gold. Vacuum 1985, 35, (4-5), 171-176.

57. Biederman, H.; Holland, L., Metal Doped Fluorocarbon Polymer-Films Prepared by Plasma Polymerization Using an Rf Planar Magnetron Target. Nuclear Instruments & Methods in Physics Research 1983, 212, (1-3), 497-503.

58. Sacher, E.; Klembergsapieha, J. E.; Schreiber, H. P.; Wertheimer, M. R., Moisture Barrier Properties of Plasma-Polymerized Hexamethyldisiloxane. Applied Polymer Symposia 1984, (38), 163-171.

59. Yasuda, H., Glow-Discharge Polymerization. Macromolecular Reviews Part D-Journal of Polymer Science 1981, 16, 199-293.

60. Woollen, A., Tetrapak Dutch Connection. Food Manufacture 1978, 53, (7), 45-&.

61. [Anon], Tetrapak in Holland. Dairy Industries International 1978, 43, (7), 26-28.

62. Granier, A.; Borvon, G.; Bousquet, A.; Goullet, A.; Leteinturier, C.; van der Lee, A., Mechanisms involved in the conversion of ppHMDSO films into SiO_2-like by oxygen plasma treatment. Plasma Processes and Polymers 2006, 3, (4-5), 365-373.

63. Granier, A.; Nicolazo, F.; Vallee, C.; Goullet, A.; Turban, G.; Grolleau, B., Diagnostics in O-2 helicon plasmas for SiO_2 deposition. Plasma Sources Science & Technology 1997, 6, (2), 147-156.

64. Nicolazo, F.; Goullet, A.; Granier, A.; Vallee, C.; Turban, G.; Grolleau, B., Study of oxygen/TEOS plasmas and thin SiOx films obtained in an helicon diffusion reactor. Surface & Coatings Technology 1998, 98, (1-3), 1578-1583.

65. Vallee, C.; Goullet, A.; Nicolazo, F.; Granier, A.; Turban, G., In situ ellipsometry and infrared analysis of PECVD SiO2 films deposited in an O-2/TEOS helicon reactor. Journal of Non-Crystalline Solids 1997, 216, 48-54.

66. Bousquet, A.; Bursikova, V.; Goullet, A.; Djouadi, A.; Zajickova, L.; Granier, A., Comparison of structure and mechanical properties of SiO_2-like films deposited in O_2/HMDSO pulsed and continuous plasmas. Surface & Coatings Technology 2006, 200, (22-23), 6517-6521.

67. Supiot, P.; Vivien, C.; Granier, A.; Bousquet, A.; Mackova, A.; Escaich, D.; Clergereaux, R.; Raynaud, P.; Stryhal, Z.; Pavlik, J., Growth and modification of organosilicon films in PECVD and remote afterglow reactors. Plasma Processes and Polymers 2006, 3, (2), 100-109.

68. Favia, P.; d'Agostino, R., Plasma treatments and plasma deposition of polymers for biomedical applications. Surface & Coatings Technology 1998, 98, (1-3), 1102-1106.

69. Favia, P.; d'Agostino, R.; Palumbo, F., Grafting of chemical groups onto polymers by means of RF plasma treatments: A technology for biomedical applications. Journal De Physique IV 1997, 7, (C4), 199-208.

70. Schiller, S.; Hu, J.; Jenkins, A. T. A.; Timmons, R. B.; Sanchez-Estrada, F. S.; Knoll, W.; Forch, R., Chemical structure and properties of plasma-polymerized maleic anhydride films. Chemistry of Materials 2002, 14, (1), 235-242.

71. Jenkins, A. T. A.; Hu, J.; Wang, Y. Z.; Schiller, S.; Foerch, R.; Knoll, W., Pulsed plasma deposited maleic anhydride thin films as supports for lipid bilayers. Langmuir 2000, 16, (16), 6381-6384.

72. Ryan, M. E.; Hynes, A. M.; Badyal, J. P. S., Pulsed plasma polymerization of maleic anhydride. Chemistry of Materials 1996, 8, (1), 37-42.

73. Manos, D. M.; Flamm, D. L., Plasma Etching: an introduction. Academic press: New York, 1989.

74. Auciello, O.; Flamm, D. L., Plasma Diagnostics. Academic Press: New York, 1989; Vol. Vol. 1.

75. Bruno, G.; Capezzuto, P.; Madan, A., Plasma Deposition of Amorphous Silicon-Based Materials. Academic Press: New York, 1991.

76. Förch, R.; Chifen, A. N., Bousquet, A.; Khor, H.-L.; Jungblut, M.; Chu, L.-Q.; Zhang, Z.; Osey-Mensah, I.; Sinner, E.-K.; Knoll, W., Recent and expected roles of plasma polymerized films for biomedical applications. CVD Journal, special edition 2006.

77. Innocenzi, P.; Martucci, A.; Guglielmi, M.; Bearzotti, A.; Traversa, E.; Pivin, J. C., Mesoporous silica thin films for alcohol sensors. Journal of the European Ceramic Society 2001, 21, (10-11), 1985-1988.

78. Igarashi, S.; Itakura, A. N.; Toda, M.; Kitajima, M.; Chu, L.; Chifene, A. N.; Forch, R.; Berger, R., Swelling signals of polymer films measured by a combination of micromechanical cantilever sensor and surface plasmon resonance spectroscopy. Sensors & Actuators B-Chemical 2006, 117, (1), 43-49.

79. Biosensors Biosensor research at Diepenbeek and London South Bank University.

80. Oran, U.; Swaraj, S.; Friedrich, J. F.; Unger, W. E. S., Surface analysis of plasma-deposited polymer films, 1 - ToF-SSIMS of plasma polystyrene before and after exposure to ambient air. Plasma Processes and Polymers 2004, 1, (2), 123-133.

81. Unger, W. E. S.; Swaraj, S.; Oran, U.; Lippitz, A., Radio frequency (r.f.) plasma-deposited polymer films: influence of external plasma parameters as viewed by comprehensive in-situ surface chemical analysis by XAS, XPS and ToF-SIMS. Surface and Interface Analysis 2006, 38, (4), 522-525.

82. D'Agostino, R.; Favia, P.; Oehr, C.; Wertheimer, M. R., Low-temperature plasma processing of materials: Past, present, and future. Plasma Processes & Polymers 2005, 2, (1), 7-15.

83. Wapner, K.; Grundmeier, G., Spectroscopic analysis of the interface chemistry of ultra-thin plasma polymer films on iron. Surface & Coatings Technology 2005, 200, (1-4), 100-103.

84. Yeo, S.; Kwon, T.; Choi, C.; Park, H.; Hyun, J. W.; Jung, D., The patterned hydrophilic surfaces of glass slides to be applicable for the construction of protein chips. Current Applied Physics 2006, 6, (2), 267-270.

85. Ohl, A.; Schroder, K.; Keller, D.; Meyer-Plath, A.; Bienert, H.; Husen, B.; Rune, G. M., Chemical micropatterning of polymeric cell culture substrates using low-pressure hydrogen gas discharge plasmas. Journal of Materials Science-Materials in Medicine 1999, 10, (12), 747-754.

86. Poll, H. U.; Schreiter, S., Problems of large scale deposition of thin plasma polymer films. Surface & Coatings Technology 1997, 93, (1), 105-111.

87. Lubbe-Wolff, G., Efficient environmental legislation - On different philosophies of pollution control in Europe. Journal of Environmental Law 2001, 13, (1), 79-+.

Chapter 2

2 Fundamentals of Plasma Polymerization and Surface Modification

2.1 Introduction

The plasma state is a mixture of electrons, negatively and positively charged particles, and neutral atoms and molecules. Plasmas have been described as the fourth state of matter, which is highly activated than in solid, liquid or gas state. Three essential items are required for plasma generation: (1) an energy source for ionization, (2) a pumping system to maintain the plasma state; vacuum or atmospheric, (3) and a reaction chamber. This energy source can be used to initiate polymerization, termed plasma polymerization or the thin film deposition process has been termed as plasma enhanced chemical vapor deposition (PECVD).

Although the formation of polymeric materials in plasma is customarily termed plasma polymerization, the term polymerization applies to many conventional (radical and ionic) methods of polymer formation and does not exactly describe the actual processes that occur in plasma polymerization. The following section presents the fundamental aspects of plasma and mechanisms of polymeric material formation in plasma.

2.2 Main Sources of Gas Discharge Plasmas

Plasma can also be created by other conditions by transferring power from an electric field to electrons or by applying intense heat to state of matter.[1-4] In most cases, a direct current (DC) glow discharge is attained by passing electric current through a gas under low pressure. The cathode is bombarded with positive ions, resulting in the generation of secondary electrons. These electrons are accelerated away from the cathode until they gain sufficient energy to ionize the gas molecules or atoms that collide with the electrons.

Another means to create glow discharge is by using alternating current. The frequency of alternation is important. At a low frequency, it can be regarded as a DC discharge with changing polarity. The positive ions become immobile upon increasing the frequency of the applied voltage because they can no longer follow the periodic changes in field polarity, and therefore respond to time-averaged fields. A frequency of about 50–100 kHz is sufficient to provide a continuous discharge. In radio frequency (rf, 13.56 MHz), no contact between the
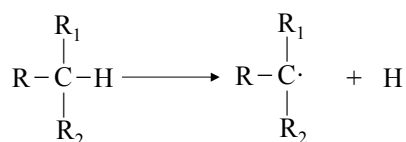
electrodes and the plasma is required. The plasma can be initiated and sustained by external inductive electrodes.

Most frequently, high frequency plasmas (f > 1 MHz) are used for PECVD of dielectric optical films, in order to avoid surface charging and plasma instabilities as recommended by ITU (International Telecommunications Union). ITU approved industrial, scientific, and medical frequencies operated at 13.56 MHz rf, or 2.45 GHz microwave, MW.

2.3   The Plasma Polymerization Mechanism

The concept of this polymerization points out that elemental reactions occurring in plasma polymerization are the fragmentation of monomer molecules, the formation of active sites (radicals) from the monomer, and recombination of the activated fragments to form a polymer. H. Yasuda described this process as the rapid step growth of polymers due to fragmentation of monomers, which occur in a glow discharge region.[4-6] This process is attributed to the various types of collisions occurring simultaneously or separately in the reaction chamber. If fragmentation and recombination operate in plasma, the starting molecules for plasma polymerization will not be restricted to unsaturated compounds such as vinyl compounds, saturated compounds can also deposit plasma polymers. The fragmentation of starting molecules in plasma is represented by two types of reactions, namely the elimination of the weak hydrogen atom and the scission of the C–C bond.

(a) Hydrogen elimination   (b) C –C bond scission

$$R-\underset{\underset{R_2}{|}}{\overset{\overset{R_1}{|}}{C}}-H \longrightarrow R-\underset{\underset{R_2}{|}}{\overset{\overset{R_1}{|}}{C}}\cdot \quad + \quad H \qquad R-\underset{\underset{R_2}{|}}{\overset{\overset{X_1}{|}}{C}}-\underset{\underset{R_2}{|}}{\overset{\overset{X_2}{|}}{C}}-H \longrightarrow R-\underset{\underset{R_2}{|}}{\overset{\overset{X_1}{|}}{C}}\cdot \quad + \quad \cdot\underset{\underset{R_2}{|}}{\overset{\overset{X_2}{|}}{C}}-R$$
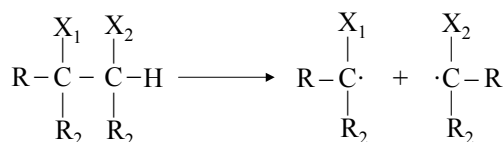
Hydrogen elimination is considered to contribute greatly to the polymer-forming process in plasma polymerization. The gas phase of a closed system after plasma polymerization of hydrocarbons is mainly composed of hydrogen as reported by Hillman and co-workers.[7]
Figure 2-1 shows an essential polymer forming process as proposed by H. Yasuda, which can be related to the elimination of hydrogen and scission of C–C bonds. When hydrogen atoms are eliminated from monomer molecules by plasma to form mono-radicals $M_i\cdot$, and bi-radicals $\cdot M_k\cdot$, and thereafter, the addition of the radicals to monomer and the recombination between two radicals proceeds to make large molecules with or without radical. Mono-radicals $M_i\cdot$ add to the monomer to form a new radical $M_j-M\cdot$. Mono-radical $M_i\cdot$ and may recombine with $M_j\cdot$

to build a neutral or stable molecule $M_i-M_j\cdot$. A bi-radical can also attack the monomer to form a new bi-radical $\cdot M_k-M\cdot$, or recombine with another bi-radical to form a new bi-radical $\cdot M_k-M_j\cdot$. The new monomer M_i-M_j is activated by plasma to form mono- or bi-functional activated species. This cycle I is the repeated activation of the reaction products from mono-functional activated species, cycle II describes the recombination of the mono and bi-radical to form larger radicals.
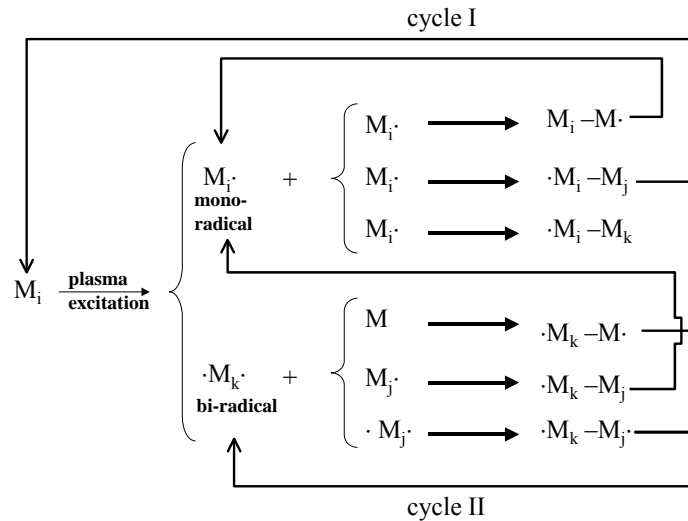
Figure 2-1: overall plasma polymerization mechanism showing a bi-cyclic step-growth. Subscripts i, j, k, merely indicate the difference in the size of species involved (i = j is possible, if i = j = 1 corresponds to original monomer)[4]

However, the fragmentation to yield these species depends on how much the electric energy (rf power) and the amount of monomer injected into the system to maintain the plasma. The polymer deposition rate has been related to the Yasuda parameter, (W/FM) which describes the ratio of input power, W to the flow rate, F and monomer molecular weight, M.[4] As soon as plasma is created, the gas phase becomes a mixture of the original monomer and species created. This implies that any material that interacts with plasma becomes a source of monomer for plasma polymerization. Figure 2-2 depicts the overall scheme of plasma polymerization, which encompasses the principle of the competitive ablation and polymerization (CAP) mechanism.[7, 8] The ablated material can be re-deposited or leaves the system as an effluent gas. Thus, the two types of plasma-mechanisms can be differentiated, the plasma-state and plasma-induced polymerization. The plasma-state polymerization describes the main route of polymer formation under the influence of plasma; whereas, plasma-induced polymerization represents the polymerization of condensed monomer on the surface by plasma interaction.

In contrast to conventional polymerization, plasma polymerization forms an irregular network-like material which varies from a low to a high cross-linked density.[8] The plasma polymerization of acetylene, ethylene, ethane, styrene and other hydrocarbons have been investigated, which showed different chemical characteristics as compared to conventional method of polymerization. Investigations were based on various operational parameters such input power, deposition pressure and monomers flow.

In a conventional polymerization, monomers are linked together through chemical reactions without any alteration of chemical structure of the monomer or, in some cases, with small alteration by loss of fragments from two monomers, e.g. condensation reaction. Therefore, the chemical structure of the formed polymer chains is well predicted from the chemical structure of the monomer. In plasma polymerization, the chemical structure of polymers formed, if the same monomer was used, is never predicted from the monomer structure. In some cases, due to atmospheric reactions, nitrogen, or oxygen are incorporated into the polymers formed by radical combination reactions.

Thus, using the conventional method to prepare polymer films involves steps such as monomer synthesis, polymerization, and preparation of coating solution, cleaning or conditioning of substrate, drying and curing. This can be replaced by a "one–step process" in the plasma polymerization, which can be credited to the complexity of the chemical reactions in such a process.
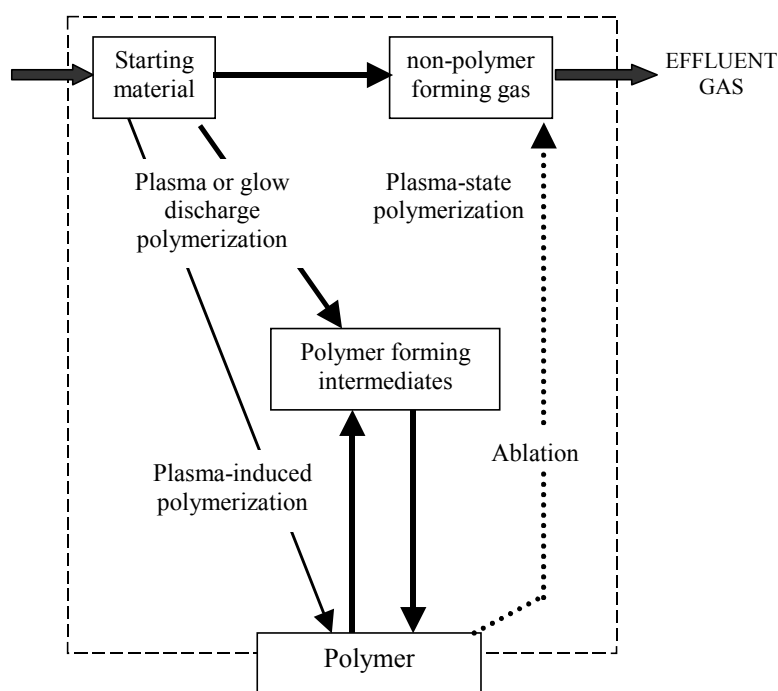
Figure 2-2: Schematic representation of plasma polymerization mechanism[4]

18

2.4   Surface Modification

The modification of the chemical structure, reactivity, and bonding characteristics of polymer surfaces has considerable technological importance in the areas of protective coatings, adhesion and biomedical compatibility. Plasma surface treatment is one type of surface modification that is commonly used. This surface treatment can be used to modify the surface of a polymer or material to improve adhesion or wettability, to provide a diffusion barrier layer, or to minimize degradation of a polymer surface during binding. A unique feature of plasma modification is that the surface structure of the polymer can be selectively modified for a specific application while the bulk properties of the polymer are unaffected, e.g. the polymerization of thin film on top of material. However, it must be noted that the complexity of the plasma itself makes it difficult to unravel the mechanisms responsible for surface modification, without the necessary diagnostic techniques.

From recent reports[9-13] on polymers surfaces, the most interesting reasons for surface modification are to;

- produce special functional groups at the surface for specific interactions with other functional groups,
- increase surface energy,
- increase hydrophobicity or hydrophilicity,
- improve chemical inertness,
- introduce surface cross-linking,
- remove weak boundary layers or contaminants,
- modify surface morphology - increase or decrease surface crystallinity and roughness.
- increase surface electrical conductivity,
- increase surface lubricity and
- improve dyeability.

Some of the various surface modification techniques implemented will be presented here.

2.5   Methods of Surface Modification

Common surface modification techniques include treatments by flame, corona, plasmas, photons, electron beams, ion beams, x-rays, γ-rays, UV-irradiation and wet chemical methods. In the <u>flame treatment,</u> excited species are produced at high temperatures (1000–2000 °C), which then react with the surface in contact. This leads primarily to increased oxygen concentration on the surface, which is regarded as an advantage over other treatment techniques.[14] The main

application of flame treatment on polymers is to improve adhesion or enhance printability in the polymer industry. One disadvantage of this method is temperature operation, which might create surface heterogeneity and thus can not be applied to a range of materials.

Corona discharge is a form of plasma pre-treatment, operated at atmospheric pressure, used widely for enhancing the adhesive properties. This discharge is produced when air (atmospheric plasma) is ionized by a high electric field and it is widely used for treating plastic films and conical containers.[15, 16] This form of treatment is limited to a small area, where the discharge strikes, and the specificity toward the type of functional groups introduced at the surface is considered to be low, which can be seen as a disadvantage over other treatment methods.

Specifically, plasma treatment encompasses any form of surface treatment in which a material is exposed to an ionized gas (plasma). This would include both flame and corona treatment. However, plasma treatment differentiates from the other methods, because of the low-pressure treatment requiring vacuum equipments. The species involved in plasma treatment are electrons, ions, and radicals. Non-polymerizable gases such as oxygen, argon, helium, hydrogen, and nitrogen have been used for surface treatment. [14, 17-20]

The ability to introduce functional groups on the surface by variation of the monomer gas used and working in a simple dry one-step process is of great advantage over other surface treatment methods. Treatment of surface films by plasma would remove loosely bonded surface contamination, thereby enhancing the total contact area, and mechanical interlocking.[21]

Wet chemical methods such as etchants, chromic or sulphuric acid have also been used to modify surfaces, which remains unfavorable due to several environmental problems and time consuming nature of the process.[22, 23]

2.6 Reference

1. Hudis, M., *Techniques and Applications of Plasma Chemistry*. John Wiley: New York, 1974.

2. Chan, C.-M.; Ko, T.-M.; Hiraoka, H., Polymer surface modification by plasmas and photons. *Surface Science Reports* **1996,** 24, 24.

3. Yasuda, H. K., Some important aspects of plasma polymerization. *Plasma Processes & Polymers* **2005,** 2, (4), 293-304.

4. Yasuda, H., *Plasma Polymerization*. Academic Press: 1985.

5. Wertheimer, M. R.; Thomas, H. R.; Perri, M. J.; KlembergSapieha, J. E.; Martinu, L., Plasmas and polymers: From laboratory to large scale commercialization. *Pure and Applied Chemistry* **1996,** 68, (5), 1047-1053.

6. Kurosawa, S.; Choi, B. G.; Park, J. W.; Aizawa, H.; Shim, K. B.; Yamamoto, K., Synthesis and characterization of plasma-polymerized hexamethyldisiloxane films. *Thin Solid Films* **2006,** 506, 176-179.

7. Yasuda, H.; Bumgarner, M. O.; Hillman, J. J., *J. Appl. Polym Sci.* **1975,** 19, (531).

8. Yasuda, H.; Yu, Q. S., Creation of polymerizable species in plasma polymerization. *Plasma Chemistry & Plasma Processing* **2004,** 24, (2), 325-351.

9. Yoshinari, M.; Hayakawa, T.; Matsuzaka, K.; Inoue, T.; Oda, Y.; Shimono, M.; Ide, T.; Tanaka, T., Oxygen plasma surface modification enhances immobilization of simvastatin acid. *Biomedical Research-Tokyo* **2006,** 27, (1), 29-36.

10. Wavhal, D. S.; Zhang, J. M.; Steen, M. L.; Fisher, E. R., Investigation of gas phase species and deposition of SiO_2 Films from HMDSO/O-2 plasmas. *Plasma Processes & Polymers* **2006,** 3, (3), 276-287.

11. Unger, W. E. S.; Swaraj, S.; Oran, U.; Lippitz, A., Radio frequency (r.f.) plasma-deposited polymer films: influence of external plasma parameters as viewed by comprehensive in-situ surface chemical analysis by XAS, XPS and ToF-SIMS. *Surface and Interface Analysis* **2006,** 38, (4), 522-525.

12. Muir, B. W.; McArthur, S. L.; Thissen, H.; Simon, G. P.; Griesser, H. J.; Castner, D. G., Effects of oxygen plasma treatment on the surface of bisphenol A polycarbonate: a study using SIMS, principal component analysis, ellipsometry, XPS and AFM nanoindentation. *Surface and Interface Analysis* **2006,** 38, (8), 1186-1197.

13. Wapner, K.; Grundmeier, G., Spectroscopic analysis of the interface chemistry of ultra-thin plasma polymer films on iron. *Surface & Coatings Technology* **2005,** 200, (1-4), 100-103.

14. Mittal, K. L., *Polymer Surface Modification: Relevance to Adhesion*. VSP BV, The Netherlands, : Utrecht, 1996.

15. D'Agostino, R.; Cramarossa, F.; Fracassi, F.; Illuzzi, F., *Plasma Deposition, Treatment, and Etching of Polymers*. Academic Press, San Diego, CA,: 1990.

16. Eliezer, Y.; Eliezer, S., *The Fourth State of Matter: An Introduction to the Physics of Plasma*. 1989

17. Bastos, A. C.; Ostwald, C.; Engl, L.; Grundmeier, G.; Simoes, A. M., Formability of organic coatings - an electrochemical approach. *Electrochimica Acta* **2004,** 49, (22-23), 3947-3955.

18. Balazs, D. J.; Triandafillu, K.; Chevolot, Y.; Aronsson, B. O.; Harms, H.; Descouts, P.; Mathieu, H. J., Surface modification of PVC endotracheal tubes by oxygen glow discharge to reduce bacterial adhesion. *Surface and Interface Analysis* **2003,** 35, (3), 301-309.

19. Samson, F., Ophthalmic Lens Coatings. *Surface & Coatings Technology* **1996,** 81, (1), 79-86.

20. Dennler, G.; Houdayer, A.; Segui, Y.; Wertheimer, M. R., Growth and structure of hyperthin SiO2 coatings on polymers. *Journal of Vacuum Science & Technology a-Vacuum Surfaces and Films* **2001,** 19, (5), 2320-2327.

21. Mittal, K. L., *Vac. Sci. Technol.* **1976,** 13, 6.

22. Chemla, M.; Levy, D.; Petitdidier, S.; Rouelle, F.; Zanna, S., Silicon chemical oxide growth by a novel wet treatment in aqueous chlorine solutions. *Electrochemistry* **2004,** 72, (4), 238-245.

23. Romero-Sanchez, M. D.; Pastor-Blas, M. M.; Martin-Martinez, J. M., Adhesion improvement of SBR rubber by treatment with trichloroisocyanuric acid solutions in different esters. *International Journal of Adhesion and Adhesives* **2001,** 21, (4), 325-337.

Chapter 3

3 Characterization Methods & Materials

Polymers have been replacing other materials such as metals, wood, glass, paper, leather, etc. in many sectors of our daily life. Therefore, many methods have been developed to the increasing importance to characterize both polymer surfaces and bulk. Due to the difference in fabrication methods between conventional and plasma polymers, not all the characterization methods are favorable for the analysis of plasma polymer films. This chapter deals with the most important techniques that have been used to characterize the plasma polymer films and multilayers in this work.

3.1   Fourier Transform Infrared (FT-IR) Spectroscopy

Infrared spectroscopy is the study of the interaction of infrared light with matter. It is used for material characterization because of the fact that the chemical bonds in a material have specific frequencies at which they vibrate corresponding to their energy levels. The resonance or vibrational frequencies are determined by the shape of the molecular potential energy surfaces, the masses of the atoms and eventually by the associated vibronic coupling.

The most important component of a FT-IR spectrometer is an interferometer based on the original design by Albert Michelson[1] in 1880, as shown in Figure 3-1. Light from the source is split into two beams by a half-silvered mirror and make one of the light beams travel a different distance than the other (one is reflected off a fixed mirror and one off a moving mirror which introduces a time delay). The difference in distance travelled by these two light beams is called optical path difference, λ (or optical retardation). The Fourier transform spectrometer is just a Michelson interferometer with a movable mirror.

Constructive or destructive interference can occur depending upon the light wavelength δ factor. A combination of both interferences can occur and the light beam intensity would be somewhere between very bright and very weak. A plot of the light intensity versus optical path difference or a large number of sinusoidal signals added together is called an interferogram. The variation of the light intensity with optical path difference is measured by the detector as sinusoidal wave. This is the fundamental measurement obtained by FT-IR, which is Fourier transformed to give a spectrum.
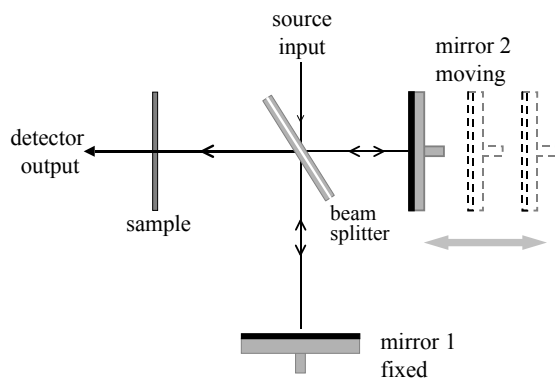
Figure 3-1: A schematic of a generic Michelson interferometer

The chemical composition of the films was characterized using a Nicolet Magna-IR spectrometer. The FT-IR spectrometer used in this work consists of infrared radiation source, interferometer, beamsplitter, detector, and a sample compartment. Once light leaves the interferometer, it passes through the sample compartment and is focused upon the detector. The detector is a simple electrical transducer, which processes the electrical signal to Fourier transformed spectrum.

Two types of detector material systems were used in this work, the Deuterated Triglycine Sulfate (DTGS) and Mercury Cadmium Telluride (HgCdTe) or "MCT" detector. The DTGS is equipped with KBr beam-splitter windows cover the mid range from $4000 - 400$ cm^{-1}. The "narrow band' MCT detectors are sensitive down to 700 cm^{-1}. This detector was cooled with liquid nitrogen to reduce the noise signal. MCT detectors are generally faster and more sensitive than DTGS detectors. The suitable detector was chosen depending upon the measurement mode.

In the transmission measurement mode, the infrared beam is passed directly through the sample. The advantages of this mode are the high signal-to-noise ratios, i.e. the spectrum quality, and the universality. A Si-wafer substrate was used for the transmission mode. In the reflectance sampling measurement mode, the infrared beam is reflected after being passed through the sample. Gold film was deposited on a glass substrate, which was used due to its higher reflectance, 98%.

The samples were irradiated with a polarized laser beam at an incidence angle of 5° from the substrate, at a 4 cm^{-1} resolution. This measurement mode is also known as the Infra-Red Reflection Absorption Spectroscopy (IRRAS). The incidence angle can be varied between 0 ° and 360 °. Thus, spectral shifts in the wavenumber may be noticed if the incidence angle is varied or measured in transmission mode. This discrepancy depends upon the in-phase motion of adjacent atoms in the vibrational mode of the molecule.[2, 3] A substrate holder that was used

designed which couples the incidence light at 5 °, which allows for the analysis of nm thick adlayers on the Au substrate.

3.2 X-ray Photoelectron Spectroscopy (XPS)

XPS is an ideal technique used for surface analysis and it possess the following attributes: quantitative atomic identification, chemical sensitivity, sampling depth variability from about 0.2 to 10 nm depending on the material, and it is insensitive to surface roughness.[4]

This technique, also known as Electrochemical Spectroscopy for Chemical Analysis (ESCA), involves the irradiation of a sample in a vacuum with soft X-rays and the energy analysis of photoemitted electrons which are generated close to the sample surface. The interaction between the X-ray photon and an inner-shell electron causes a complete transfer of the photon energy to an electron. This electron then has enough energy to leave the atom and escape from the surface (photoelectron).[5] The basic XPS equation was stated by Rutherford in 1914:

$$E_k = hv - E_b \qquad \text{eqn. 3-1}$$

whereby E_k is the photoelectron kinetic energy, hv the exciting photon energy, E_b the electron binding energy in the sample.[4]
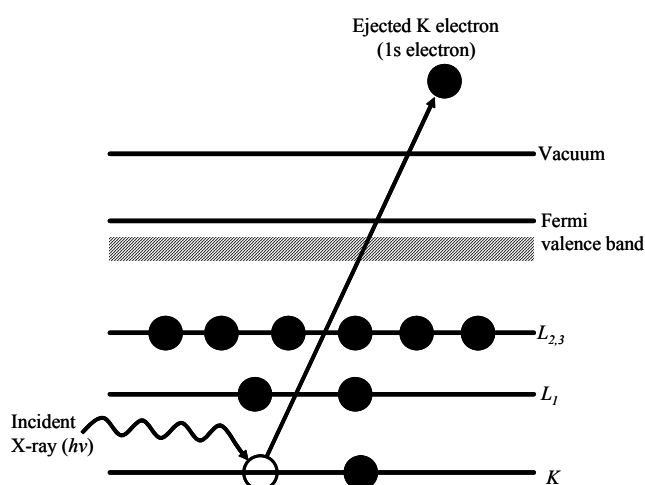
Figure 3-2: schematic diagram of the XPS process, showing photoionization of an atom by the ejection of a 1s electron

XPS set-up usually consists of a vacuum vessel with its associated pumping system and sample introduction systems, an X-ray source, an electron energy analyser with an electron–optical lens, an electron detection system and a workstation (PC) which controls the spectrometer operation and processes the obtained data. In order for electrons to reach the analyzer without being scattered by residual gas molecules, an ultra high vacuum ($1.33 \cdot 10^{-9}$ mbar) is used.[6]

The electron energy analyzer measures the binding energy (BE) of a particular shell of an atom, which is then plotted as intensity (counts per sec) versus binding energy, known as the XPS

spectrum. The process of photoemission is shown schematically in Figure 3-2, where an electron from the K shell is ejected from the atom (a 1s photoelectron).

In this work, the XPS spectra were recorded using a Perkin Elmer PHI 5600 spectrometer[*], whereby the Mg Kα radiation (1253.6 eV) is non-monochromated. The instrument was calibrated using a reference of Cu 2p^3 (932.725 eV), Au 4f (84.0 eV) and Ag 3d^5 (368.35 eV). Samples were analyzed at a take off angle of 45°. Survey spectra were recorded using a pass energy of 187.85 eV in 0.8 eV steps. Detail spectra of carbon, oxygen and silicon were collected at a pass energy of 11.75 eV in steps of 0.025 eV. The spectra were calibrated with respect to the C 1s peak at 284.8 eV for direct comparison to literature values.[7] Line-shape analyses were done using a least-square deconvolution routine employing line shapes with 100 % Lorentzian character.

3.3   Surface Plasmon Resonance (SPR)

The term surface plasmons (SPs) has been known for quite a long time. The main principles and theories governing SPs are so far well defined and numerous publications have discussed their properties in detail.[8-11]

In this section only the basics of this technique will be discussed. Surface plasmon resonance spectroscopy (SPR, SPS or SPRS) is more than a century old technique which can be referred to the findings of Wood's anomaly seen in the reflected light from diffraction gratings.[12]
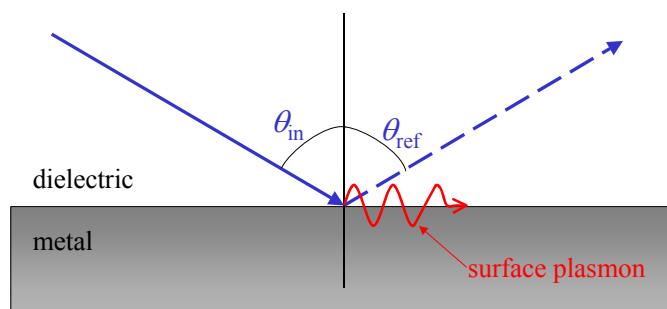
Figure 3-3: surface plasmon excited at the interface due to reflection of light ray at an interface of a metal and a dielectric

Surface plasmons are electromagnetic waves which can be excited at the interface between a metal (e.g. Au, Ag, Pt) and a dielectric material. Plasmons are basically light waves that are bound to the surface by the interaction with free electrons of the conductor, as illustrated in Figure 3-3. As a result, the free electrons respond collectively by oscillating in resonance with the light wave. The resonant interaction between the surface charge oscillation and the

---

electromagnetic field of the light constitutes the SPs and strongly depends on the optical properties of the system.

The relationship that expresses the dispersion of the plasmon along this interface between the x-component of the wave vector of the plasmon K_{photon}, and both dielectric materials functions, ε_M (metal), ε_D (medium: air or water) has been derived for a homogeneous dielectric (ε_1) as follows:

$$K_{photon} = \frac{\omega}{c}\sqrt{\varepsilon_1}$$

eqn. 3-2

The electron charges on a metal boundary can perform coherent oscillations, termed surface plasmon polaritons (SPPs). These charge oscillations can be localized in the z-direction, and accompanied by a mixed transversal and longitudinal electromagnetic field that propagates along the x-axis and disappears at $z \rightarrow \infty$ on both sides of the metal/ dielectric interface, whereby its maximum is at |z| = 0. Therefore, to achieve plasmon resonance with photons, the conservation of energy and momentum should be fulfilled. Thus, the wave vector of the photon in the dispersion direction must be adapted to wave vector of the plasmon to obtain a resonance.

3.3.1 The Reflection Measurement Mode

For a thin, non-adsorbing layer defined by a thickness d and a refractive index n, the resonant angle displacement $\Delta\theta$ is proportional to the optical thickness, $n \cdot d$ of the layer.

$$\Delta\theta = n \cdot d$$
$$n = (n_{film} - n_{dielectric})$$

eqn. 3-3

The relationship between the refractive index and the dielectric constant, ε is expressed in the complex form as follows;

$$\varepsilon = n^2 = (n+ik)^2 = n^2 + 2ikn - k^2 = \varepsilon' + \varepsilon''$$

eqn. 3-4

whereby, n = real part of the refractive index; ik = imaginary part of the refractive index (corresponds to the absorption); ε'= real part of the dielectric constant, $(\varepsilon' = n^2 + k^2)$; ε''= imaginary part of the dielectric constant, $(\varepsilon'' = 2kn)$.

The imaginary part of the eqn. 3-4 is equal to zero, if the film is non-adsorbing, then the dielectric constant would be ε = n^2. A drawback to this method is that the refractive index and thickness cannot be determined simultaneously. If the refractive index is known from another measurement technique, e.g. ellipsometry, then the Fresnel's equation can be used to convert the shift in incidence angle to film thickness. In this thesis, the refractive indices of all the films used were determined using ellipsometry. The prism and Au film refractive indices were based on the

manufacturer and literature data respectively. The reflection curves were fitted by the Winspall software, developed by A. Scheller at the Max Planck Institute for Polymer Research. The software calculates the Fresnel coefficients of each film / layer with a recursion formalism.[13]

3.3.2 Prism Coupling Geometry

The impulse of light in a dielectric is too small to couple to a surface, since a direct coupling of incident light is not possible on a smooth surface. This can be improved, by passing the photons through a medium with a higher refractive index than the dielectric. Thus, a high refractive index prism and a reflecting surface can be used, so that the coupled surface plasmons are excited by the evanescent field of the reflected light under total internal reflection conditions. If light is reflected at a metal surface covered with a dielectric medium, e.g. a glass prism, the momentum of the photons, p, is increased. If the incidence angle is altered, then it is possible to modify the wave vector so that it corresponds to the wave vector of the plasmon $K_{plasmon}$. Plasmon resonance can only be monitored if these angles are equal. Both wave vectors can be coupled using a prism geometry. Two prism coupling geometries are possible, the Otto[11, 14] and the Kretschmann-Raether configuration.[8] The prism can be triangular, half cylindrical or hemispherical shape.

In this thesis, the Kretschmann-Raether configuration and a triangular prism was used, because it is easy to build than creating an air gap between the prism and the metal, as in the Otto –configuration.

In this Kretschmann-Raether configuration, light is reflected by the metal film deposited on glass, beneath the prism, as shown in Figure 3-4. A finite thickness of the metal layer is necessary to influence the coupling angle θ, and efficiency, i.e. the minimum reflectivity. The surface plasmons are excited by the evanescent field of the reflected light, the resulted electric field in the dielectric medium decays exponentially in the x- and z- axis.
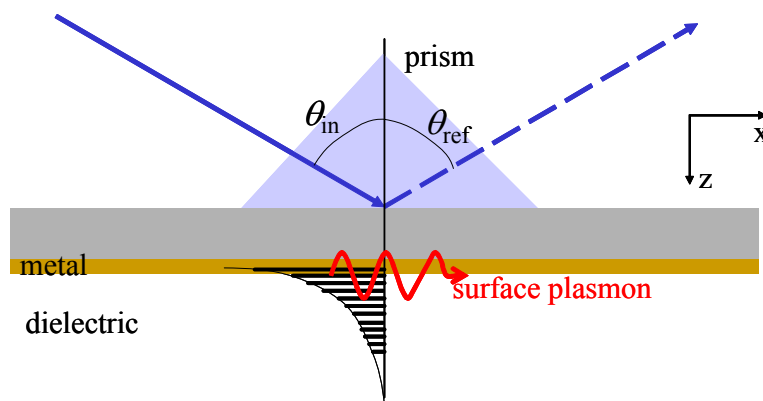

Figure 3-4: schematic representation of the prism coupling geometries in the Kretschmann – Raether configuration

Experimentally, a thin metal film, Au is evaporated directly onto a glass substrate. The glass substrate is coupled to the base of the prism, with an index-matching fluid for optical reasons, thus both materials have the same refractive index. A single dust particle (~ 1μm) or air bubble at the interface can obstruct the plasmons. Only the plasmons at the metal / dielectric interface are of importance to monitor any changes in the dielectric medium. Damping of the evanescent field of the reflected beam can occur, if the maximal thickness of the metal film is exceeded. Optimal thickness is about 48 nm Au, using a He–Ne laser light for excitation.[15]

3.3.3 Surface Plasmon Fluorescence Spectroscopy (SPFS)

Another section of this work will concentrate on the binding of fluorophore encapsulated vesicles and then the lysis of these vesicles using an enzyme (chapter 6).

In the biochemical industry, many analytical methods based on fluorescence detection techniques have been used due to their high sensitivity and short time scale at which fluorescence occurs. Several binding or dissociation steps can be monitored with the help of fluorescence molecules, the lifetimes of which are in the range of 10^{-8} sec.[16] In this work, fluorescence detection mode of the SPR was used to monitor binding and disruption of bio-molecules. Therefore, the change in fluorescence intensity with respect to time will be monitored. This will give an insight into the binding or disruption process occurring on the dielectric layer.

3.3.4 The combined SPR and SPFS Set-up

Figure 3-5 shows a home-built SPR and Surface Plasmon-Enhanced Fluorescence Spectrometer (SPFS) set-up, which was used in this work for the combined SPR and fluorescence measurements.[22]

The excitation beam is produced by the He-Ne laser (λ = 633 nm, 5 nm, Uniphase), which passes through the chopper at a frequency of 1333 Hz. The beam modulation by the chopper is controlled by the lockin amplifier. This excitation beam then passes through two polarizers, which serve for intensity and plane of polarization adjustments. A programmable shutter is placed in front of these polarizers, which is mostly used during the fluorescence measurements, in order to reduce the bleaching effect of the fluorescent dye. The sample holder and the photodiode (detector) are mounted on a coaxial goniometer (HUBER), thus enabling an independent tuning of angular positions at angle steps of 0.001° controlled by the SPR software on the workstation. The sample holder can be adjusted on the xy–axis, which is required for an optimal set-up alignment.

The incident beam is reflected at the base of the coupling prism (Schott, 90°, LASFN$_9$) by the evaporated Au metal, and the reflected intensity is focused by a lens (lens pd, f = 50 mm, Ovis) for detection by the photodiode. The photodiode is connected to a lockin amplifier, so that noise and foreign light intensity, such as daylight or any light source in the lab, is reduced. The amplifier selects all the frequencies that are modulated by the operation frequency of the attached chopper.

A collecting lens (lens pm, f = 50 mm, Ovis) is placed perpendicular to the substrate holder that focuses the emitted light through an interference filter (λ = 670 $\pm$ 2nm, LOT) into a photomultiplier unit (pm, Hamamatsu), which measures fluorescence emission. The pm is connected to a counter and then the data is processed at the workstation. The attenuator is a neutral filter, which attenuates the fluorescence in the case of high fluorescence intensity.
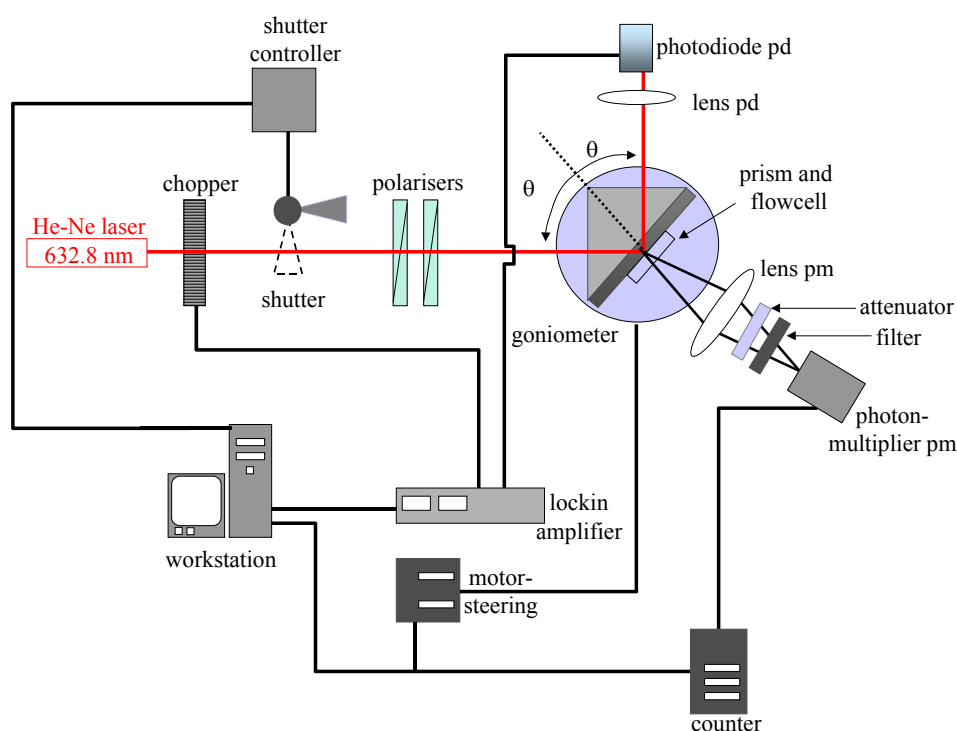
Figure 3-5: schematic surface plasmon fluorescence spectroscopy set-up

For the system alignment, two apertures are needed, for the incident and reflected beam. First, the detector arm is adjusted, then the sample holder. The sample holder can also be tilted or shifted in the z-axis, so as to optimize the alignment. The SPR and fluorescence systems were all controlled by Winspall software and the data were analyzed by Waspview software. Both programs were written by A. Scheller of MPI-P, Mainz.

3.3.5 Flow Cell and Sample Handling
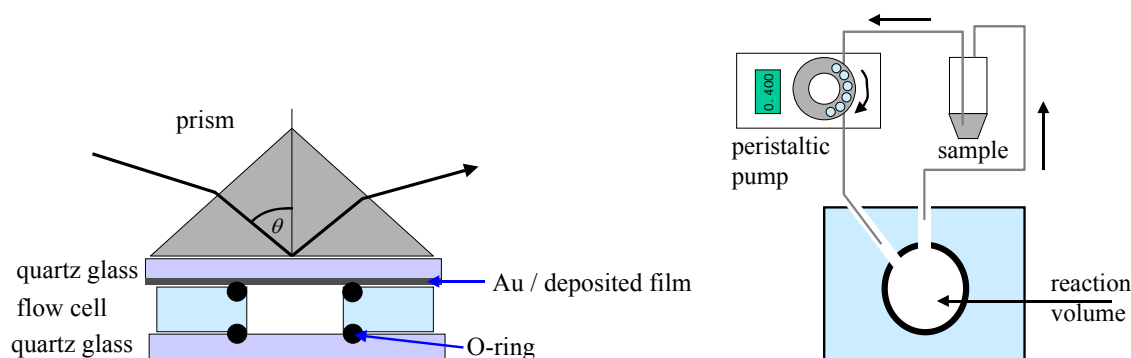
Figure 3-6: set-up of the prism, sample and flow cell sealed using an o-ring

The flow cell represented in the schematic in Figure 3-6 is home made. The prism, glass, flow cell and sample are mounted on the sample holder. A reaction volume is created by a bottom quartz glass (Herasil, Schott) sealed by a viton O-ring on the sample holder and the Au / sample. The flow cell is equipped with an inlet and outlet, which can hold a volume of about 100 µl, pumped by a peristaltic pump (Ismatec, Switzerland) over the sample surface. One difficulty here is to avoid air bubbles in the cell, which might lead to false measurements. The air bubbles were avoided by gradually increasing the liquid circulation flow rate until the cell volume was filled.

The circulation flow rate was 0.5 ml min^{-1} for optimized analyte delivery, minimizing mass transport effects, the prevention of backward flow and disruption in the reaction volume.

SPR response

In SPR spectroscopy, the reflectivity is measured with respect to the incidence ray. The exponential decay of the evanescent field of a surface plasmon wave into the dielectric medium at a distance of several hundreds of nm makes this technique extremely sensitive to monitor optical changes at the metal –dielectric interface.

If light passes through a high refractive index prism, the dispersion of the free photons changes. This implies, changing the dielectric constant of one of the medium would also influence the wave vector of the surface plasmon resonance along the x-axis of the prism. Based on this theory, the deposition of a thin and non-adsorbing film, (thickness less than the decay length along the z -axis), with a different dielectric constant, would also affect the total dielectric constant over the evanescent field. This will cause the SPR angle to shift to the right as shown in Figure 3-7. It is possible to obtain resonance of the system by changing the incidence angle θ (of the incoming laser beam) until the wave vector of the photons in the x-axis is equal to product of the photons wave vector and sin θ, (i.e. $k_{ph,x} = k_{ph}\sin\theta$). The system is in resonance, when the

surface plasmons have been excited by the energy of the incident light and the intensity of the reflected light decreases.
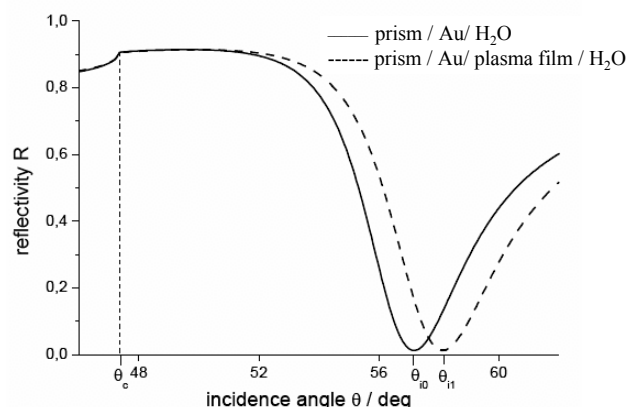
Figure 3-7: resonance curve for a Au / H_2O and Au / plasma film system

Fluorescence Detection

The detection of the fluorescence from the backside of the sample holder by the photomultipliers during an angle scan was also controlled by the Winspall software. The actual fluorescence intensity measured by the counter also collects the reflectivity from the lockin-amplifier simultaneously. Hence, the resulting fluorescence scan curve (counter-scan) was assigned to the same incidence angles to the measured reflectivity. A neutral filter (attenuator) was used occasionally to attenuate the fluorescence in cases of a high intensity, thus the pm was kept in a linear range (< 1-$2 \cdot 10^6$ cps).

3.3.6 SPR and SPFS Measurement Sequence

In general the following measurement sequence was frequently used to monitor binding or disruption processes on the surface for all the SPR and SPFS measurements in this work.

1. Scan curve: To determine the thickness of the evaporated metal film and to obtain a measurement for the fluorescence background of the sample, an angle scan was recorded. Thereafter, the cell was filled with the pure buffer, which was used for all aqueous medium measurements. During an angle scan, the pm unit detects the fluorescence intensity, because the goniometer moves both the pm unit and the pd detector with the sample in assigned angle steps by 2θ and θ respectively. Thus, the resulting fluorescence scan curve (counter-scan) can be assigned to same incidence angles as the reflectivity collected from the lockin amplifier.[14]

2. Kinetic run: The analyte to be bound is injected into the flow cell after the observed baseline (reflectivity constant) was found to be stable. After the adsorption process was

finished, the sample was rinsed with pure buffer, so as to remove bulk analytes and unspecifically bound molecules from the sample surface. In the case of stability measurements, the reflectivity change is monitored at a constant angle for a continuous buffer flow.

3. Scan shift: In comparison with the reference scans the change in thickness and fluorescence signal was determined. In case of non-adsorbing layers ($\varepsilon \geq 0$), the measured shift is proportional to the change of the optical layer thickness n · d.

3.3.7 The Kinetic Measurement Mode

SPR spectroscopy can be used to monitor online kinetic processes, i.e. physical or chemical changes occurring with respect to time. At a fixed incidence angle, where the angle scan curve portrays a linear gradient, the detected reflectivity is measured versus time. The resonance will shift to higher angles if the reflectivity increases. Some assumptions must be considered at this point, such as, the resonance minimum shift and the optical thickness are proportional.

Figure 3-8 shows a constant value, R_1 will be reached, when no significant change in the adsorption process occurs. This process can be also irreversible, e.g. dissociation, dissolution or removal of a layer is occurring. The shape of the curve represents the rate of change. In this work, the kinetics was monitored for both binding and dissociation processes.

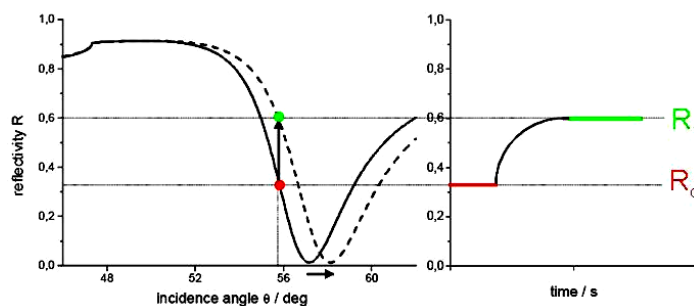Figure 3-8: schematic representation of a kinetic measurement, measured at a constant incident angle for a over a period of time.

3.4   Ellipsometry

Ellipsometry is an optical diagnostic method which is used to determine the complex refractive index and thickness of a film, which is usually deposited on top of a known substrate material.[17] The fundamental background of this technique is shown in Figure 3-9.
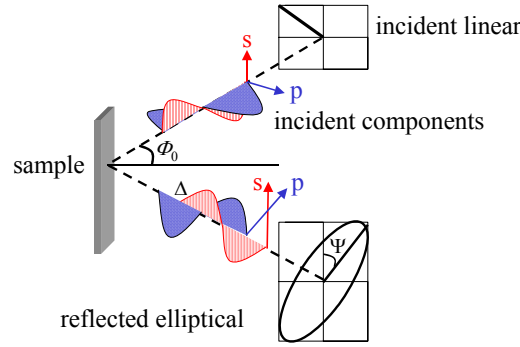
Figure 3-9: schematic overview of the meaning of the ellipsometric parameter Ψ and Δ.

The main principle of this technique is based on the difference in reflection coefficient for perpendicular (s-direction) and parallel polarized (p-direction) light. This means that, upon reflection at a sample surface, the polarisation direction of light will be altered. The change itself is dependent on the optical properties of the material where the reflection takes place.[18] The complex reflection ratio (ρ) of the parallel and perpendicular reflection coefficient, r_p and r_s respectively, is given by:

$$\rho = \frac{r_p}{r_s} = \frac{|r_p|}{|r_s|} \exp\left[i\left(\delta_p - \delta_s\right)\right] = \tan(\Psi)\exp(i\Delta) \qquad \text{eqn. 3-5}$$

Where δ_p and δ_s are the individual phase shifts at reflection for the parallel and perpendicular component respectively. When the film at which the light is reflected is assumed to be a semi-infinite material, then it is easy to calculate the complex refractive index from these parameters. In that case, the so called two phase model can be used, which is mostly used for bulk materials.[19] The Fresnel equations for optical isotropic materials, obtained from boundary conditions for the electric field components at the surface are given by the eqn. 3-6 and eqn. 3-7:

$$r_p = \frac{n_0 \cos\Phi_0 - n_1 \cos\Phi_1}{n_0 \cos\Phi_0 + n_1 \cos\Phi_1} \qquad \text{eqn. 3-6}$$

$$r_p = \frac{n_1 \cos\Phi_0 - n_0 \cos\Phi_1}{n_1 \cos\Phi_0 + n_0 \cos\Phi_1} \qquad \text{eqn. 3-7}$$

Here n_0 and n_1 are the complex refractive indices of respectively ambient and the sample, ϕ_1 and ϕ_2 describe the angle of incidence and the angle of refraction respectively. Combining the Fresnel equations and the complex reflection ratio (eqn. 3.5), the complex refractive index equation can be derived:

$$n_1 = n_0 \sin\Phi_0 \sqrt{1 + \left(\frac{1-\rho}{1+\rho}\right)\tan^2\Phi_0} \qquad \text{eqn. 3-8}$$

This equation can also be used for substrates with single or multilayer plasma films. However, the refractive index obtained will characterize the whole layer and not the individual film. This is the two-phase model of characterization, whereby the surface does not differ from the bulk properties. If the optical properties of the bulk material do differ from the surface, then a three or more phase model needs to be applied. The single films deposited in this work were assumed to be homogeneous, and therefore, a two-phase model was used for characterization.

A variable angle spectroellipsometer (SE or VASE) EP^3 Nanofilm, Germany, was used to determine the refractive index, n, and thickness, d, of the layers. VASE was used to measure the relative phase change of a reflected polarized light beam expressed as psi, φ and delta, Δ. The data was acquired at 5 different wavelengths (range $\sim 611 - 650$ nm) at 60° angle of incidence. The VASE was equipped with the data analysis EP^3 view software, which was used to model the n and d of each layer from the φ and Δ data based on eqn. 3-5.

3.4.1 Characterization of Film Thickness

The film thickness was also determined using a surface profiler (P-10, KLA Tencor, U.S.A.) on reference Si-wafers. The analyzed silicon wafers were partly covered with a piece of microscopy glass slide during the plasma deposition. To analyse the thickness of the plasma polymers, the glass slide was removed and the step height was measured.

3.5   Contact Angle Goniometry

When a drop of liquid falls on a solid surface, e.g. a plasma film, the edge forms a defined angle that depends on the properties of the liquid, the solid and the vapor phase. This is known as the contact angle. If the liquid drop spreads on the surface completely (contact angle $\Theta = 0$), then a finite angle is established.[20, 21] The force balance at this three-phase has been described by Young's equation, which relates the contact angle to the interfacial tension of the solid in equilibrium with the vapor γ_{SV}, the liquid in equilibrium with its saturated vapor γ_{LV}, and the solid in equilibrium with the liquid γ_{SL}:[22]

$$\gamma_{LV} \cos \Theta = \gamma_{SV} - \gamma_{SL} \qquad \text{eqn. 3-9}$$

In this work, the water contact angle is used to predict some static or dynamic conditions such as surface wetting phenomena, chemical heterogeneity, surface roughness and even swelling. These conditions may cause variations of the contact angle along the three-phase contact line, if measured over a period of time.[23, 24] Figure 3-10 shows the contact angle effect of oxygen plasma surface treatment on a plasma polymerized film after deposition. The as-

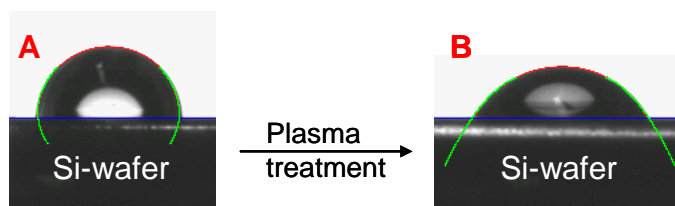deposited film showed a contact angle of 105.6 ° and after surface treatment 55° $\pm$ 2 was measured.

Figure 3-10: the difference in water contact angle can be seen clearly for this plasma polymerized hexamethyl disiloxane film (A) as-deposited 105.6 ° and (B) after 5 sec, 55 °, surface treatment under 50 W O_2 plasma

The most common method of measuring the contact angle is to observe a sessile drop with a microscope. The contact angle is then determined by a goniometer or the image is recorded by a video system and the contour is fitted, e.g. using Young – Laplace, height-width, or polynomial method.
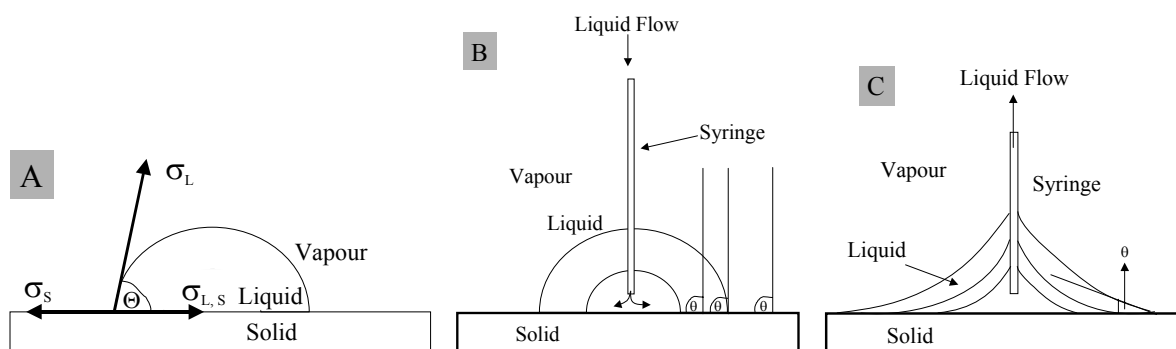
Figure 3-11: schematic diagram showing the A: sessile, B: advancing, and C: receding contact angle.

If the contact angle is measured while the volume of the drop is increasing, the three phase line advances, this is called the advancing contact angle Θ_{adv}. If the drop volume is decreased, and the wetting line is receding, this is described as the receding contact angle Θ_{rec}. The difference $\Theta_{adv} - \Theta_{rec}$ is called contact angle hysteresis, which is often related to surface roughness, inhomogeneity, surface mobility of functional groups, and adsorption and desorption of liquid molecules which is accompanied by the dissipation of energy.[25, 26]

Another widely used technique is the Wilhelmy plate method, which is based on force required to prevent a plate (e.g. coated with plasma polymer) from being drawn into the liquid. This force is $2\gamma_L \, l \cos \Theta$, here l is the width of the plate, and the contact angle is larger than zero.[27]

The capillary rise method is usually used to determine the speed of the liquid rise of porous materials, powders pressed in a capillary tube. This method relies on many assumptions, which makes it unreliable.

In this work, the water contact angles (WCA) were measured by the sessile drop technique using a microscope equipped with a horizontal light path and a goniometer eyepiece (DSA10, Kruss GMBH, Germany). MilliQ-H_2O was used as test liquid with a drop volume of 4 µl. All values reported in this thesis are the average of five measurements per sample.

3.6   Electrochemical Impedance Spectroscopy

Electrochemical impedance spectroscopy (EIS) is a powerful method of characterizing electrical properties of materials, films and their interfaces. EIS has been used to investigate the dynamics of bound or mobile charges in the bulk or interfacial regions of any material, from ionic to insulators.[28] This method has been implemented in materials research and development because it is a non-destructive analytical tool. EIS can be automated and the results may be correlated with many complex materials variable: rates of chemical reaction, dielectric properties, defects, microstructure and compositional influences on the conductance of the materials.[29-31]

In this thesis, the EIS is used for the characterization of the stability and electrical properties of plasma polymerised multilayers films in aqueous medium. The basic theory of electrochemical impedance theory will be presented here.

3.6.1 Impedance

Impedance (Z) is a measure of opposition to a sinusoidal alternating electric current, which takes into account the combination of the resistive, capacitive and inductive properties of the material in the current path. Mathematically, impedance is the ratio of the phasor voltage across an element to the phasor current through the element. Impedance is a vector: it has both a magnitude and a direction, and therefore can often conveniently be expressed as a complex number.

Impedance spectroscopy is used in this work to measure how easily a material (plasma polymer) conducts current when a AC voltage is applied across it. This technique gives a fast response to changes in the film properties. Schiller *et al*. used impedance measurements to characterize the stability of plasma polymerized maleic anhydride in a 0.1M KCl solution over a period of 11 hours.[32] This property has also been used to determine the corrosion stability of thin polymer films on metal, the dielectric property or reactive polymers.[30, 33-36]

Basics of Alternating Current Theory and Applications to Impedance Spectroscopy

An alternating current (AC) is an electrical current whose magnitude and direction vary cyclically, as opposed to direct current, whose direction remains constant. Alternating currents are accompanied by alternating voltages (potential), which can be described as a mathematical function of time as follows:

$$V_t = \Delta V \sin \omega t \qquad \text{eqn. 3-10}$$

whereby ΔV is the peak amplitude voltage, $w = 2\pi f$ (f = frequency) and t = time (sec). When an AC potential is then applied to a circuit, then an AC current flows, this can be expressed as:

$$I_t = \Delta I \sin \omega t + \phi \qquad \text{eqn. 3-11}$$

The resultant current, I remains sinusoidal but may be out of phase with the potential by a given time, ϕ.
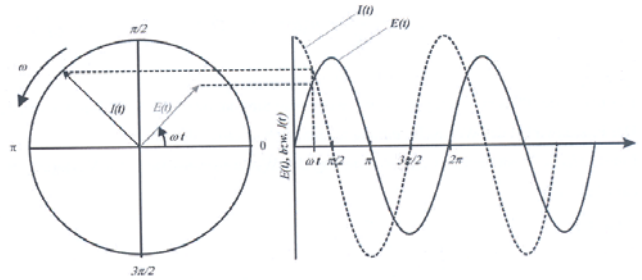
Figure 3-12: phasor diagram for an alternating voltage

From this phasor diagram, the behaviour of the AC across the circuit (resistors, capacitors and inductances) can be considered.

(a) Impedance of a Resistor

A resistor is a two terminal electrical component that resists an electric current by producing a voltage drop between its terminals in accordance with Ohm's law, as a ratio between voltage, V and current, I.

$$R = \frac{V}{I} \qquad \text{eqn. 3-12}$$

Substituting eqn. 3-10 into the Ohm's law, would yield a current that has the same phase as the potential when an AC potential is applied to a resistor, i.e. $\phi = 0$.

$$I = \frac{\Delta V}{R} \sin \omega t \qquad \text{eqn. 3-13}$$

(b) Impedance of a Capacitor

Capacitors are electrical devices that can store charges in the electric field between a pair of closely spaced conductors, separated by a dielectric material. The capacitor's capacitance (C) is a measure of the amount of charge (Q) stored on each plate for a given voltage (V) that appears between the plates:

$$Q = CV \qquad\qquad \text{eqn. 3-14}$$

$C = \dfrac{\varepsilon_r A}{d}$, whereby A = plate area, d = distance between plates and ε_r = permittivity of material

Since the current *I,* through the capacitor is the rate at which charge, *Q* is forced through the capacitor ($I = \mathrm{d}Q/\mathrm{d}t$), this can be substituted into eqn. 3-11, which would yield the AC potential: $I = \omega C\, \varDelta E \cos \omega t$. In a linear system, the response signal, $I_{(t)}$, is shifted in phase ϕ and has a different amplitude, I_0, thus: $I_{(t)} = I_0 \cos (\omega t - \phi)$. This can be expressed analogous to Ohm's law to calculate the impedance.

It is known that impedance (*Z*) is simply a generalized form of resistance that takes into account both the way in which resistors and capacitors can *impede* electrical current, defined as; $Z = \varDelta V/\varDelta I$, and has a phase ϕ. Thus:

$$Z = \frac{E(t)}{I(t)} = \frac{E_0 \cos(\omega t)}{I_0 \cos(\omega t - \phi)} = Z_0 \frac{\cos(\omega t)}{\cos(\omega t - \phi)} \qquad\qquad \text{eqn. 3-15}$$

3.6.2 Impedance of a Parallel and Series RC circuit
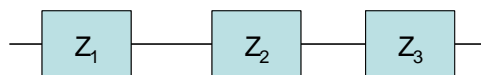

Figure 3-13: Impedances circuits in series.

For linear impedance elements in series, the equivalent impedance is calculated from:
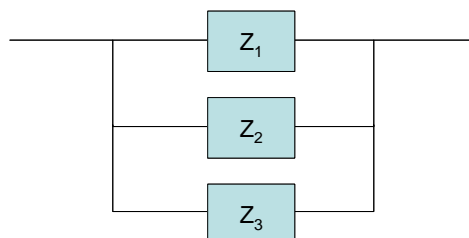
$Z_{eq} = Z_1 + Z_2 + Z_3$

Figure 3-14: Impedances circuits in parallel.

Due to the complexity of a real electrochemical system, the impedance can be calculated or modeled from parallel and series RC circuits. Very few electrochemical cells can be modeled

using a single equivalent circuit element. Fortunately, there are simple formulas that describe the impedance of circuit elements in both parallel and series combinations.[28]

If the impedances elements are in parallel, then the inverse equivalent impedance is calculated as the sum of the impedance inverse of each element, i.e. $1/Z_{eq} = 1/Z_1 + 1/Z_2 + 1/Z_3$. Generally, impedance would increase, but capacitance decreases when capacitors are connected in series. This is a consequence of the inverse relationship between capacitance and impedance.

3.6.3 Impedance Data Analysis

The characterization of electrochemical systems with impedance spectroscopy requires the interpretation of the data with the help of suitable models based on equivalent circuits. The experimental data is fitted to the model equivalent circuit in order to to estimate parameters that adequately describe the experimental data and can be used to predict the behavior of the system under various conditions.

Equivalent Circuit Models

These are models built with the help of known passive elements, resistors and capacitors, which represent a real system. These elements can be combined in series and parallel to give complex equivalent circuits. Each element has a physical meaning that corresponds to the system under investigation. These models were used in this work because of the easiest interpretation of the dielectric behavior of the plasma polymers in terms of the several polarization mechanisms, which might occur upon contact with the electrolyte.

Figure 3-15 shows the simplest equivalent circuit used in this work. A resistor is in parallel with a capacitor, which is attributed to the dielectric characteristics of the polymer film.
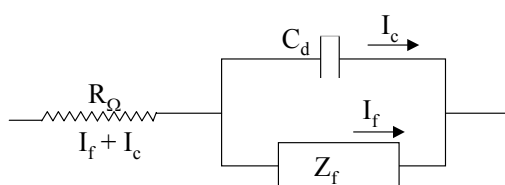
Figure 3-15: simple RC equivalent electrical circuit of an electrochemical cell for a simple electrode process. R_Ω is the solution resistance, of the electrode materials, Z_f the impedance of the electrode process, and C_d the double layer capacity.

The equivalent circuit of the plasma polymers will consider both resistance and capacitance properties, e.g. the transport of charges through the polymer and would reflect the physical and chemical properties of the film.[28, 37] Resistance is proportional to the polymer thickness, whereas the capacitance is inversely proportional to thickness. Thus, if the polymer swells or delaminates

from the electrode, this can be measured by following the change in resistance and capacitance values or from the impedance spectra.

Likewise for a multilayer, two single RC elements are switched in series with the resistance component of the electrolyte. A capacitance component is also used for the Au layer, which is in series with the both RC elements.
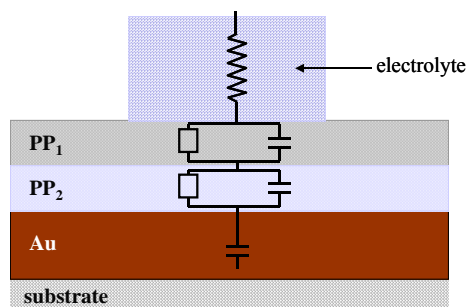
Figure 3-16: equivalent circuit for multilayer films, PP (plasma polymer), showing the resistance and capacitance components of each layer and the electrolyte resistance.

3.6.4 Data Presentation

To obtain impedance spectra $Z(\omega)$, the time or frequency domain can be used. The frequency domain was used in this thesis. The spectra are obtained by sequential measurements of $E(t)$ and $I(t)$ for different frequencies over specific time periods.

The obtained impedance spectra in this work were plotted in the so-called *Bode plot*, where the absolute value $Z(\omega)$ and the phase shift $\phi(\omega)$ is presented as a function of frequency ω. The plot uses the logarithm of frequency to allow a very wide frequency range to be plotted on one graph. This is an advantage for the identification of small impedance in the presence of large ones.

The Bode plot has the advantage that it provides all the necessary start values needed to model the values of the equivalent circuit values, R_Ω and Z_f.

3.6.5 EIS Measurement Set-up

For the characterisation of the plasma polymers layers, a home built three-electrode arrangement electrochemical cell was used. This arrangement consists of a saturated AgCl as reference electrode, and a Pt counter electrode with the working electrode being the 50 nm Au deposited on BK7 glass and the plasma deposited film. The plasma polymerized layers were deposited on the working electrode, whereby, plasma polymers were deposited on the Au-electrodes. The volume of the electrolyte (0.1M NaCl) solution was 5 ml used for all experiments. All EIS experiments were carried out at room temperature, inside a Faraday cage, as shown in Figure 3-17. Impedance measurements were periodically made at open circuit potential, in the frequency range 10^{-2}–10^{+5} Hz with an amplitude of 0.5 mV rms using a

potentiostat (Autolab PGSTAT 30) equipped with a Frequency Response Analyser (FRA) controlled by a PC with the FRA software package (ecochemie). For stability experiments, impedance loop measurements were carried out for over 24 hours.
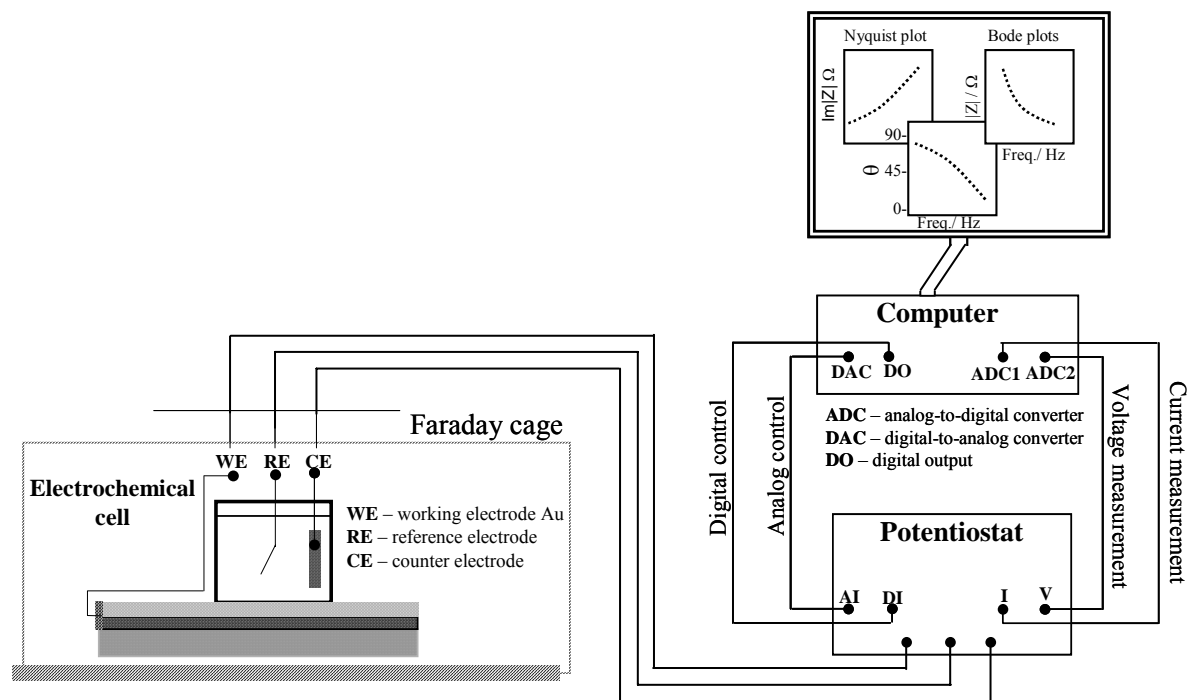
Figure 3-17: electrochemical impedance spectroscopy (EIS) configuration used in the experiment, which consists of pp films deposited on the WE (Au), CE (platinum wire), RE (AgCl). Configuration is enclosed in a faraday cage.

3.7 Microscopy of surfaces

In this section, two experimental techniques of surface characterization that have been used in this work will be briefly presented.

3.7.1 Scanning Electron Microscopy

Scanning Electron Microscope (SEM) is widely used to study surfaces of solid objects, which utilizes a beam of focused electrons as an electron probe that is scanned in a regular manner over the specimen.[38] Electron microscopes are now available that are easy to operate and reliable and that give point-to-point resolutions of less than 0.2 nm. In addition to this lateral resolution, the high depth of field is an advantage of SEM, it enables the imaging of a 3–D impression of a sample. In SEM, the electron beam is emitted from a heated filament or field emission tip. The electrons are accelerated by an electric potential in order of 1– 400 kV. A condenser lens projects the beam from the source onto the condenser aperture. The beam is focused by an objective lens and raster-scanned by scanning coils over the sample. The spot size

of the primary electron beam determines the resolution of the instrument. When the primary electrons hit the sample surface, they pass part of their energy to electrons in the sample, resulting in the emission of secondary electrons. The secondary electrons are collected by a detector and their intensity is displayed versus the position of the primary beam on the sample. The secondary electrons are viewed on a cathode-ray tube (CRT).[39]

A Leo Gemini SEM apparatus was used for characterisation of the pp films on Si-wafer and polycarbonat substrates. To avoid surface charging, the SEM was operated between $1 - 3$ kV of (low) energy. Otherwise, the samples need to be made conductive, e.g. by evaporating a metal film on the sample.

3.7.2 The Atomic Force Microscope

Atomic force microscopy (AFM), in which a sharp probe is employed for profiling surfaces has developed into an invaluable multi-disciplinary technique for advanced characterization of polymer materials.[40]

AFM was used in this work because it provides high-resolution imaging of surface structures between scales of a few nm to hundreds of μm high sensitivity and accuracy.

The AFM measures deflection of a cantilever due to capillary, electrostatic, van der Waals, and frictional forces between the tip and the surface. The fine tip which is mounted onto a piezoelectrically positioned cantilever spring provides the means to measure surface forces in the range from 10^{-13} to 10^{-6} N. The cantilever is typically silicon or silicon nitride with a tip radius of curvature in the nm scale range. Surface imaging is realized with the electronic feedback system, which uses a signal from the optical positional detector, i.e. vertical and horizontal segments. These segments measure the cantilever deflections caused by normal and lateral tip-sample forces respectively. All these functions are realized using an electronic controller, which also communicates with an image acquisition computer. The variations in the cantilever-sample separation are converted into a height image with bright (dark) contrast assigned to high (low) surface locations. The resolution in this technique depends on radius of curvature of cantilever tip. The image size of the AFM is limited around 150 μm^2.

The primary modes of operation are contact and dynamic mode. In the contact mode operation, the static tip deflection is used as a feedback signal. The force between the tip and the surface is kept constant during scanning by maintaining a constant deflection. Because the measurement of the contact mode is prone to noise and drift, low stiffness cantilevers are used to strengthen the deflection signal. A drawback of AFM is the destruction of fragile objects on the sample. This can be avoided by using the tapping mode, whereby the cantilever is vibrated at its

resonance frequency. The oscillation amplitude, phase, and resonance frequency are modified by tip-sample interaction forces; these changes in oscillation with respect to the external reference oscillation provide information about the sample's characteristics.[41]

AFM measurements can be made on almost all surfaces, conducting, non-conducting, organic, and inorganic surfaces. Numerous probes have been used, including attaching a several micrometer colloidal particle to a cantilever as described by Butt and co-workers.[42]
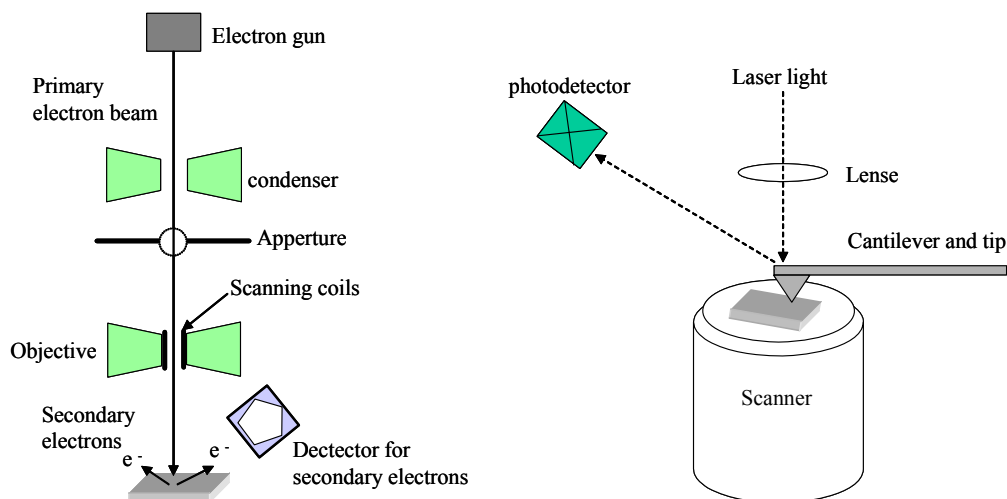
Figure 3-18: schematic representation of a scanning electron microscopy (left) and atomic force microscopy (right)

The surface morphology and roughness of the films were studied in this work using atomic force microscopy (AFM) on a Dimension™ 3100 (Digital Instruments) at ambient pressure and room temperature. The topographic images were obtained in the tapping mode using a resonant oscillating frequency of 250–350 kHz (Olympus). The surface roughness (Root Mean Square, RMS) of all the films in this work was calculated for a 250 x 250 nm scan size.

3.8   Lipids and Membranes

The binding of model membranes on plasma polymerized multilayers and subsequent lysis of model membranes with an enzyme was investigated, which will be presented in chapter 6.

3.8.1 Model Membranes

Membranes function to organize biological processes by compartmentalizing them.[43] The basic unit of life, the cell, is essentially defined by its enveloping membrane. Biological membranes are organized assemblies of lipids and proteins with small amounts of carbohydrates. These structures regulate the composition of the intracellular medium by controlling the flow of nutrients, waste products, ions, etc., into and out of the cell. Many fundamental biochemical processes occur on or in this 2D matrix membranous scaffolding, which is held together by non-covalent interactions.
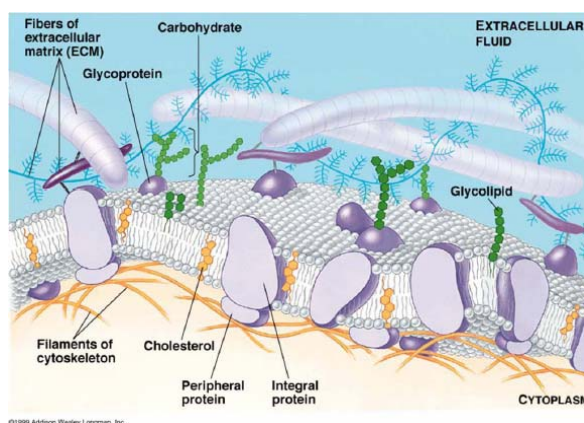
Figure 3-19: schematic diagram of a plasma membrane as described by Singer and Nicolson, courtesy Addison Wesley Longman, Inc.

Figure 3-19 shows a biological membranes as described by Singer and Nicholson,[43-45] bio-membranes composed of proteins associated with a lipid bilayer matrix. The membrane proteins carry out dynamic processes and are operationally classified according to how tightly they are associated with membranes. The space between the proteins is filled with phospholipids. Phospholipids are amphiphilic molecules with non-polar (hydrophobic) aliphatic "tails" and polar (hydrophilic) phosphoryl –X "heads". Phospholipids form a bilayer, as depicted in Figure 3-20, which serves as a barrier between extra-cellular fluid and the cytoplasm. Major components of animal plasma membranes are cholesterol. Due to the chemical structure, it contains polar OH groups which provide the weak amphiphilic character, and a fused ring system which is responsible for the rigidity.[43] Due to the complexity of the lipid fraction in

biological membranes, several model membranes such as tethered bilayer, black lipid membrane and vesicles have been used to study the dynamic processes associated with membranes.[43, 45, 46]
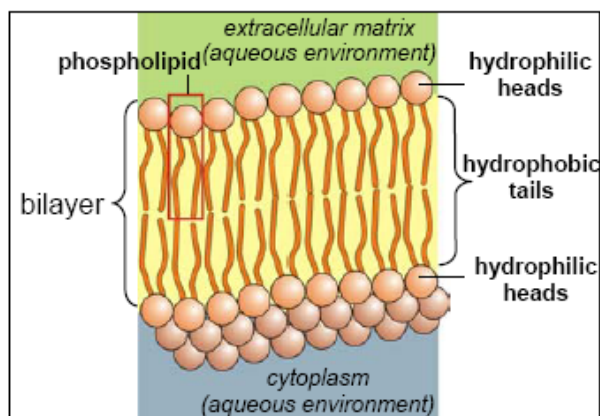
Figure 3-20: schematics of lipid bilayer matrix formed by phospholipids.

3.9 Vesicles

Vesicles are microscopic sacs that enclose a volume with a molecularly thin membrane.[43, 47, 48] Such membranes are generally self-directed assemblies of amphiphilic molecules with a dual hydrophilic-hydrophobic character. Vesicles are vital for cell function and are principally lipids, with a molecular weight less than 1 kDa. They can be prepared from biological amphiphiles by extrusion or sonification.

Vesicles and biomembranes have existed since the first cells and play critical roles in compartmentalization functions as varied as nutrient transport and DNA protection.[49] Whereas phospholipids are the natural amphiphiles of cell membranes, vesicle-forming materials used in products ranging from cosmetics to anticancer agents can be synthetic as well as biological.[50] When suitably mixed in water or similar solvents, the oily parts of the amphiphiles tend to associate while the more hydrophilic parts face inner and outer solutions, helping to delimit the two interfaces of the membrane,[51] as shown in Figure 3-21.
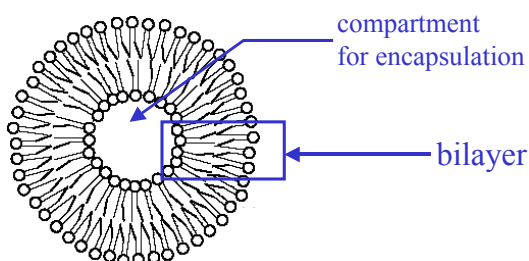
Figure 3-21: cross-sectional schematic representation of a phospholipid vesicle

Another section of this work presents the binding of stable phospholipids vesicles on plasma polymerized multilayer, which could serve as a biosensor. The stable vesicles have been used as a biomembrane to encapsulate fluorophores.

Upon mechanical disruption or lysis of the vesicle, the encapsulated fluorophores may diffuse through the membrane, which can be detected by surface plasmon-enhanced fluorescence spectroscopy (SPFS). The release of the fluorophore molecules initiated by a physical or chemical mechanism makes the system suitable for drug delivery applications in the pharmaceutical industry.[50] The polar character of the vesicle core enables polar drug molecules to be encapsulated. If the vesicle is surface bound (otherwise unstable, which may rupture mechanically), then potential fluorophore release mechanism by disruption of the membrane may be driven chemically or physically, e.g. some enzymatic activity causes lysis of a lipid vesicles. Vesicle systems using a thiol-lipid bound-support lipid bilayer have been studied by various research groups, however the systems subsequently rupture upon rinsing of the surface to form a bilayer. [52, 53]

3.9.1 Chemical Structure of Phospholipase A_2 Enzyme

In this work, phospholipase A_2 (PLA_2) will be used to catalyze the dissociation of the vesicle to release the encapsulated fluorophore.
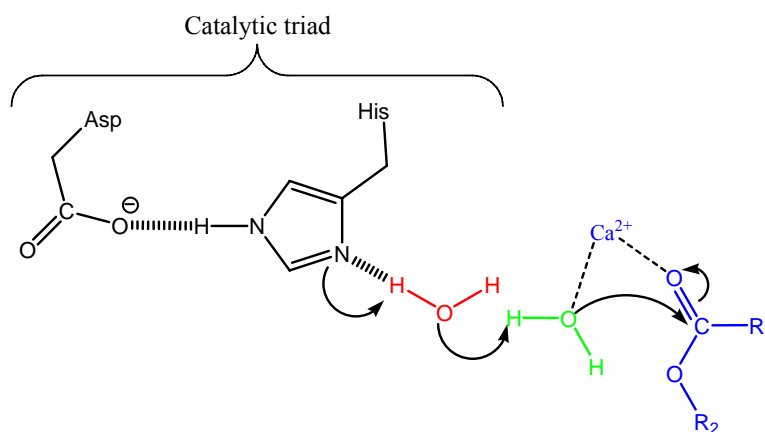
Figure 3-22: structure and mechanism of phospholipase A2. Asp = Aspartic acid, His = Histidine. The catalytic triad activates a second water molecule to attack the scissile carbonyl carbon with Ca2+ coordinating to the activated water molecule as well as electrostatically stabilizing the resulting tetrahedral intermediate.

Phospholipase A2 (PLA_2) are a large family of enzymes that specifically deacylate fatty acids from the 2nd C-atom (SN_2- reaction) of the triglyceride backbone of phospholipids, producing a free fatty acid and a lyso-phospholipid.[51, 54, 55] Many PLA_2's are obtained from cobra venom and bee venom, which are classified based on location of activity (e.g. pancreatic and

secretory) or mode of activity (calcium dependent and calcium independent).[56] Figure 3-22 shows the structure of a PLA$_2$, which consists of a catalytic triad, (two amino acids; Aspartic acid and Histidine) with a water molecule and a catalytically important Ca^{2+} ion with hydrogen bonds over the H$_2$O molecule.

3.10 Plasma Reactor

Figure 3-23 shows the schematic representation of the home-built set-up used for the all the plasma deposition described in this work.[57, 58] The reaction chamber consist of a Pyrex glass cylindrical tube, (l = 30 cm, d = 10 cm). This chamber is enclosed in a Faraday cage. Gases fed through the system pass two cold traps, cooled with liquid nitrogen, for collection of excess reactant before reaching the pump (Leybold Trivac, D16BCS/PFPE). A MKS baratron (Type 627B) was connected near the inlet to monitor the pressure inside the chamber. Side arms at the reactor inlet allow for the introduction of monomer vapors. Side arms at the reactor tube inlet allow the introduction of non-polymerizable gases such as oxygen, nitrogen and argon, and the monomer vapors.

A rf power generator (ENI 300 W) generates the power of this capacitively coupled cylindrical radio frequency (RF), 13.56 MHz plasma reactor. The power flows through a watt meter and a matching network, and then it is supplied to the reactor chamber via an external concentric coil (anode). The external concentric coils are 9 cm apart and the power electrode is earthed. A Tektronix TDS 340 pulse generator controls the pulsing of the radio frequency signal. The plasma can be operated either in the continuous wave (cw) or in the pulsed mode.

The reactor inlet and monomer supply were equipped with a home-built heating jacket. The temperature of the reaction chamber was monitored and controlled by a temperature indicator regulator (TIR), which was built-in at the outlet arm of the reactor. The plasma vapor temperature was measured using a thermo-sensor (PT-100), which was mounted inside the reactor arm outlet.

The reactor used at the Chemistry Department, University of Bath, UK has the same geometry as the one used at the Max-Planck Institute for Polymer Research. However, the power was generated by a RF generator (Coaxial Power System Ltd, RFG150). Despite polymerization at the same plasma conditions, it is known that, the smallest geometrical difference, reactor leakage, or difference in monomer quality can yield to large difference in deposition rate and chemistry. Therefore, all the results presented here have been carefully compared to avoid discrepancies.
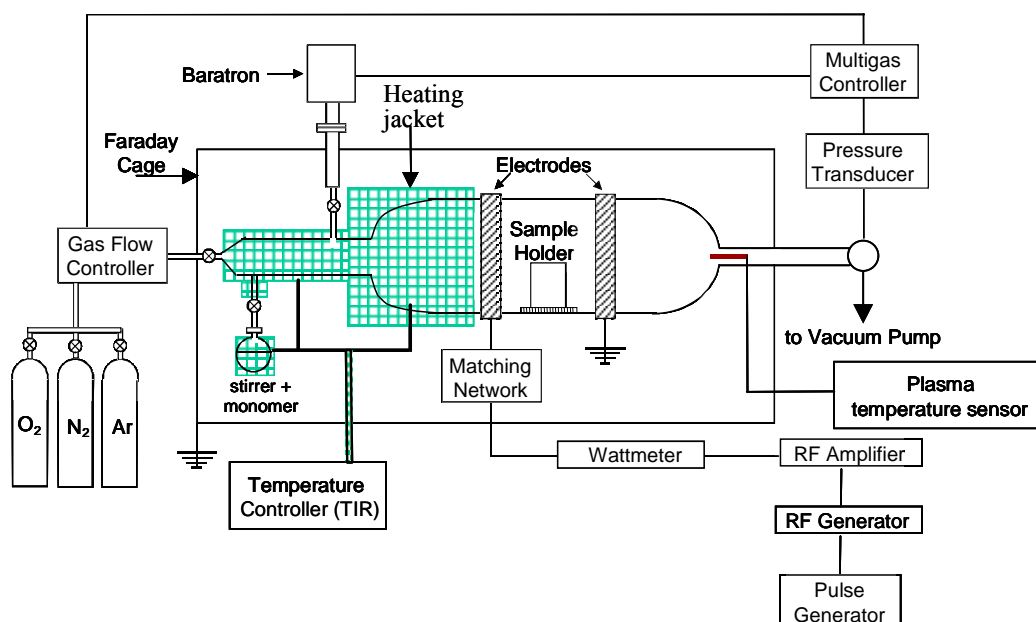
Figure 3-23: schematic representation of the plasma reactor, electrical components and temperature unit.

3.11 Precursors and Sample Preparation

For the fabrication of the different thin plasma polymer films, various precursors were used to achieve the desired film property. Depending upon the characterization methods, all the films were deposited on either Si-wafer and/or gold films on a glass substrate.

Hexamethyl disiloxane (HMDSO, $(CH_3)_3$–Si–O–Si–$(CH_3)_3$) was purchased from ACROS Organics, Germany, at 99.99% purity. The gas flow rate was controlled using a needle valve and kept constant for all experiments (1 sccm), while the oxygen gas flow was controlled by a MKS gas flow meter (Type 1295C). HMDSO and excess oxygen gas was used for the fabrication of SiO_2 –like films.

Maleic anhydride (Sigma-Aldrich, Germany, 99.5% purity) was ground into fine powder and placed into a 25 ml round bottom flask attached to the reactor. Maleic anhydride powder was not purified further and the flask was merely evacuated before polymerisation. Maleic anhydride films were plasma polymerized on the SiO_2 –like films, which were used to bind stable phospholipid vesicles.

Allylamine and Styrene were purchased from ACROS Organics (purity 99.99 %). Both monomers were placed in 10 ml round bottom flask and their gas flow rates were controlled using a floating ball flow meter (Kobold, Germany). Both monomers were degassed by three consecutive freeze-thaw cycles, but were used without any further purification. Both monomers were covalently bonded on SiO_2 films to investigate the stability and adhesion properties of SiO_2 film.

Substrate preparation

Depending upon the method of characterization, either (1 x 2 cm) piece of Si(100)–wafer or (2 x 4 cm) glass were used as the substrate. The BK7 glass was coated with 80 nm of Au for IRRAS measurements. LaSFN9 glass was coated with 50 nm of Au by thermal evaporation (Edwards FL 400) for SPR measurements. The samples were placed on a 3 cm high glass holder placed between the anode and cathode electrode. The reactor chamber was evacuated to a typical base pressure of less than 0.001 mbar before the monomers were introduced, in order to achieve purity in the deposition system.

Thermal Evaporation of Au

For all the SPR measurements, 48 nm Au (99.99 %, Balzers) were deposited on to clean LaSFN$_9$ wafers by thermal evaporation at a deposition rate of 0.1 nm/s under UHV conditions ($5 \cdot 10^{-5}$ mbar) in an evaporation apparatus (Edwards, FL400, M-BAE 250). The adhesion of the Au film to the glass substrate was improved by first evaporating 2 nm thin chromium film onto the glass surface.

3.12 Reference

1.   Brian, C. S., *Fundamentals of Fourier Transform Infrared Spectroscopy* CRC   Press: New York, 1996.

2.   Kirk, C. T., Quantitative-Analysis of the Effect of Disorder-Induced Mode-Coupling on Infrared-Absorption in Silica. *Physical Review B* **1988,** 38, (2), 1255-1273.

3.   Lucovsky, G.; Richard, P. D.; Tsu, D. V.; Lin, S. Y.; Markunas, R. J., Deposition of Silicon Dioxide and Silicon-Nitride by Remote Plasma Enhanced Chemical Vapor-Deposition. *Journal of Vacuum Science & Technology a-Vacuum Surfaces and Films* **1986,** 4, (3), 681-688.

4.   Briggs, D., *Surface analysis of polymers by XPS and static SIMS*. Cambridge University Press: 1998.

5.   Alexander, M. R.; Short, R. D.; Jones, F. R.; Stollenwerk, M.; Zabold, J.; Michaeli, W., An X-ray photoelectron spectroscopic investigation into the chemical structure of deposits formed from hexamethyldisiloxane/ oxygen plasmas. *Journal of Materials Science* **1995**.

6.   Watts, J. F.; Wolstenholme, J., *An Introduction to Surface Analysis by XPS and AES*. Wiley & Sons: West Sussex, England, 2003; p 224.

7.   Alexander, M. R.; Short, R. D.; Jones, F. R.; Michaeli, W.; Blomfield, C. J., A study of HMDSO/O_2 plasma deposits using a high-sensitivity and -energy resolution XPS instrument: curve fitting of the Si 2p core level. *Applied Surface Science* **1999,** 137, (1-4), 179-183.

8.   Raether, H., *Surface Plasmon on Smooth and Rough Surfaces and on Gratings*. Springer: Berlin, 1988.

9.   Yeh, P., *Optical Waves in Layered Media* John Wiley & Sons: New York, 1988.

10.   Agranovich, V. M., *Surface Polaritons*. North Holland, Amsterdam, 1982.

11.   Knoll, W., *MRS Bulletin* **1991,** XVI, (7).

12.   Wood, R. W., On a remarkable case of uneven distribution of light in a diffraction grating spectrum. *Philosophical Magazine* **1902,** 4, (396).

13.   Kovacs, G., *Electromagnetic Surfaces Modes*. John Wiley & Sons: New York, 1982.

14.   Knoll, W., Interfaces and Thin Films as seen by Bound Electromagnetic Waves [Review]. *Annual Review of Physical Chemistry* **1998,** 49, 569-638.

15.   Neumann, T. Strategies for Detecting DNA Hybridisation Using Surface Plasmon Fluorescence Spectroscopy. Max-Planck Institute for Polymer Research, 2001.

16.   Valeur, B., *Molecular fluorescence*. Wiley - VCH: Weinheim, 2002.

17.   Tompkins, G.; Harland, A., *Handbook of ellipsometry*. Springer: Heidelberg, 2005; p 870.

18.   Azzam, R. M. A., *Ellipsometry and polarized light*. North-Holland: Amsterdam, 1979.

19.   Azzam, R. M. A., *Selected papers on ellipsometry*. SPIE Optical Engineering Press: Bellingham, 1991.

20. Adamson, A. W.; Gast, A. P., *Physical Chemistry of Surfaces*. John Wiley & Sons: New York, 1997.

21. Brezesinki, G.; Mögel, H.-J., *Grenzflächen und Kollöide*. Spektrum Akademischer Verlag: Heidelberg, 1993.

22. Young, T., *Phil. Trans. Roy. Soc. London* **1805,** 95.

23. Gengenbach, T. R.; Griesser, H. J., Post-deposition ageing reactions differ markedly between plasma polymers deposited from siloxane and silazane monomers. *Polymer* **1999,** 40, (18), 5079-5094.

24. Chan, C.-M.; Ko, T.-M.; Hiraoka, H., Polymer surface modification by plasmas and photons. *Surface Science Reports* **1996,** 24, 24.

25. Garbassi, F.; Morra, M.; Occhiello, E.; Barino, L.; Scordamaglia, R., *surface interface analysis* **1989,** 14.

26. Eick, J. D.; Good, R. J.; Neumann, A. W., *Journal of Colloid & Interface Science* **1975,** 53, 235.

27. Butt, H.-J.; K., G.; Kappl, M., *Physics and Chemistry of Interfaces*. Wiley-VCH: Weinheim, 2003.

28. Macdonald, J. R., *Impedance spectroscopy*. Wiley: New York, 1987.

29. Basarir, F.; Choi, E. Y.; Moon, S. H.; Song, K. C.; Yoon, T. H., Electrochemical properties of PP membranes with plasma polymer coatings of acrylic acid. *Journal of Membrane Science* **2005,** 260, (1-2), 66-74.

30. Bastos, A. C.; Ostwald, C.; Engl, L.; Grundmeier, G.; Simoes, A. M., Formability of organic coatings - an electrochemical approach. *Electrochimica Acta* **2004,** 49, (22-23), 3947-3955.

31. Han, L. C. M.; Rajeshwar, K.; Timmons, R. B., Film chemistry control and electrochemical properties of pulsed plasma polymerized ferrocene and vinylferrocene. *Langmuir* **1997,** 13, (22), 5941-5950.

32. Jenkins, A. T. A.; Hu, J.; Wang, Y. Z.; Schiller, S.; Foerch, R.; Knoll, W., Pulsed plasma deposited maleic anhydride thin films as supports for lipid bilayers. *Langmuir* **2000,** 16, (16), 6381-6384.

33. Bellucci, F.; Maio, V.; Monetta, T.; Nicodemo, L.; Mijovic, J., Impedance spectroscopy of reactive polymers .4. An improved experimental procedure for measurement of effective resistivity. *Journal of Polymer Science Part B-Polymer Physics* **1996,** 34, (7), 1277-1280.

34. Mijovic, J.; Andjelic, S.; Fitz, B.; Zurawsky, W.; Mondragon, I.; Bellucci, F.; Nicolais, L., Impedance spectroscopy of reactive polymers .3. Correlations between dielectric, spectroscopic, and rheological properties during cure of a trifunctional epoxy resin. *Journal of Polymer Science Part B-Polymer Physics* **1996,** 34, (2), 379-388.

35. Nguyen, P. T.; Rammelt, U.; Plieth, W., Electrochemical impedance spectroscopy for characterization of coatings with intrinsically conducting polymers. *Macromolecular Symposia* **2002,** 187, 929-938.

36.   Grundmeier, G.; Thiemann, P.; Carpentier, J.; Barranco, V., Tailored thin plasma polymers for the corrosion protection of metals. *Surface & Coatings Technology* **2003,** 174, 996-1001.

37.   Vandeleur, R. H. M., A Critical Consideration on the Interpretation of Impedance Plots. *Journal of Physics D-Applied Physics* **1991,** 24, (8), 1430-1435.

38.   Rochow, T. G.; Rochow, E. G., *An Introduction to Microscopy by Means of Light, Electrons, X-Rays, or Ultrasound* 1978.

39.   Lee, R. E., *Scanning electron microscopy and X-ray Microanalysis*. Prentice-Hall: NJ, 1993.

40.   Binnig, G.; Quate, C. F.; Gerber, C., *Physical Review Letters* **1986,** 56, 930.

41.   Hinterdorfer, P.; Dufrene, Y. F., Detection and localization of single molecular recognition events using atomic force microscopy. *Nature Methods* **2006,** 3, (5), 347-355.

42.   Butt, H.-J.; Gerharz, B., *Langmuir* **1995,** 11, (4735).

43.   Voet, D.; Voet, G., *Biochemistry*. Wiley & Sons: USA, 2004.

44.   Cowan, S. W., Bacterial porins: Lessons from three high-resolution structures. *curr. opin Struct. Biol.* **1993,** 3.

45.   Cullis, R. R.; Hope, M. J., *Physical properties and functional roles of lipids in Membranes*. Elsevier: 1991.

46.   Gruhn, T.; Lipowsky, R., Temperature dependence of vesicle adhesion -. *Physical Review E* **2005,** 7101, (1 Part 1), 1903.

47.   Pignataro, B.; Steinem, C.; Galla, H. J.; Fuchs, H.; Janshoff, A., Specific adhesion of vesicles monitored by scanning force microscopy and quartz crystal microbalance. *Biophysical Journal 78(1 Part* **2000,** 78, (1 Part 1), 487-498.

48.   Petsev, D. N., Interaction and adhesion of vesicles: Coupling between attractive interactions and bilayer membrane flexibility. *Langmuir* **1999,** 15, (4), 1096-1100.

49.   Lipowsky, R.; Sackmann, E., *Structure and Dynamics of Membranes - from Cells to Vesicles* Elsevier Science: Amsterdam, 1995.

50.   Lasic, D. D.; Papahadjopolous, D., *Medical applications of Liposomes*. Elsevier: 1998.

51.   Storch, J.; Kleinfeld, A. M., The lipid structure of Biological Membranes. *Trends Biochem. Sci* **1985,** 10.

52.   Boukobza, E.; Sonnenfeld, A.; Haran, G., *J. Phys. Chem. B* **2001,** 105, 12165-12170.

53.   Williams, T. L.; Vareiro, M. M. L. M.; Jenkins, A. T. A., Fluorophore-encapsulated solid-supported bilayer vesicles: A method for studying membrane permeation processes. *Langmuir* **2006,** 22, (15), 6473-6476.

54.   Navon, A.; Ittah, V.; Scheraga, H. A.; Haas, E., Formation of the hydrophobic core of ribonuclease A through sequential coordinated conformational transitions. *Biochemistry* **2002,** 41, (48), 14225-14231.

55.   Six, D. A., the expanding superfamily of Phospholipase A2 enzymes: classification and characterisation. *Biochimica et Biophysica Acta.* **2000,** 1488.

56. Garima Singh; S. Gourinath; K. Saravanan; Sujata Sharma; A. Srinivasana; Singh, P., Sequence-induced trimerization of phospholipase A2: structure of a trimeric isoform of PLA2 from common krait (Bungarus caeruleus) at 2.5 angstrom resolution. *protein structure communications Acta Crystallographica Section F - Structural Biology and Crystallization Communications* **2004,** 61, (Part 1).

57. Van Os, M. T. Surface Modification by Plasma Polymerization. Film Deposition, Tailoring of Surface Properties and Biocompatibility. CIP, Den Haag, 2000.

58. van Os, M. T.; Menges, B.; Foerch, R.; Vancso, G. J.; Knoll, W., Characterization of plasma-polymerized allylamine using waveguide mode spectroscopy. *Chemistry of Materials* **1999,** 11, (11), 3252-3257.

<div align="right">

Chapter 4

</div>

4   Results – Fabrication of thin SiO$_2$ –like films

(Part of this work has been submitted to Plasma Processes & Polymers – Jan. 2007.)

Abstract

The application of SiO$_2$-like films in the semi-conductor, biomedical, and food-packaging industries has gained a lot of credit due to its unique mechanical,[1,2] optical properties,[2, 3] and chemical properties. These properties obtained are dependent upon the fabrication technique.[4-8] One of the most promising and efficient techniques to achieve the desired properties is using Plasma Enhanced Chemical Vapor Deposition (PECVD) of organometallic monomers.[9-13] As a result of their interesting properties, these polymeric materials based on their organometallic compositions continue to attract the attention of many researchers and magnufacturers, in the field of protective coatings, up to materials with variable refractive indices.[14, 15] In this section, the fabrication of SiO$_2$-like thin films from plasma polymerized hexamethyl disiloxane (pp-HMDSO) and oxygen monomer will be presented. SiO$_2$-like (inorganic) films refers here to films with very small amount of other components other than silicon and oxygen, i.e. carbon, where HMDSO is used.

4.1   Results and Discussion

This section presents the effect of varying the various process parameters in order to optimize the fabrication of the SiO$_2$ –like films.

Sample preparation

The deposition process of the pp organosilicon films was investigated by a series of experiments. First, oxygen gas and HMDSO vapour were introduced into the reactor in ratios of 2:1, 5:1, 10:1, and 30:1 at a pressure of 0.2 mbar under 90 W RF input power. In a second series of experiment, the O$_2$ to HMDSO ratio was kept constant at 10:1, and the RF input power was varied between 30 and 180 W. The process was optimised to obtain 18 ± 2 nm pp-HMDSO films at low deposition rate of 1.32 nm/sec. In simple words, each parameter has been varied individually, while the other deposition parameters were kept constant. Table 4-1 shows an overview of the deposition parameters.

Monomer:gas Ratio	HMDSO:O$_2$ (1:10)	Monomer:gas Peak power (W)	HMDSO:O$_2$ 90 W
Peak power (W)	30 60 100 150 180	Monomer:gas (HMDSO:O$_2$) Ratio	1:2 1:5 1:10 1:30
Pressure (mbar)	0.2	Pressure (mbar)	0.2
Thickness (nm)	27 ± 3	Thickness (nm)	27 ± 3
Deposition rate (nm/min)	1.32	Deposition rate (nm/min)	1.32

Table 4-1: overview of the plasma parameters used for the deposition of the SiO$_2$-based films.

4.1.1 Influence of Input Power on Deposition Rate

At constant monomer ratio and pressure, the deposition rate of HMDSO:O$_2$ strongly depends on the Yasuda parameter (W/FM), as shown in Figure 4-1A. A deposition time of 30 sec was used for all the films. At 20 W (0.061 J/cm^3), deposition rate of 0.64 nm/sec was attained, whereas at the highest Yasuda factor, 0.68 J/cm^3, (at 220 W input power), the deposition rate of 1.55 nm/sec was measured. Figure 4-1B shows the increasing angular shift with respect to input power due to the change in optical thickness as measured by SPR. The film thickness was simulated using the WINSPALL software.

Two deposition regions can be distinguished in Figure 4-1A, low input power (low deposition gradient, Yasuda factor < 0.25 J/cm^3) and high input power (high deposition gradient, Yasuda factor > 0.25 J/cm^3). These regions characterize the increasing plasma density with an adequate amount of energy which speeds up the reaction deposition rate.

The increasing Yasuda factor suggests a transition from an energy-deficient to a more energetic state. Thus, more energy per unit mass of the monomer is available at high input power, leading to the generation of more reactive species and an increase in deposition rate of the films.
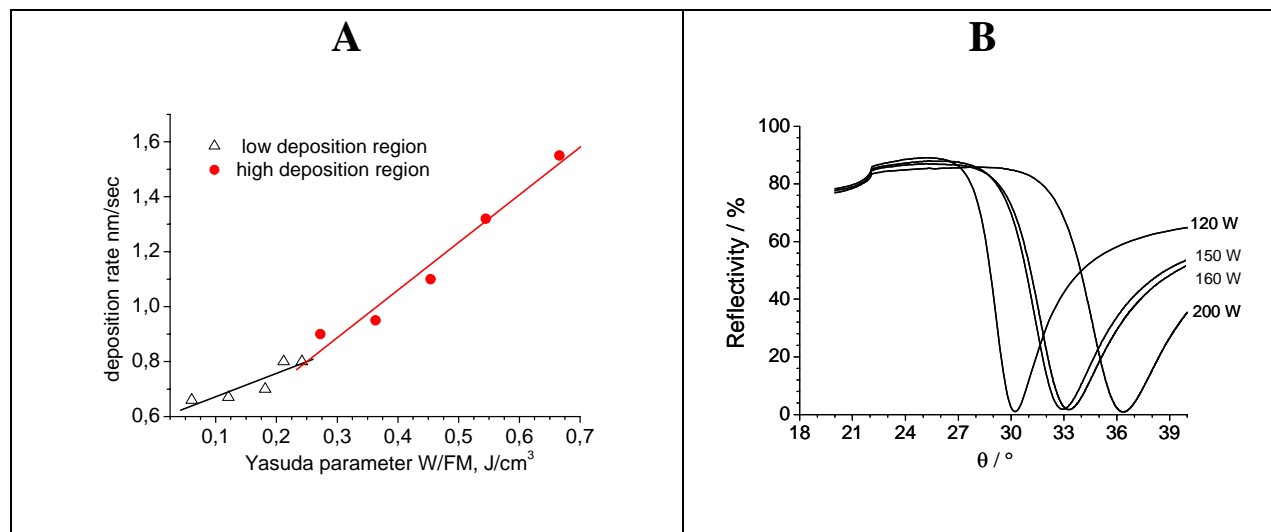
Figure 4-1: (A) deposition rate of HMDSO:O_2 under different input power at constant deposition time of 30 sec, (B) SPR scan of 30 min plasma polymerized films showing increase in film thickness with Yasuda parameter.

The position of the substrate holder in the plasma reactor is essential to achieve reproducible results. Various positions within the reactor (outside the electrodes) were characterized by depositing films with respect to input power and flow rate separately, which showed inconsistent deposition rates. The results presented here were obtained from the same position within the electrodes in the plasma reactor, as described in chapter 3.11.

4.1.2 Influence of Pressure on Deposition Rate

The deposition rate as a function of different chamber pressure at increasing input power is depicted in Figure 4-2. Generally, the deposition rate increases with increasing pressure and input power. At low input power, 20 W, a steep increase in deposition rate could be seen from 0.1 mbar to 0.2 mbar. The increase in deposition rate is more evident at 180 W as compared to the other deposition input powers, 20 W – 150 W. However, at 180 W, a minor increase in the deposition rate between 0.2 mbar and 0.35 mbar was observed.

For all the depositions at the various input power, it is evident that the deposition rate increases with the deposition pressure. This is due to the increasing HMDSO monomer molecules which is proportional to the system pressure. This leads to an increase in total number of collisions of the molecules, thereby forming actives species which are responsible for higher deposition rates.[16-18]
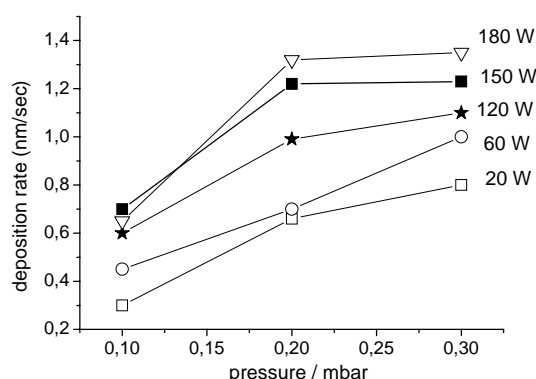
Figure 4-2: deposition rate of HMDSO/O_2 as a function of input power at different deposition pressure.

At high deposition pressures in vacuum processes, a threshold value can be attained. Above this value the reactants (HMDSO and O_2) are saturated in the chamber which would reduce the radical path length. Thereby, this would lead to a reduction in dissociation rate at higher input pressure values. This threshold value can be correlated to the 0.2 mbar deposition pressure. Figure 4-2 shows a slight increase in deposition rate at 180 W input power from 1.3 nm/sec to 1.4 nm/sec for 0.2 mbar to 0.3 mbar respectively.

Kobayashi and others have reported that a higher amount of bonded oxygen within plasma deposited HMDSO/O_2 films can be obtained at optimized low deposition pressure and under constant input power. [8, 16, 19] Thus, it was necessary to work at lower input pressures (0.2 mbar) and higher input power in order to obtain SiO_2 –like films.

4.1.3 Plasma Input Power Effects on Films Wettability

Figure 4-3 shows the water contact angle (WCA) measurements for pp-HMDSO films deposited on Au substrates as a function of input power. The WCA decreases as input power increases, the highest (ca. 102.5° $\pm$ 4 °) and lowest (ca. 96° $\pm$ 4 °). This decrease in wettability reveals monomer dissociation due to the input power, thus dissociation of non-polar (–CH_3) groups from the precursor. Kurusawa *et al* also reported WCA values for pp-HMDSO films between 105°and 110° ($\pm$ 2°) fabricated under 100 W input power respectively.[20] The WCA values of the pp-HMDSO/O_2 surface film can be reduced by a subsequent oxygen plasma treatment, as shown in Figure 4-3. This procedure of exposing the deposited HMDSO/O_2 films to an additional oxygen plasma treatment step will be defined here as a *post-treatment* step.
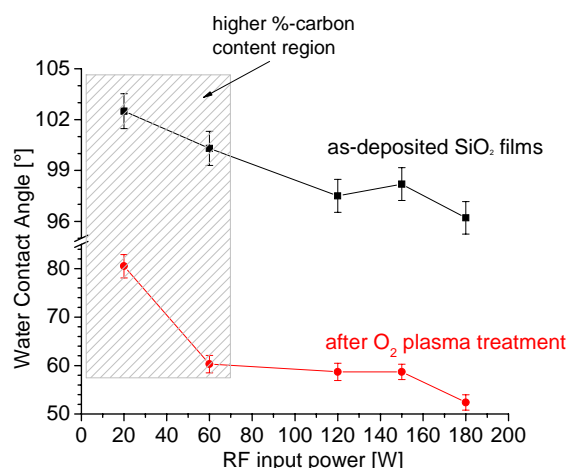
Figure 4-3: Contact angles determined by the sessile drop method on HMDSO/O_2 films, showing the effect of increasing the RF input power at constant HMDSO:O_2 (1:10) ratio.

The treatment of these surfaces with oxygen plasma for 5 sec showed a decrease in the WCA from 81° ($\pm$ 4 °) for the 30 W films and to 52° ($\pm$ 4 °) for the 180 W deposited films. This suggests the introduction of polar groups (e.g. –OH bond) at the surface, may be related to the observed increase in hydrophilicity. This effect of the O_2 plasma post-treatment with respect to the WCA is due to increased higher energy state created by the oxygen radicals. This creates an increase in surface tension from the formation of surface polar groups.[21-23] A. Hofrichter implemented this surface treatment step to enhance the adhesion of polycarbonate onto SiO_2 layers, the resistance to temperature and moisture was also significantly improved.[21]

4.1.4 Effect of Input Power on the Refractive Index

Figure 4-4: refractive index and C/O atomic ratio of plasma polymerized HMDSO/O2 (gas ratio 1:10) under different rf input power. Samples were post-treated by 5 sec O_2 plasma.

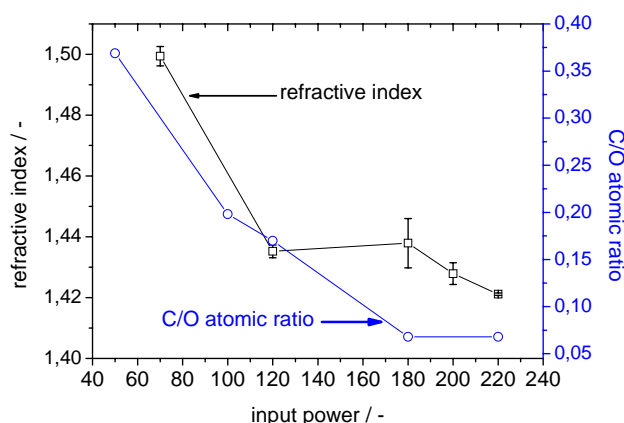Figure 4-4 shows that the refractive index decreases upon increasing input power, from about 1.499 for low input power, 70 W to a minimum of 1.42 at the highest deposition input power employed, 220 W. The C:O atomic ratio decreases from 0.35 for low input power to 0.05 for high input power. According to Figure 4-4, the impact of the input power on the monomer causes a decrease in carbon and an increase in oxygen within the deposited film.

The decrease in refractive index upon increasing input power can be explained by different contents of organic residuals in the films, which depends upon the reaction parameters of the HMDSO/O_2 polymerization. The refractive index at high input power (above 200 W) showed a value of 1.427, which corresponds to silica films.[24, 25]

4.1.5 Chemical Composition of Films – Analyzed by IRRAS

Input Power Effect

The structure and bonding in the pp-HMDSO/O_2 films for the deposition of SiO_2-like films have been studied by means of IRRAS spectroscopy to verify the influence of the deposition conditions on the internal chemical structure.

Figure 4-5 shows the IRRAS spectra of HMDSO:O_2 films deposited at different input power at constant pressure, 0.2 mbar and monomer ratio, 1:10. As a result of the chemical conversion of the HMDSO precursor to SiO_2-like films, typical Si-O-Si absorption bands were observed between 1250–1160 cm^{-1} for all samples. This absorption band shifts from low to high wavenumbers upon increase in input power, as can be seen for 30 W and 180 W films showing their spectra peak at 1160 cm^{-1} and 1250 cm^{-1}, respectively. This can be explained by the different optical modes in the O-Si-O group. Till date, three transverse optical (TO) modes at 460 cm^{-1}, 800 cm^{-1}, and 1075 cm^{-1} have been reported. These modes have been identified as the rocking, bending, and asymmetric stretching modes of the Si–O–Si bond. Infra Red Reflection Absorption Spectroscopy (IRRAS) introduces an angle of incidence to the polarized laser light incident on the sample during the measurements, which leads to additional longitudinal optical (LO) absorption bands from Si–O around 1250 cm^{-1}, 1165 cm^{-1}, and 1200 cm^{-1}.[26-28]

Additionally, Lucosky and Naiman separately reported the vibration of the Si–O–Si bond in the Transverse Optical (TO) mode, which depends on the incidence angle of the polarized IR light.[29, 30] This means the bonds move transverse to the chain and their displacement are restored by an external confining potential, i.e. mutually repulsive. Thus, the frequency of the Si–O–Si bond, due to the vibration initiated by the IR light, is related to the wavenumber. By contrast, the much weaker Si–O–Si bending mode at 808 cm^{-1} seems unaffected by this effect.

However, this shift reflects the changes in the chemical composition of the deposited films from mostly organic character to mostly inorganic SiO_2 character. For the films deposited at 150 W or higher there was virtually no evidence in the IRRAS spectra for hydrocarbons within the films.

Especially the films deposited at low input power (< 100 W), which show bands at 1273 cm^{-1} and 2967 cm^{-1} characteristically for $Si-CH_2R$ – residuals and methyl groups respectively. The intensity of these hydrocarbon bands decreases upon increase in RF input power due to increasing monomer dissociation as a result of the input power.

Different peak positions have been reported by many research groups for pp HMDSO films, and the proposed wavenumber ranges have been summarized in Table 4-2. The position of the Si–O–Si bond stretching vibration is strongly linked to the $(Si-O)_x$ stoichiometry. Its vibration frequency increases as the oxygen ratio tends to two. Furthermore, this shift can be a consequence of the local environment of Si–O–Si groups which varies with the deposition conditions. These shifts have been related to fabrication methods which yield film stress, porosity, or different film composition. In this work, all the films were prepared under comparable conditions, large deviations from stoichiometry as well as porosity may be excluded.

Vibrational mode	Frequency (cm^{-1})
Si–O bending	800 – 750
CH_3 rocking in $Si-CH_3$	980 – 860
Si–O–Si, Si–O– C asymmetric stretching	1200 – 1020
CH_3 symmetric bending in $Si-CH_x$	1450 – 1250
Si–H stretching	2150 – 2100
C–C, CH_3 asymmetric stretching	2960 – 2800
–OH stretching in free Si–OH	3300 – 3100

Table 4-2: frequencies and possible functional groups in plasma polymerized films from HMDSO/O₂.[31-35]

The shift variation of the intensity of the Si–O–Si bond in the pp–HMDSO film as a function of the input power suggests a profound effect of the fragmentation of Si–C and C–H bonds of HMDSO monomers, which could not be seen on the spectra.[36-39] Pfuch, Bensch, and Sahli separately reported that this shift in Si-O-Si spectra peak from low to higher wavenumbers indicates a stronger binding between Si-O-Si bridges.[28, 40] Furthermore, Pfuch integrated the area under the main Si-O-Si spectra, which showed an increase in area with growing input power.[25]
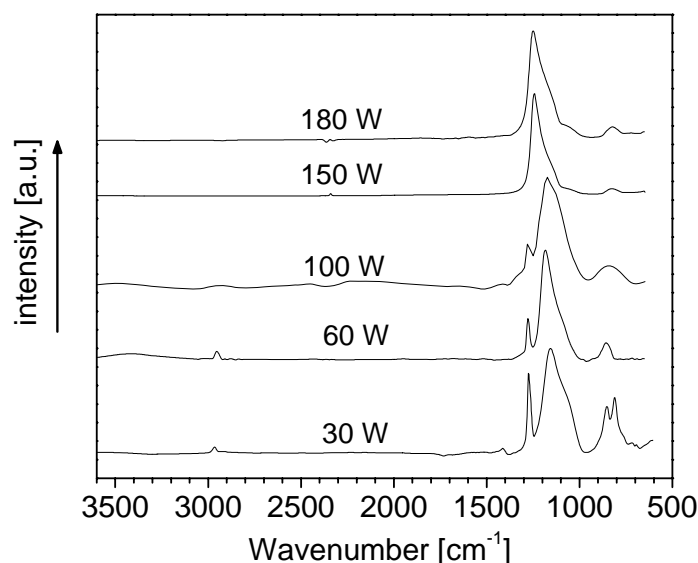
Figure 4-5: IRRAS spectra showing plasma polymerized HMDSO/O$_2$ films under different input powers at constant HMDSO:O$_2$ ratio and deposition rate.
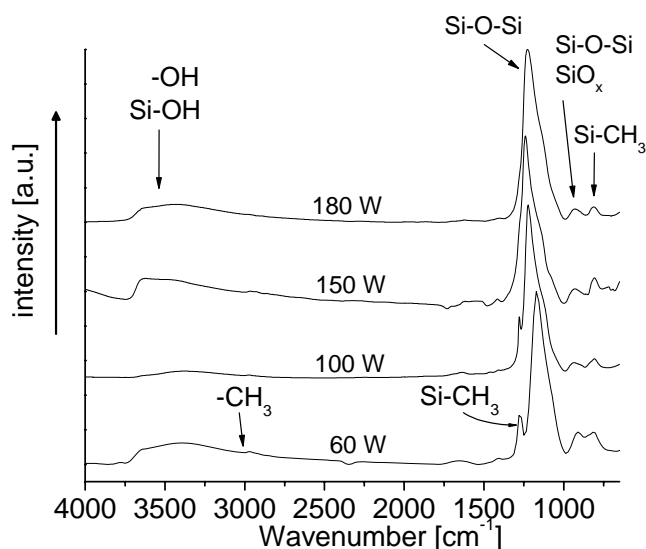
Figure 4-6: IRRAS chemical analysis of pp–HMDSO films (30 nm) deposited at different input power, after post-treatment in oxygen plasma, 10 sccm, 50 W, 5 sec.

In comparison to the as-deposited films, the surface modification of the SiO$_2$-like films by O$_2$ plasma treatment also led to changes in the IRRAS spectra as shown in Figure 4-6. The appearance of low intensity peaks at 935 cm^{-1} and 3360 cm^{-1} in the IR spectra indicates the formation of Si–OH and –OH related bonds respectively. The introduction of –OH bonds at the surface leads to the observed increase in hydrophilicity reported in section 4.1.3. Apparently, an

increase in conversion of the organic residuals under 50 W and 10 sccm oxygen flow was enough to initiate the oxidation of the Si–CH$_3$ and hydrocarbon groups. It should be noted that the film thickness for all the samples was found to be the same after treatment.

Effect of Monomer/Gas Ratio
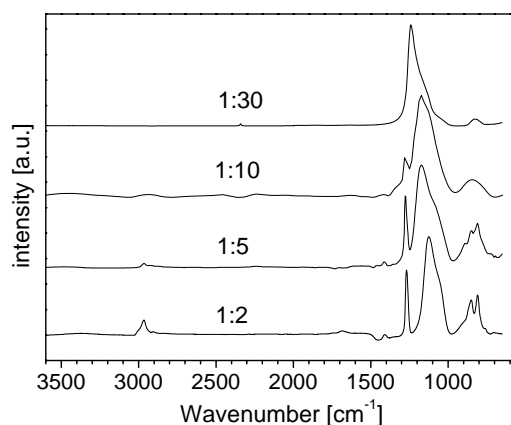
Figure 4-7: IRRAS spectra of 30 nm pp–HMDSO film deposited under 90 W input power at different HMDSO:O$_2$ ratio (as indicated on graph), showing the effect of increasing the O$_2$ ratio.

Figure 4-7 shows the effect of increasing the oxygen ratio in the gas mixture at a constant input power under 90 W. The stretching and bending bands attributed to Si–O–Si are clearly observable in the ranges 1120 –1230 cm^{-1} and 750 –810cm^{-1}. Moreover, the spectra show a broad band at wavenumbers between 850 and 800 cm^{-1}. This is formed by two adjacent bands as reported earlier, and may be assigned to the stretches of Si–OH and Si–CH$_3$ respectively.[4-6, 12, 26-28, 33, 35, 41-43] At the lowest HMDSO:O$_2$ (1:2) ratio, the highest intensity of the hydrocarbon could be seen at 2975 cm^{-1}. Another prominent peak is seen around 1260 cm^{-1}, which represents the Si–CH$_x$ group. On this same spectra, the broad band intensity at 807 cm^{-1} belongs to the Si–C group, which diminishes upon increasing oxygen content.

The effect of increasing the oxygen ratio for the plasma polymerisation of the HMDSO/O$_2$ increased the dissociation of the HMDSO monomer, and an increased intensity of the Si-O-Si bond, due to increased oxygen radicals was noticed.

4.1.6 Chemical Composition of Films – Analyzed by XPS

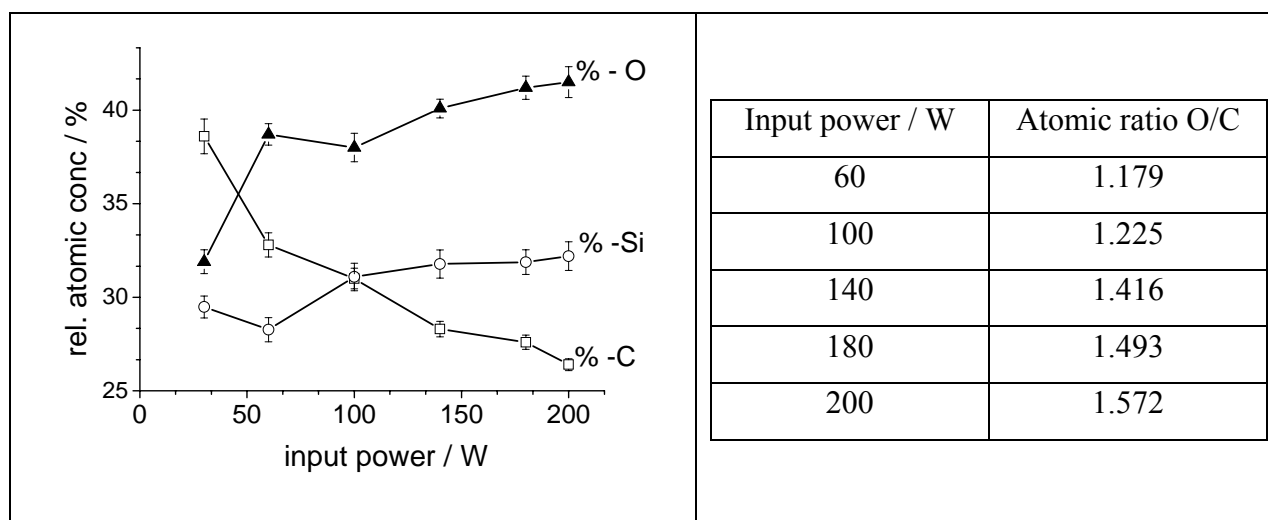| Input power / W	Atomic ratio O/C
60	1.179
100	1.225
140	1.416
180	1.493
200	1.572

Figure 4-8: XPS elemental analysis for plasma deposited $HMDSO/O_2$ (1:10) films, (20 nm) and the corresponding C:O atomic ratio.

The data obtained from XPS in Figure 4-8 shows the relative elemental percentage composition of pp–$HMDSO/O_2$ films, under different input power ranging from 30 W to 200 W. The as–deposited films under 30 W (low power) show about 29 % silicon, 39 % carbon, and 32 % oxygen content.

The increase in input power also yields an increase in temperature, which provides the required energy to induce the dissociation of the HMDSO monomer.[44] This implies that increasing the input power favors the radical formation through bond scission of the monomer, thus the chemical composition of the films will be influenced.

The carbon content decreases continuously with increase in deposition power, whereas the relative oxygen content increases. At the highest input power employed, 200 W, the lowest ratio of O/C ratio (1.572) was obtained. Furthermore, it was noticed that the Si:O surface ratio decreased from about 1:1.3 to 1:1.1, from 200 W to 30 W input power respectively. For silica films, the Si:O ratio corresponds to 1:2, thus the surface 1:1.3 for Si:O reported in this section do not correspond to SiO_2-like films, because of high C-atomic content.

An oxygen plasma post–treatment step of 5 seconds was carried out to increase the Si:O ratio. Figure 4-9 shows the relative atomic percentages of carbon, oxygen, and silicon obtained after post treatment. At low input power (30 W) of HMDSO deposition, a relatively small change of the carbon content is noticed after the treatment. The HMDSO deposition at higher input power (>150W) depicts a decrease in carbon and an increase in oxygen content after the O_2 plasma treatment. At 220 W input power, the residual carbon content was significantly reduced to less than 5 % atomic concentration. The stoichiometry of the O_2 plasma post–treated deposited

HMDSO/O_2 films attained was $Si_1O_{1.89}C_{0.11}$, thus "SiO_2-like" films. This 5 sec post–treatment time showed a reduction of the hydrocarbon content in the deposited films. The results of the films chemical compositional changes are consistent with the IRRAS measurements earlier reported, which showed a decrease in carbon content with increasing in input power, as well as after the post treatment.
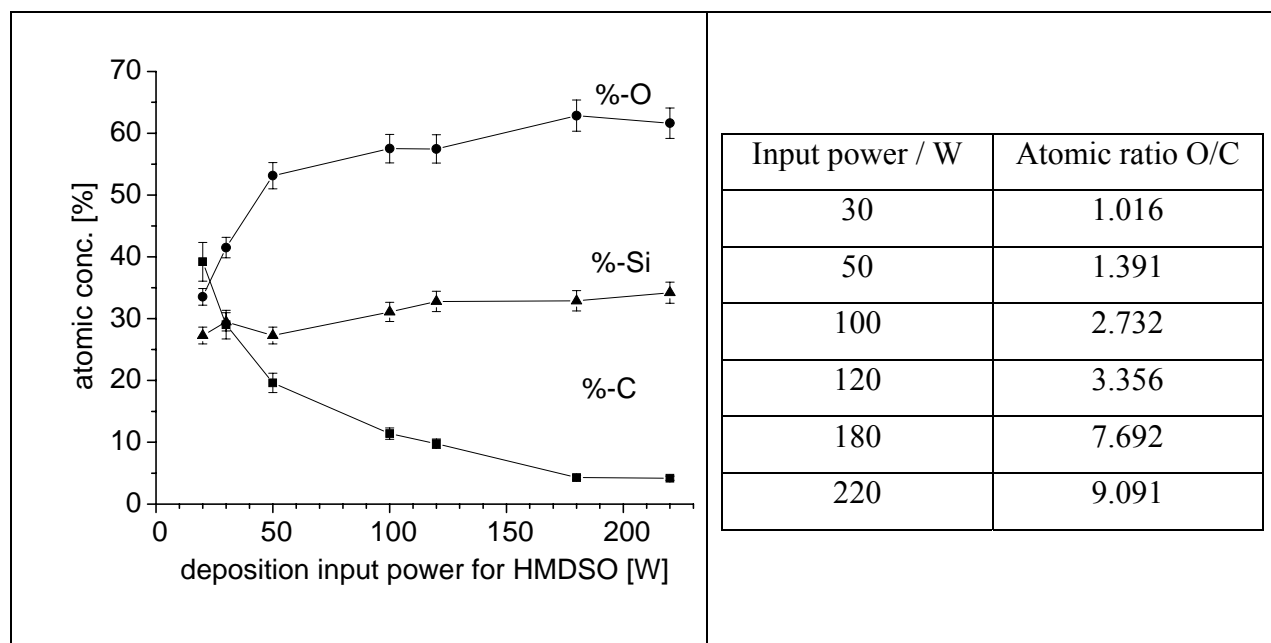

Input power / W	Atomic ratio O/C
30	1.016
50	1.391
100	2.732
120	3.356
180	7.692
220	9.091

Figure 4-9: XPS elemental analysis for the plasma deposited HMDSO/O_2 films after post–treatment with O_2 plasma for 5 sec, at 50 W. The corresponding C:O ratio versus input power is shown on left.

Figure 4-10 shows high–resolution Si 2p spectra for films deposited at low (60 W) and high input power (150 W), before and after O_2 plasma post treatment.

The changes in the chemical structure of the films as a result of the O_2 plasma modification reflect the relative binding energies of the Si 2p peaks. At low deposition input power, the Si 2p peak is seen at 102.3 eV and after post–treatment, an increase in binding energy to 102.7 eV was observed. Likewise at high deposition input power, an increase or shift in binding energy due to plasma post–treatment is seen from 102.3 eV to 103.4 eV. Also, the area under the spectra increases after post–treatment for both low and high deposition input power, indicating chemical interactions of the $Si(-O)_xC_y$ environment in the deposited film with the O_2-plasma, whereby $x + y = 4$. These binding energy shifts have previously been related to various chemical combinations of carbon and oxygen atoms bonded to silicon. Configurations such as $Si(–O)_1C_3$, $Si(–O)_2C_2$, $Si(–O)_3C_1$ and $Si(–O)_4$ have been proposed, with the $Si(-O)_4$ configuration showing the highest binding energy for the Si 2p electrons.[25, 32, 34, 46]
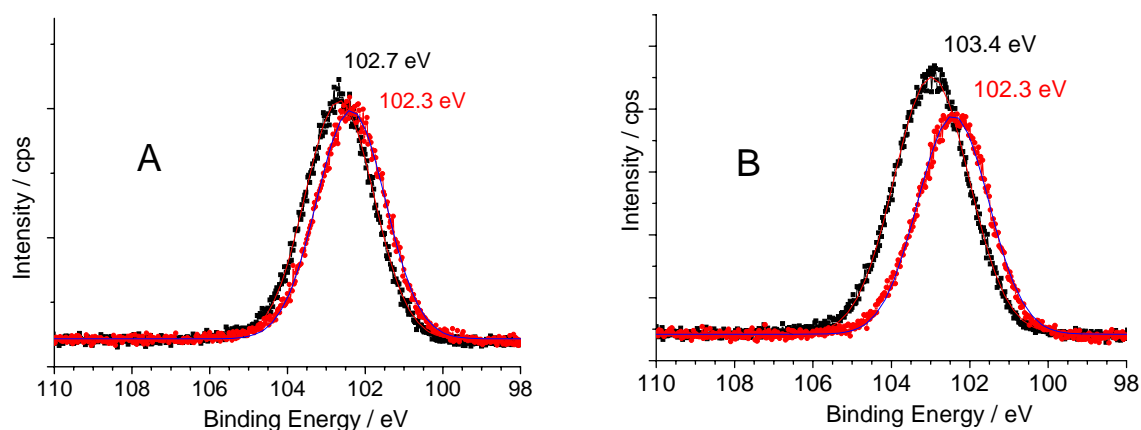
Figure 4-10: Si 2p high–resolution XPS spectra of as–deposited (lower BE) and films treated with O_2 plasma for 5 sec under 50 W (higher BE). Films were deposited under (A) 60 W, (B) 150 W, HMDSO/O_2 plasma.

Following this interpretation, we can assume that those films deposited at 60 W input have a higher concentration of Si(–O)$_1$ for which the Si 2p peaks is observed at 102.3 eV. After oxygen plasma surface modification the Si 2p peak shifts to 102.7 eV, suggesting a mostly Si(-O)$_3$C$_1$ character. Films deposited using 150 W RF input power showed a higher binding energy of 103.4 eV after treatment, which is a typical value for a highly oxidized silicon environment as reported for quartz films.[47, 48] This shift further indicates the dissociation of the hydrocarbon from the deposited film with increasing input power has been enhanced by the post–treatment to yield SiO$_2$-like films.

The peak values of the BE obtained versus the various input power have been plotted in Figure 4-11. The post-treated films showed a linear increase in the BE shift with increasing deposition input power, whereas the as–deposited films showed a slight increase up to BE value of 102.4 eV at 200 W, which corresponds to the Si(–O)$_2$ chemical environment. The lower BE values of the as–deposited films may be explained by the fact that, after the plasma power is switched off, some radicals, unfragmented monomer (molecules), and other species are still present in the reaction chamber, which is then deposited on the film. This "off–plasma" deposition may be responsible for the high hydrocarbon environment detected for the as-deposited (un-treated) films.

It can be concluded that the wide range of Si(-O)$_x$ chemical environment obtained upon treating the deposited HMDSO/O_2 films can be related to the Si 2p binding energy shifts, which tends to SiO$_2$ –like films for high input powers.
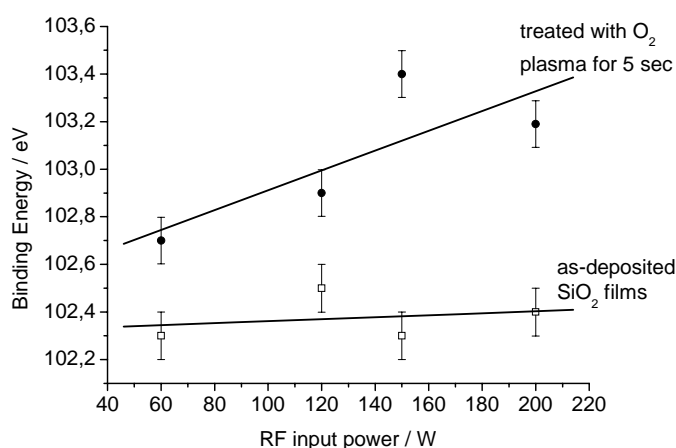
Figure 4-11: effect of RF input power on the binding energy of silicon atomic orbital (Si 2p) for the as–deposited and treated film.

4.1.7 Surface Morphology – AFM Measurements

Figure 4-12 and Figure 4-13 show the 3D micrographs from the AFM measurements of the deposited HMDSO films at 60 W (low input) and 150 W (high input) power respectively. The figures (a) represent the untreated films, while figures (b) depict the post–treated films.

The surfaces of the HMDSO/O_2 deposited films studied in this work were always smooth with the surface roughness root mean square (RMS) values below 0.5 nm. The AFM micrographs showed that the surface roughness increases with input power, illustrated in Figure 4-14. After the O_2 plasma post-treatment for 5 seconds, the surface roughness value decreased to about 0.3 nm at 200 W input power. The post-treated films above 120 W showed negligible differences in surface roughness, which might be related to changes in the surface chemical composition. R. Mahlberg and co-workers used AFM to investigate the changes in topography and surface free energy of plasma treated HMDSO on wood (for 15 sec at 60 W and 100 W). They also showed the surface morphology and surface roughness decreased for very short treatment times.[50]
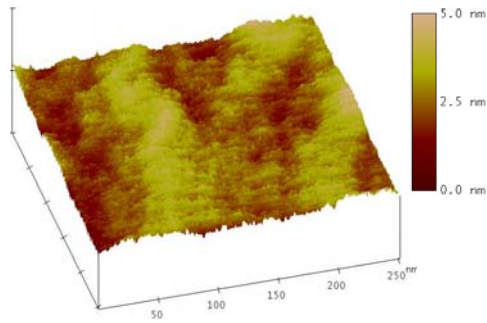
(a) as-deposited   **(b) treated 5 sec**
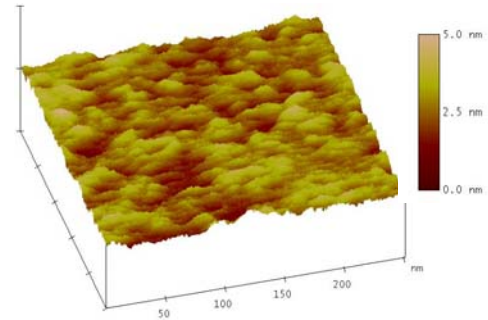
Figure 4-12:AFM micrograph of a SiO$_2$-like film deposited under **60 W** input power (a) as-deposited and (b) treated with O$_2$ plasma for 5 sec
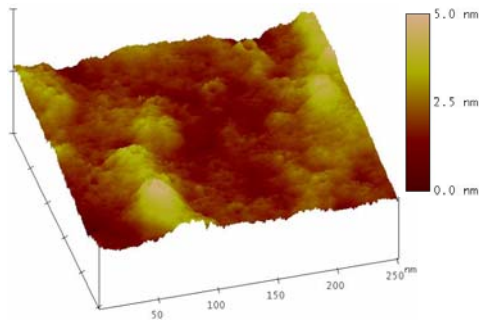
(a) as-deposited   **(b) treated 5 sec**
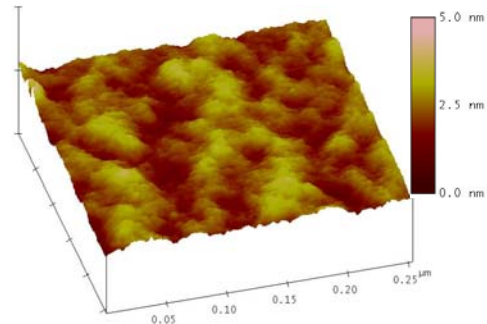
Figure 4-13: AFM micrograph of a SiO$_2$-like film deposited under **150 W** input power (a) as-deposited and (b) treated with O$_2$ plasma for 5 sec.
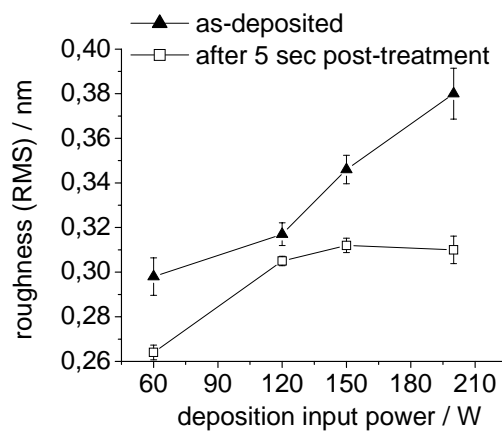
Figure 4-14: surface roughness of plasma deposited HMDSO/ O$_2$ at different input power, HMDSO:O$_2$ ratio 1:10, as-deposited and after surface treatment (for 5 sec at 50 W).

4.1.8 Conclusion – Fabrication of SiO$_x$C$_y$ and SiO$_2$ –like Films

The results presented here show the significant effect of various deposition parameters on the deposition of the SiO$_2$-like films, from hexamethyl disiloxane and oxygen. The films deposited were analyzed by IRRAS, ellipsometry, AFM, and XPS. At low input power as shown by the XPS results, high amount of carbon is retained in the deposited film. Upon oxygen plasma post-treatment, the atomic %-carbon decreases, and the atomic %-oxygen increases with the input power of the HMDSO deposition. These results are consistent with the chemical analysis from the IRRAS experiments.

4.2   References

1.   Aitchison, L., A History of Metals. Interscience Publishers 1960, 2, (351).

2.   Bunshah, R. F.; Deshpandey, C. V., Hard Coatings. Vacuum 1989, 30, (10), 955.

3.   Samson, F., Ophthalmic Lens Coatings. Surface & Coatings Technology 1996, 81, (1), 79-86.

4.   Mota, R. P.; Galvao, D.; Durrant, S. F.; Demoraes, M. A. B.; Dantas, S. D.; Cantao, M., HMDSO Plasma Polymerization and Thin Film Optical Properties. Thin Solid Films 1995, 270, (1-2), 109-113.

5.   Vautrin-Ul, C.; Boisse-Laporte, C.; Benissad, N.; Chausse, A.; Leprince, P.; Messina, R., Plasma-polymerized coatings using HMDSO precursor for iron protection. Progress in Organic Coatings 2000, 38, (1), 9-15.

6.   Bousquet, A.; Bursikova, V.; Goullet, A.; Djouadi, A.; Zajickova, L.; Granier, A., Comparison of structure and mechanical properties of SiO2-like films deposited in O-2/HMDSO pulsed and continuous plasmas. Surface & Coatings Technology 2006, 200, (22-23), 6517-6521.

7.   Vanooij, W. J.; Surman, D.; Yasuda, H. K., Plasma-polymerized coatings of trimethylsilane deposited on cold-rolled steel substrate. - Effect of deposition conditions on corrosion performance [Review]. Progress in Organic Coatings 1995, 25, (4), 319-337.

8.   Yasuda, H., Plasma Polymerization. Academic Press: 1985.

9.   Dennler, G.; Houdayer, A.; Raynaud, P.; Seguy, I.; Segui, Y.; Wertheimer, M. R., Growth modes of SiOx films deposited by evaporation and plasma-enhanced chemical vapor deposition on polymeric substrates. Plasmas and Polymers 2003, 8, (1), 43-59.

10.   Dennler, G.; Houdayer, A.; Segui, Y.; Wertheimer, M. R., Growth and structure of hyperthin SiO2 coatings on polymers. Journal of Vacuum Science & Technology a-Vacuum Surfaces and Films 2001, 19, (5), 2320-2327.

11.   Lamendola, R.; dAgostino, R., RF plasma deposition of barrier thin films from hexamethyldisilazane and hexamethyldisiloxane containing feeds. Abstracts of Papers of the American Chemical Society 1997, 213, 499-POLY.

12.   Schmachtenberg, E.; Costa, F. R.; Gobel, S., Microwave assisted HMDSO/oxygen plasma coated polyethylene terephthalate films: Effects of process parameters and uniaxial strain on gas barrier properties, surface morphology, and chemical composition. Journal of Applied Polymer Science 2006, 99, (4), 1485-1495.

13.   Walkiewicz-Pietrzykowska, A.; Espinos, J. P.; Gonzalez-Elipe, A. R., Type of precursor and synthesis of silicon oxycarbide (SiOxCyH) thin films with a surfatron microwave oxygen/argon plasma. Journal of Vacuum Science & Technology A 2006, 24, (4), 988-994.

14.   Martin-Palma, R. J.; Gago, R.; Tores-Costa, V.; Fernandez-Hidalgo, P.; Kreissig, U.; Martinez Duart, J. M., Optical and compositional analysis of functional SiOxCy:H coatings on polymers. Thin Solid Films accepted 25 July 2006, (in press).

15.   Fernández-Hidalgo, P.; Martín-Palma, R. J.; Conde, A.; Gago, R.; Martinez Duart, J. M., Structural and chemical characterization of functional SiO xCy:H coatings for polymeric lenses. J. Vac. Sci. Technol. B 2004, 22, (5).

16.   Yasuda, H. K., Some important aspects of plasma polymerization. Plasma Processes & Polymers 2005, 2, (4), 293-304.

17.   Kurosawa, S.; Hirokawa, T.; Kashima, K.; Aizawa, H.; Han, D. S.; Yoshimi, Y.; Okada, Y.; Yase, K.; Miyake, J.; Yoshimoto, M.; Hilborn, J., Detection of deposition rate of plasma-polymerized films by quartz crystal microbalance. Thin Solid Films 2000, 374, (2), 262-267.

18.   Yasuda, H., Glow-Discharge Polymerization. Macromolecular Reviews Part D-Journal of Polymer Science 1981, 16, 199-293.

19. Lasorsa, C.; Morando, P. J.; Rodrigo, A., Effects of the plasma oxygen concentration on the formation of SiOxCy films by low temperature PECVD. Surface & Coatings Technology 2005, 194, (1), 42-47.

20. Kurosawa, S.; Choi, B. G.; Park, J. W.; Aizawa, H.; Shim, K. B.; Yamamoto, K., Synthesis and characterization of plasma-polymerized hexamethyldisiloxane films. Thin Solid Films 2006, 506, 176-179.

21. Hofrichter, A.; Bulkin, P.; Drevillon, B., An interfacial study of a hydrogenated carbon interlayer for adhesion enhancement of plasma deposited silica thin films on polycarbonate. Journal of Adhesion Science & Technology 2002, 16, (4), 395-407.

22. Takada, T.; Nakahara, M.; Kumagai, H.; Sanada, Y., Surface modification and characterization of carbon black with oxygen plasma. Carbon 1996, 34, (9), 1087-1091.

23. Yoshinari, M.; Hayakawa, T.; Matsuzaka, K.; Inoue, T.; Oda, Y.; Shimono, M.; Ide, T.; Tanaka, T., Oxygen plasma surface modification enhances immobilization of simvastatin acid. Biomedical Research-Tokyo 2006, 27, (1), 29-36.

24. Alexandrov, S. E.; McSporran, N.; Hitchman, M. L., Remote AP-PECVD of silicon dioxide films from hexamethyldisiloxane (HMDSO). Chemical Vapor Deposition 2005, 11, (11-12), 481-490.

25. Pfuch, A.; Heft, A.; Weidl, R.; Lang, K., Characterization of SiO2 thin films prepared by plasma-activated chemical vapour deposition. Surface & Coatings Technology 2006, 201, (1-2), 189-196.

26. Kirk, C. T., An FT-IR study of silicon dioxides for VLSI microelectronics. Physical Review B 1988, 38.

27. Lange, P., Journal of Applied Physics 1989, 66, (1).

28. Bensch, W., Bergholz, W. , An FT-IR study of silicon dioxides for VLSI microelectronics. Semicond. Sci. Technol 1990, 5.

29. Lucovsky, G.; Manitini, M. J.; Srivastava, J. K.; Irene, E. A., J. Vac. Sci. Technol. B 1987, 5.

30. Naiman, M. L.; Kirk, C. T.; Aucoin, R. J.; Terry, F. L.; Wyatt, P. W.; Senturia, S. D., J. Electrochem. Soc. 1984, 131, 637.

31. Goujon, M.; Belmonte, T.; Henrion, G., OES and FTIR diagnostics of HMDSO/O2 gas mixtures for SiOx deposition assisted by RF plasma. Surface and Coatings Technology 2004, 188-189, 756-761.

32. Alexander, M. R.; Short, R. D.; Jones, F. R.; Michaeli, W.; Blomfield, C. J., A study of HMDSO/O2 plasma deposits using a high-sensitivity and -energy resolution XPS instrument: curve fitting of the Si 2p core level. Applied Surface Science 1999, 137, (1-4), 179-183.

33. Alexander, M. R.; Short, R. D.; Jones, F. R.; Michaeli, W.; Stollenwerk, M.; Mathar, G.; Zaold, J., The heteregeneous nature of HMDSO plasma deposits. In Ceramic Films and Coatings, British Ceramic Proceedings: UK, 1995; Vol. 54, p p. 89.

34. Wavhal, D. S.; Zhang, J. M.; Steen, M. L.; Fisher, E. R., Investigation of gas phase species and deposition of SiO2 Films from HMDSO/O-2 plasmas. Plasma Processes & Polymers 2006, 3, (3), 276-287.

35. Hegemann, D.; Vohrer, U.; Oehr, C.; Riedel, R., Deposition of SiOx films from O2 /HMDSO plasmas. Surface & Coatings Technology 1999, 119, 1033-1036.

36. Czeremuszkin, G.; Wertheimer, M. R.; Latre`che, M.; Da Silva, M. L. P., Plasmas and Polymers 2001, 6, (107).

37. Felts, J. T., Proc. 36th Ann. Tech. Conf. Society of Vacuum Coaters 1993, 324.

38. Da Silva Sorbrinho, M. L. P.; Czeremuszkin, G.; Latre`che, M.; Wertheimer, M. R. In Material Symposium Society Proceeding,

Plasma Deposition and Treatment of Polymers, Werrendale, PA, 1999; W.W. Lee, R. D. A., R. Wertheimer Ed. Material Research Society Publisher,: Werrendale, PA, 1999.

39.   Vassallo, E.; Cremona, A.; Laguardia, L.; Mesto, E., Preparation of plasma-polymerized SiOx-like thin films from a mixture of hexamethyldisiloxane and oxygen to improve the corrosion behaviour. Surface & Coatings Technology 2006, 200, (9), 3035-3040.

40.   Sahli, S.; Segui, Y.; Ramdani, S.; Takkouk, Z., Rf Plasma Deposition from Hexamethyldisiloxane Oxygen Mixtures. Thin Solid Films 1994, 250, (1-2), 206-212.

41.   Borvon, G.; Goullet, A.; Granier, A.; Turban, G., Analysis of low-k organosilicon and low-density silica films deposited in HMDSO plasmas. Plasmas and Polymers 2002, 7, (4), 341-352.

42.   Vautrin-Ul, C.; Roux, F.; Boisse-Laporte, C.; Pastol, J. L.; Chausse, A., Hexamethyldisiloxane (HMDSO)-plasma-polymerised coatings as primer for iron corrosion protection: influence of RF bias. Journal of Materials Chemistry 2002, 12, (8), 2318-2324.

43.   Hegemann, D.; Oehr, C.; Fischer, A., Design of functional coatings. Journal of Vacuum Science & Technology A 2005, 23, (1), 5-11.

44.   Yasuda, H.; Bumgarner, M. O.; Hillman, J. J., J. Appl. Polym Sci. 1975, 19, (531).

45.   Iftiquar, S. M., J. Phys. D: Appl. Phys. 1998, 31.

46.   Fracassi, F.; D'Agostino, R.; Favia, P.; Van Sambeck, M., Plasma Sources Sci. Technol. 1993, 2, 106.

47.   Alexander, M. R.; Short, R. D.; Jones, F. R.; Stollenwerk, M.; Zabold, J.; Michaeli, W., An X-ray photoelectron spectroscopic investigation into the chemical structure of deposits formed from hexamethyldisiloxane/ oxygen plasmas. Journal of Materials Science 1995.

48.   Alexander, M. R.; Jones, F. R.; Short, R. D., Mass spectral investigation of the radio-frequency plasma deposition of hexamethyldisiloxane. Journal of Physical Chemistry B 1997, 101, (18), 3614-3619.

49.   Granier, A.; Borvon, G.; Bousquet, A.; Goullet, A.; Leteinturier, C.; van der Lee, A., Mechanisms involved in the conversion of ppHMDSO films into SiO2-like by oxygen plasma treatment. Plasma Processes and Polymers 2006, 3, (4-5), 365-373.

50.   Mahlberg, R.; Niemi, H. E. M.; Denes, F.; Rowell, R. M., Effect of oxygen and hexamethyldisiloxane plasma on morphology, wettability and adhesion properties of polypropylene and lignocellulosics. International Journal of Adhesion and Adhesives 1998, 18, (4), 283-297.

<div align="right">

Chapter 5

</div>

5 Fabrication and Characterization of Functional Multilayers – Improved Interlayer Adhesion using treated SiO$_2$-like Films

(Part of this work has been submitted to Plasma Processes and Polymers Jan. 2007 and Langmuir (in press) – Feb. 2007.)

Abstract

The importance of multilayer hard films in the coating, packaging and semiconductor industries can be traced as far back to the 1960's. These films showed very good properties on most substrates in air. Nowadays, the task of fabricating stable thin functional films in native environments for the biological sector is a challenge. One method to improve the stability of thin films in such environments is to build a multilayer, which would increase the inter-layer adhesion of the functional film and the substrate.

This chapter deals with the fabrication of multilayers, which consist of a surface functional film covalently bonded to an adhesion promoting layer. The various functional films were plasma polymerized under different deposition conditions using styrene, allylamine and maleic anhydride monomers. These films were deposited on optimized SiO$_2$-like films, obtained from plasma polymerized hexamethyl disiloxane monomer. The SiO$_2$-like film served as an adhesion promoter in the multilayer. The stability of the multilayers in aqueous medium for over 24 h was characterized using Electrochemical Impedance Spectroscopy and Surface Plasmon Resonance spectroscopy techniques. The chemical composition of the multilayers was studied using Infra-Red Reflection Absorption Spectroscopy and X-Ray Photoelectron Spectroscopy.

Furthermore, the SiO$_2$-like film was compared to the commonly used self assembled monolayer (SAM) as an adhesion promoting layers. The multilayer built with SAM layer proved to be less stable than the optimized SiO$_2$-like film as an adhesion film.

5.1   Introduction

It is generally known that plasma polymerized functional films show good adhesion properties on most substrates. However, when immersed in solution the adhesion properties are often reduced or even completely lost.[1-3] Many strategies have been developed to obtain different levels of film stability in aqueous solution.[4] For polymeric substrates, the most convenient method of adhesion improvement is a short exposure to an activating plasma, such as an oxygen plasma. This leads to the formation of reactive sites on the polymeric substrate. These can be utilized in the subsequent plasma polymerization of the precursor molecule and allow for covalent bonding between the substrate

material and the depositing film. Increasing the input power during the deposition or, for pulsed processes, increasing the duty cycle (DC) also allows for a certain level of adhesion improvement. This, however, leads to increased fragmentation of the precursor molecule, different reaction mechanisms and subsequently less functionality in the polymer film structure.[5]

One great advantage of fabricating multilayer via plasma polymerization is the cleanliness and effectiveness, which has not been achieved using other chemical methods of multilayer fabrication. The SiO_2-like film was used here due to its mechanical and chemical properties, which have been explained explicitly in chapter 4 in this work.

The SiO2-like films used in this chapter were obtained from plasma polymerized HMDSO in the presence of oxygen using a gas ratio of 1:10 (HMDSO:O_2) at a process pressure of 0.2 mbar and an input power (cw) of 150 W. However, to obtain a stable and reactive interface layer that will allow for covalent binding with subsequently plasma polymerized functional film, the SiO_2-like films were post-treated in O_2 plasma, for 5 sec under 50 W. This activation step introduces reactive oxygen groups and radicals at the surface which are then available to participate in subsequent deposition processes enabling covalent coupling at the surface functional films.[1, 2, 6, 7]

Maleic anhydride was used as one of the surface films because of its highly reactive anhydride groups, which can be retained using pulsed plasma polymerization.[8] S. Schiller, A. T. Jenkins and co-workers used pulsed plasma polymerized maleic anhydride films as a supports for biological molecules.[9, 10] They used low duty cycles during the plasma deposition, which showed a high retention of the reactive groups in the polymer film. From basic chemistry it is known that anhydride groups are highly reactive, for example towards amines. This makes these polymeric thin films particularly interesting for bio-material applications. While these films potentially exhibit excellent chemical properties, their major drawback is a lack of stability in aqueous solution. In the past, this has have solved by chemically binding the plasma polymer layers to a metal surface using self assembled monolayers (SAM's) as interface adhesion layers.[10] While this has been sufficient for previous applications, more recent studies in this area have required an improvement over the past results. One particular criterion was the improved stability on silicon-based materials, rather than metallic surfaces.

Allylamine monomer was also plasma polymerized on top of the SiO_2-like films. Plasma polymerized allylamine film is an interesting candidate to create cell adhesion surfaces for cell culture because of the presence of amine groups, which has been investigated by some researchers.[11-13] The surfaces deposited are generally marked by a high reactivity characteristic of the functional groups they contain. A unique coupling possibility can be attained, that presents a number of challenges with respect to loss of reactivity over time when it comes in contact with air and biological media. Thus, any chemical instability of the functional groups of the polymeric deposit would generally retard their application for device designing.[3, 14, 15]

Styrene was also plasma polymerized on top the SiO_2-like film, which could be further activated to yield carboxylic groups or implemented as insulators in sensor design.[16, 17] Greenwood *et al* have shown that corona treated polymerized styrene films under atmospheric conditions increased their surface oxygen content from zero to 30.9 % carbon–oxygen functionalities. Approximately, one third of these functionalities were carboxylic acid and the rest comprised primarily of carbonyl derivatives (-C=O).[18] Also, a co-polymer of polystyrene and maleic anhydride has been used to immobilize bioactive molecules at solid / liquid interfaces, whereby a wet chemical method was used to covalently bind the co-polymer on a SiO_2 surface.[19] Thus, not only bio-polymers are important in biosurface engineering, but also important is the stability of the platform for subsequent bimolecular applications. The results presented here analyze the improved adhesion of different chemical compositional surface functional films, which have been fabricated under various plasma process parameters, on an optimized SiO_2-like film. This one step process of fabricating stable multilayer without exposing to ambient conditions aims at can be implemented to design surface films for diverse application in the sensor industry.

5.2   Results & Discussion

Deposition Rates of the Functional Films
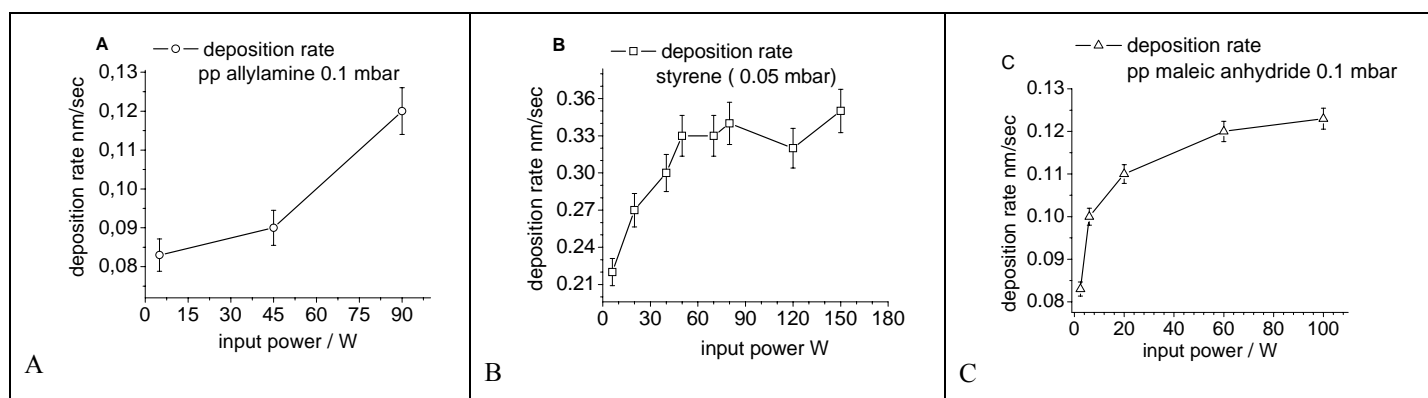
Figure 5-1: deposition rate versus input power of (A) allylamine, (B) styrene and (C) maleic anhydride, deposited at different input pressures as stated.

Figure 5-1 shows the deposition rate versus input power for the plasma polymerization of allylamine (pp-AA, 0.1 mbar), styrene (pp-PS, 0.05 mbar) and maleic anhydride (pp-MA, 0.1 mbar) monomers. The deposition rates of all the three films increased with input power, whereas the deposition rates were all below 0.3 nm/sec, due to the low pressure at which they were deposited. These parameters increase with input power because the plasma intensity causes an increase in ionic bombardment, thus higher molecular collisions which lead to increase in deposition rates.[1]

5.2.1 Chemical Analysis

SiO$_x$ – pp-Allylamine Multilayer

IRRAS spectra of pp-AA (17 nm $\pm$ 3 nm) on the SiO$_2$-like (30nm) film is shown in Figure 5-2, which shows the sum of the individual spectra of SiO$_2$–like and pp-AA film upon increasing input power.

The major peaks in Figure 5-2 with respect to the pp-AA film noticed are the amine (-NH), nitrile (-CN), amide (-CONH$_2$), and hydrocarbon (-CH$_x$) groups, which correspond to 3298 cm^{-1}, 2183 cm^{-1}, 1697 cm^{-1}, and 2939 cm^{-1} respectively. Figure 5-2 shows that the peak intensity of the amine group decreases with increasing input power while the hydrocarbon peak increases. The higher density of the amine peak suggests that under low energy plasma polymerization the amine functionality is retained to a greater extent than in the high energy process. The formation of the nitrile groups (2183 cm^{-1}) in pp-AA films suggest the transformation of the primary amino groups, whereby the intensity of these peaks increases with input power.

The presence of the oxygen radicals from the O$_2$ plasma activation, and residual free radicals in the plasma film would result to an aging process of pp-AA films in ambient air, which can be attributed to C=O stretching in amide groups around 1628 cm^{-1}. Furthermore, around this wavenumber, amines, alkenes and imines do contribute to the intensity of this peak. The Si-O-Si band appears strongly at 1230 cm^{-1} and 490 cm^{-1} for all the films, because the deposition condition for HMDSO/O$_2$ was not altered, this has been explained in chapter 4.
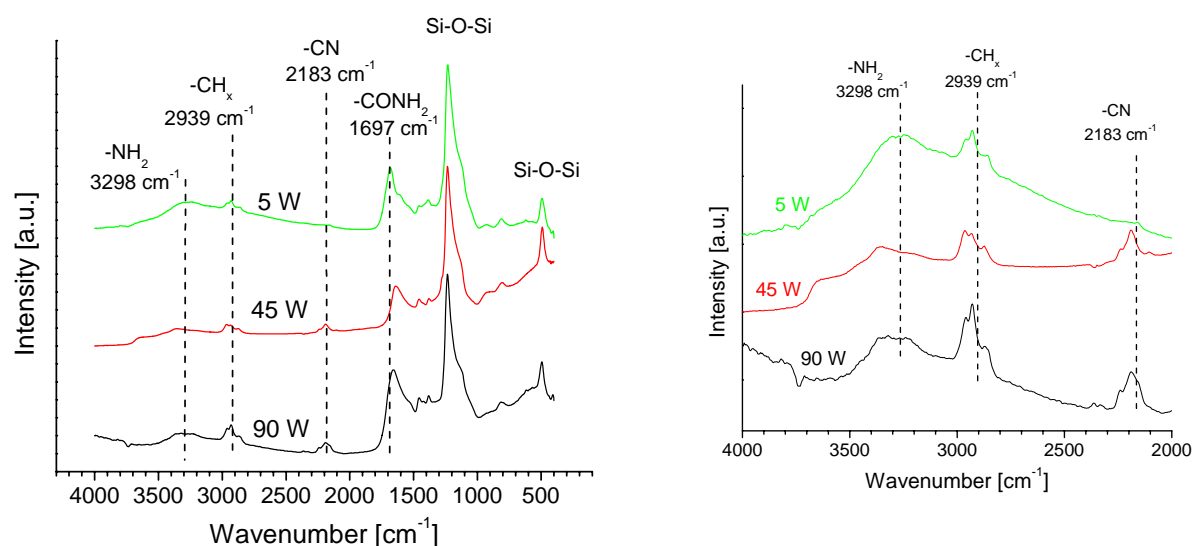

Figure 5-2: IRRAS spectra of SiO$_2$ – pp AA multilayer, the SiO$_2$ layer was deposited under 180 W input power, at 0.2 mbar. The pp AA films were deposited at 0.1 mbar, under different input powers 5 W, 45 W, and 90 W.

SiO$_x$ – pp-Styrene multilayer

Figure 5-3 depicts the effect of increasing the input power upon deposition of the plasma polymerized styrene (pp-PS) films (18 nm $\pm$ 3 nm) on SiO$_2$ like films.

The broad absorption band between 1070 cm^{-1}–1259 cm^{-1} was assigned to the asymmetric stretching modes of Si-O-Si, Si-OH, Si-CH$_3$ bands. Two main regions can be highlighted from the spectra in Figure 5-3: one region is defined from 700 cm^{-1} to 2000 cm^{-1} and the one around 2873 cm^{-1}. In the first region, the Si-O-Si peaks occur at 1230 cm^{-1}, a phenyl ring vibrations mode (at 745 cm^{-1}) and a phenyl ring bending modes at 1458 cm^{-1} and 1696 cm^{-1} can be observed. The intensities of the phenyl groups increase upon increasing in input power, demonstrating a loss of aromacity for the plasma films.

The detection of C-C vibration modes at 2224 cm^{-1} may be explained by the presence of residual styrene monomer inside the bulk of the film, which increases upon input power.

In the second region, the characteristic C-H stretching symmetric and asymmetric modes bands at correspond to the peaks at 2917 cm^{-1} and 2933 cm^{-1} respectively. The increase of these methyl end group peak with increasing input power can be explained by the fact that the plasma polymers tend to be more crosslinked.

W. Unger and other researchers have plasma polymerized styrene films, and they reported branching and cross-linking of the polymer as measured by Secondary Ion Mass Spectrometer (SIMS), whereby the aromacity was maintained for low input power and was fragmented to hydrocarbons at high input power.[20, 21]

The band assignments for other fragmented species of the pp-AA and pp-PS films are given in Table 5-1 and Table 5-2 respectively.
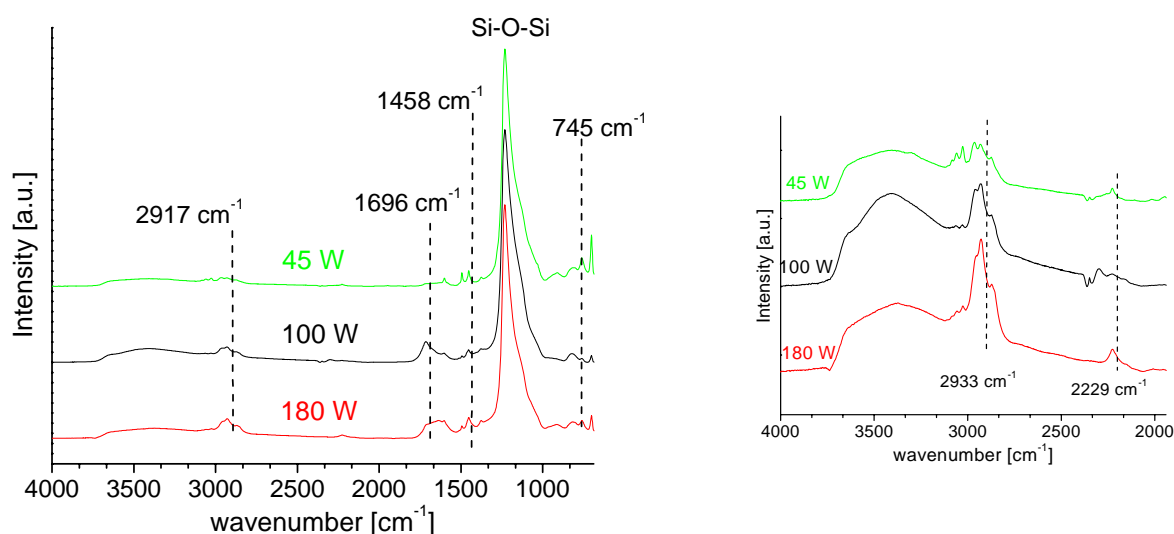

Figure 5-3: IRRAS spectra of SiO$_2$/ pp-PS multilayers, SiO$_2$ layer was deposited at 180 W, 0.2 mbar, styrene was plasma polymerized under different input powers as indicated, at 0.05 mbar.

Wavenumber (cm^{-1})	Band assignment
1560-1640	NH$_2$, amines
1225	C–N
1650–1690	C=N–H
1000–1100	C–OH
3030, 3300	NH
2400-2100	C≡C, C≡N
1650	R-N-C=O, amides
3100, 3600	–OH

Table 5-1: characteristic wavenumbers for plasma polymerized allylamine films[22-25]

Wavenumber (cm-1)	Band assignment
3070	Benzene ring
3300, 1600	–OH
2950–2850	C–C, CHx
1860, 1646 1780, 1737, 1746	C=O, carbonyl groups
1300 -1000	C–O
1647	C=C
690–750	Benzene ring
3020, 900, 1460–1600	C=C
1450,1500, 1580, 1600	aromatic C=C

Table 5-2: characteristic wavenumbers for plasma polymerized styrene films[26-29]

SiO$_x$ – pp-Maleic Anhydride multilayer

The IRRAS spectra in Figure 5-4 of the multilayer (SiO$_2$-MA) show the characteristic bands of both layers: the main SiO$_2$ band is observed at 1230 cm^{-1}, whereas the O$_2$ plasma modification step indicates an additional band at 920 cm^{-1}.

The IR-bands typical of the pp-MA layer are observed in the spectra between 1600 and 1900 cm^{-1}, as seen in Figure 5-4. MA deposited under cw (5W) conditions exhibited a carbonyl band around 1710 cm^{-1} and the typical anhydride doublet at 1795 and 1870 cm^{-1}, respectively. With the introduction of a duty cycle which was changed from 10/40 to 1/40, the band at 1710 cm^{-1} decreased in intensity and the typical bands for anhydride peaks (1795 cm^{-1} and 1870 cm^{-1}) increased in relative intensity, suggesting that more anhydride groups were retained by decreasing the duty cycle. It was noticed that these peaks show a small shift to higher wavenumbers in comparison to previous work.[9, 10, 30] This may reflect covalent bonding between the SiO$_2$ layer and the pp-MA layer and the presence of a thin, mixed interface layer in which Si-O bonds are linked with the MA-polymer. IRRAS

measurements of the films after immersion in aqueous medium showed the loss of anhydride group functionality as a result of rapid hydrolysis to carboxylic acid groups in the film, as has been reported earlier.[10]
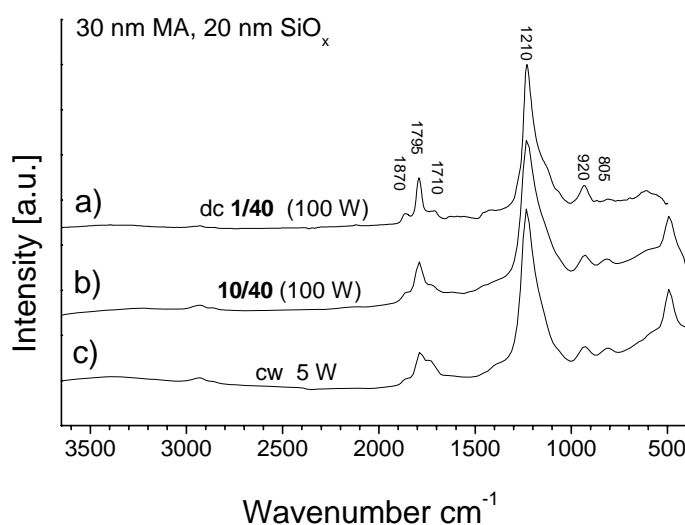

Figure 5-4: IRRAS measurements of SiO_2–MA films showing the retention of MA functionality of the pp-MA films. The pp-MA films on SiO_2-like surfaces were deposited at low duty cycle. (a) dc 1/40 at 100 W input power, (b) dc 10/40 at 100 W input power, (c) cw 5 W input power.

5.2.2 Multilayer Stability measured using Electrochemical Analysis Method

Figure 5-5 shows the Bode plot for the SiO_2-like layer on Au. This diagram is characterized by two well defined capacitive regions at high and low frequency. The physical meaning of the phase shift is related to the time constant of the circuits, which will be emphasized in this work. This time constant defines the shortest time domain over which the cell will accept a significant perturbation, which would probably occur at the interface of the films. Whereas, the magnitude of the impedance (modulus, |Z|) represents the multilayer structure and surface heterogeneity.[31, 32]

The phase angle of the pure Au layer approaches a pure capacitive behavior at low ω, which can be identified as θ tending to -90 °. And at high ω, it portrays a resistor showing almost a phase angle of zero. Upon deposition of the SiO_x layer on Au, the phase angle decreases at low ω, and increases at higher ω. This low frequency region is related to the charge transfer resistance and double layer capacitance of the electrode, while the high frequencies indicates the presence of a surface film, which contains both capacitive and resistive properties.

Figure 5-5 also shows that the impedance increases linearly from high to low frequencies upon addition of the SiO_x layer. The impedance values of Z for both Au and Au–SiO_2 –like layers were determined by fitting the experimental data, showing about 0.04 MΩ cm^2 and 0.2 MΩ cm^2. Therefore, a significant increase of charge transfer resistance due to the SiO_2 -like layer was observed. The fitting also takes into consideration the change in thickness, which would as well influence the resistance.
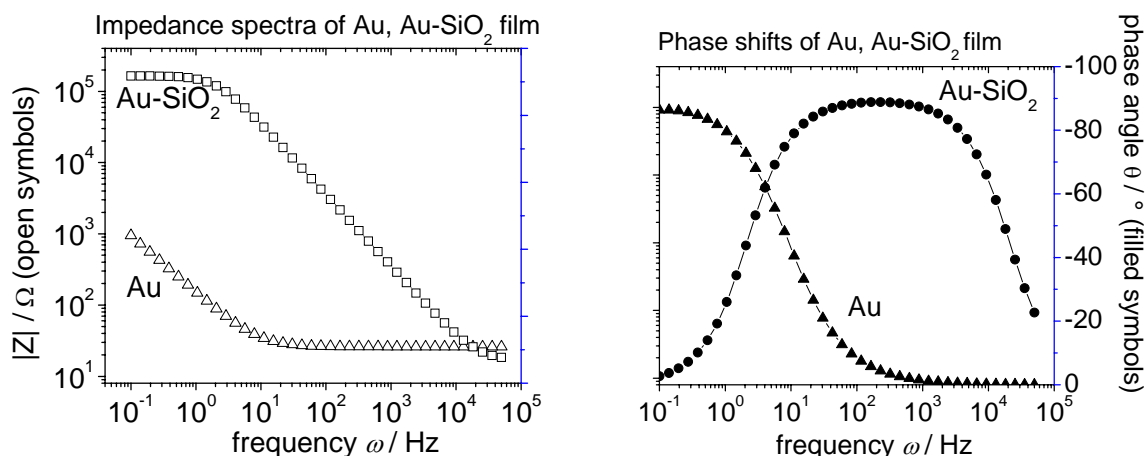
Figure 5-5: Bode plot showing the modulus impedance |Z| and phase angle vs. lg frequency of the working electrode Au, (open symbols) and SiO_2-like films (filled symbols) deposited on the Au surface.

The behaviour of all the multilayers were monitored after 30 minutes of immersion in the electrolyte solution up to 24 hours, which allows for the detection of any instability of the impedance spectra. All the plots were fitted based on a single Resistance-Capacitance (RC) element as indicated in Figure 3-16.[33, 34]

Stability of SiOx / pp-AA multilayer

Figure 5-6: Phase shift (left) and impedance spectra (right) obtained on pp AA (5 W, 50 W, 90 W) - SiO_2-like films, stable spectra were monitored for a 24 h loop measurement.

Figure 5-6 shows the phase and impedance plots of the pp-AA on plasma activated SiO_2-like film. The experimental results show defined time constants, which have been earlier explained to be related to the difference in film chemical compositions. Thus, the frequency between 10^0 and 10^2 Hz signifies the domain of ion perturbation within the multilayer, which probably occurs at the interface and indicates a change in chemical composition.

The time constant could have been influenced by the electrolyte conductivity or by changing the thickness of the working electrode; these parameters were kept constant for all the EIS measurement in this work. However, the presence of an interface does not necessarily influences the multilayer to be unstable, but the behavior of the impedance over a period of measurement in the electrolyte characterizes the stability. The impedance spectra in Figure 5-6 depict the effect of increasing the input power on the pp-AA film. The impedance spectra increase upon input power, which is more prominent above the interface region, i.e. at lower frequencies. Nevertheless, a stable spectrum was obtained from 24-hour loop EIS measurements for all the films, which indicated no delamination or dissolution of the functional pp-AA film from the SiO_2 film.

Stability of SiO_x / pp-Styrene multilayer

Figure 5-7 shows the EIS spectra obtained from pp-Styrene on SiO_2 film, whereas styrene was pp under 45 W, 90 W and 180 W. The phase shift depicts a single time constant for high input power pp-Styrene films, whereas at the lowest input power (45 W) a prominent double time constant was noticed. The impedance measurements do not show a clear trend with increasing input power, however this property was used to determine the film stability in the electrolyte for over 24 hours measurement.

The stability studies of this SiOx / pp-PS multilayer used in this work were carried out within 24 hours on the same film, which showed less than 5% decrease of impedance calculated. This minimal decrease may be related to the better interlayer adhesion achieved due to the O_2-plasma activation step.
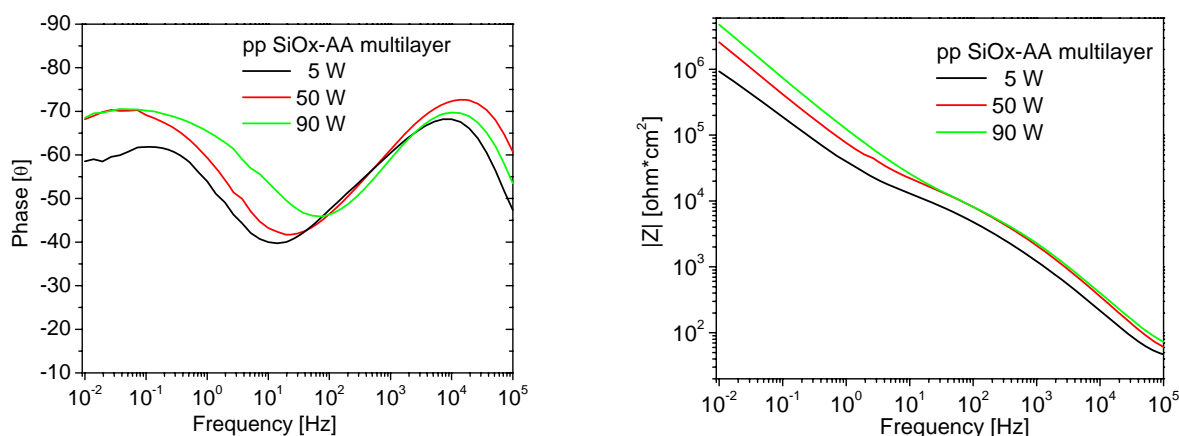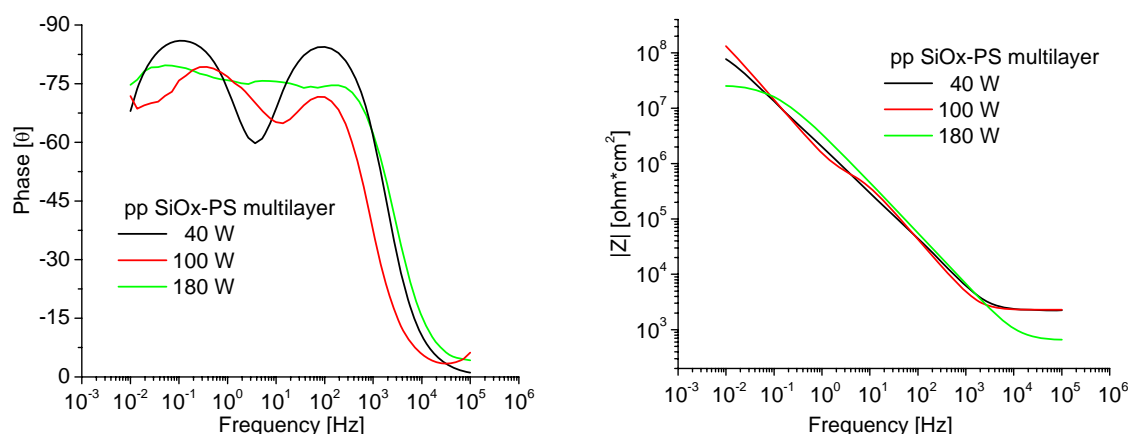

Figure 5-7: Phase shift and impedance spectra obtained on pp-PS (45 W, 180 W) SiO2-like films, stable spectra were monitored for a 24 h loop measurement.

Stability of SiOx / pp-MA multilayer

Figure 5-8 shows the phase shift of SiO_2 / pp-MA multilayer (left) and the corresponding apparent resistivity and conductivity modeled from a single RC element for a 1/40 pp-MA of the multilayer (right). The fittings of the experimental data reported the following values as depicted in Figure 5-8; R = 0.4 MΩ cm^2 and C = 1 x 10^{-7} F cm^{-2}, which are indicative of an impermeable SiO_x layer, and a low cross-linked pp –MA layer, showing that the multilayer film contains both capacitive and resistive properties. Due to the presence of only one time constant for both duty cycle and continuous wave film, it may be concluded that the pp-MA film is covalently bonded to the SiO_x-film. The stability studies of all the multilayers in this work were carried out within 24 hours on the same film, which showed less than 5% decrease of impedance calculated. This minimal decrease may be related to the better interlayer adhesion achieved due to the O_2-plasma activation step.
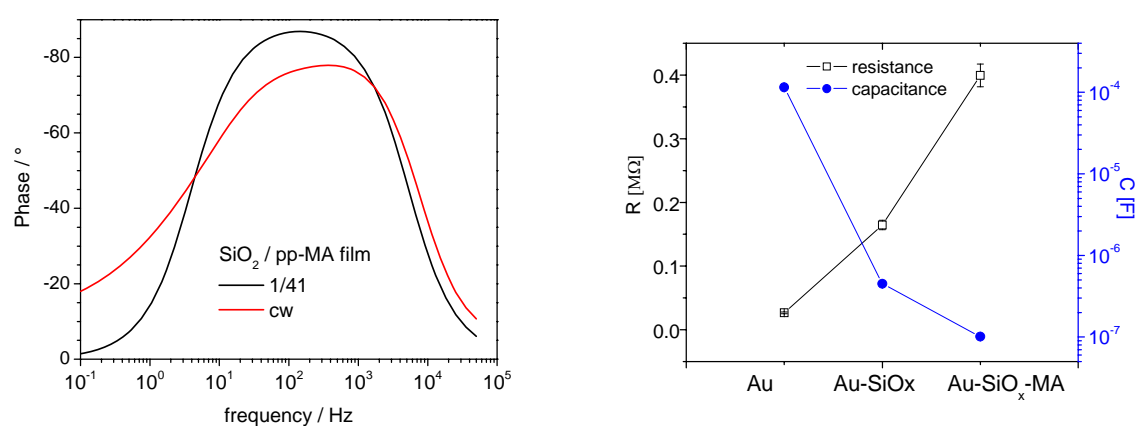
Figure 5-8: phase shift of SiO_2 / pp-MA multilayer (left) and the apparent resistivity and conductivity modeled from a single RC element for a 1/40 pp-MA of the multilayer (right).

Figure 5-9 shows the impedance spectra of the experimental results of SiO_2 / pp-MA as well as the stability of the film after 24 hours in electrolyte solution. The spectra measured after 24 hours showed a minimal decrease of the impedance, which further indicates an improved interlayer adhesion achieved due to the O_2-plasma activation step.

In a control experiment, the pp–MA film was deposited onto the SiO_x layer without O_2-plasma activation step. As expected, the organic layer delaminated from the SiO_x layer. The delamination was noticed by the floating of the organic layer on top of the electrolyte solution. Also, the θ - diagram obtained showed a double time phase constant, and the |Z|-diagram was unstable for low frequencies below 10^2 Hz.

Figure 5-9: Impedance spectra (left) of SiO_2 / pp-MA multilayer film and the multilayer stability measured for over 24 hours.

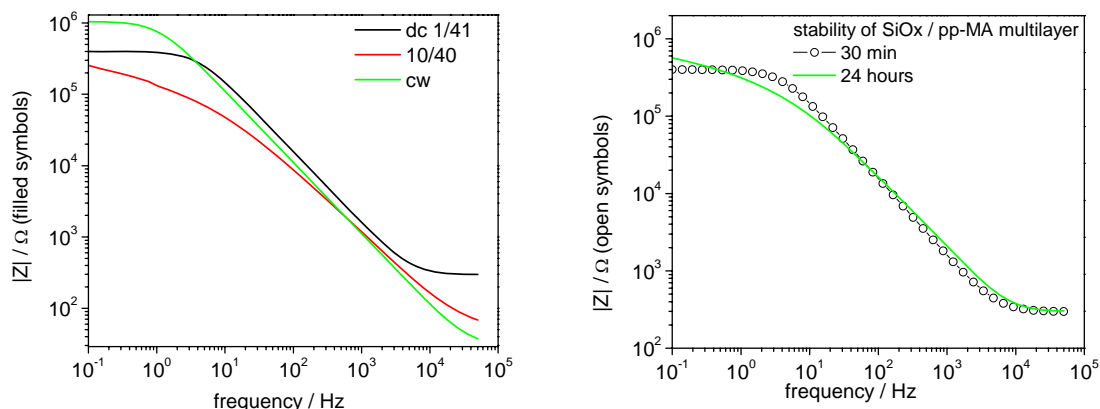Placing the plasma polymer in water would yield to hydrolysis and swelling in water, therefore both its resistance and capacitance will be altered. This effect has been reported by A. T. Jenkins *et al.*[10] Therefore the formation of conducting pathways through the polymer caused by the hydrated acid in the polymer will have a strong effect on the film resistance. This implies the capacitance will change when the polymer swells and the dielectric constant will obviously increase due to adsorption, which might also affect the film stabiliy in aqueous environments. All these parameters would affect the phase shift, however the presence of a second parameter, the impedance was used to analyze the multilayer stability. All the impedance spectra recorded in this work were constant for over 24 hours of measurement, thus the interlayer adhesion was improved due to the SiO_2 film treatment with oxygen plasma.

Jenkins and co-workers reported difficulties in measuring the electrochemical behavior of the pp-MA films on Au due to dissolution.[10] Therefore, the implementation of the dielectric SiO_2 –like layer served as a permeation barrier and also improved the well-known poor adhesion of pp-MA films on gold surfaces.

Due to the improved stability and functional groups retained in the Au–SiO_x–pp-MA multilayer system designed, these multilayer were implemented for direct coupling of biomolecules on the surface. This will be described in chapter 6.

5.2.3 Optical Thickness Change of the Au–SiO_x–pp-MA Multilayer

When comparing the stability of this double-layer structure on Au to pp-MA (35 nm) films stabilized using a SAM layer on gold, a profound improvement could be observed in the SPR kinetic scans. Figure 5-10 shows that upon immersion of pp-MA on gold in milliQ H_2O, with no adhesion layer, a continuous decrease in the reflectivity measured using SPR was observed. This decrease in %-reflected light can be directly related to a decrease in the film optical thickness $n \cdot d$ and thus a loss of

polymer from the gold surface. The Δd was calculated from the angle scan before and after immersion, which corresponded to about 11 nm decrease. Even after 25 hours the film thickness continued to decrease and it can be expected that longer exposure lead to a complete dissolution of the film.

R. Förch and co-workers also showed that plasma films deposited at low DC, however, show a substantial decrease in the optical thickness.[3] This proposed decrease in $n\,d$ occurs if one assumes the polymer to be swelling, which would imply an increase in thickness but also dilution of the polymer network. Thus, if the polymer is not covalently bonded to the substrate this could lead to dissolution, hence decrease in film optical thickness.
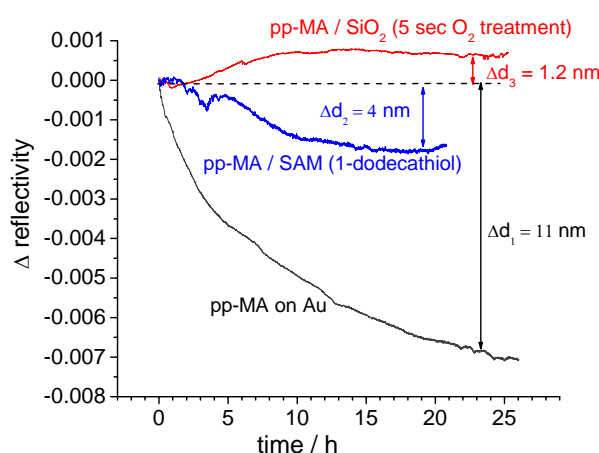
Figure 5-10: Change in reflectivity over immersion time in milli-Q water for pp-MA deposited on SiO$_2$ –like film, on SAM on gold and on bare gold, see Figure 5-11 for morphology of the immersed films.
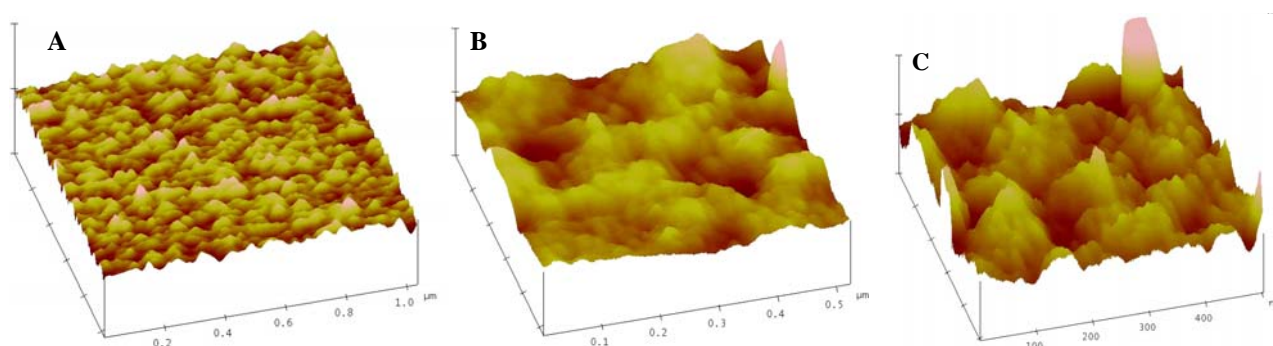
Figure 5-11: surface roughness of SiO$_2$ – MA film measured (A) as deposited RMS = 0.23 nm, (B) immersed 20 min in H$_2$O, RMS = 0.94 nm, and (C) immersed 120 min in milliQ H$_2$O, RMS = 1.43 nm

The topography of the pp-MA / SiO$_2$ films were measured using AFM before immersion into the aqueous solution, as shown in Figure 5-11A, and also after immersion for 20 min and 120 min as depicted in Figure 5-11B and Figure 5-11C.

After 20 min immersion in milliQ H$_2$O, the films showed an increase in surface roughness (RMS), 0.94 nm. The formation of wells and islands could be seen, which might be related to the film swelling. After 120 min immersion in milliQ H$_2$O, the surface roughness increased to 1.43 nm. This

roughness value remained almost constant for higher immersion time, indicating the stability of the layer. In the case of pp-MA films on gold layer, it was difficult to measure the surface roughness in milli-Q H_2O due to dissolution of pp-MA layer.

Additionally, Figure 5-10 shows that when introducing a SAM of dodecanethiol as an adhesion layer, a significant improvement in film stability was observed in comparison to the bare gold. Over a time frame of 15 hours the reflected light decreased by about 2 %, which was calculated from the angle scan shifts and corresponds to a change in thickness of 4 nm ($\pm$ 0.4 nm). After this time the film was relatively stable and no further loss of material could be observed. It was noted that during the first 5 hours of immersion there is some signal fluctuation, which may suggest processes such as swelling of the film and removal of material occurring at the same time, leading to variations in thickness and refractive index. However, using the SAM as an adhesion layer showed inconsistent results (not shown here), e.g. the reflectivity was seen after 2 hours of immersion measurement to decrease more than 80 % reflectivity upon immersion. This inconsistency of the MA films on SAM's has also been reported by K. Bender[14]. Similar results in the past have restricted the use of pp-MA films to subsequent experiments for only a few hours.

Due to the loss of material from the surface, and also the complete hydrolysis of the anhydride groups to form surfaces rich in –COOH, the pp-MA film was deposited on optimized SiO_2-like surfaces. As depicted in Figure 5-10, the pp-MA /SiO_2 layer shows an increase reflectivity, which corresponds to about 1.2 nm ($\pm$ 0.2 nm) thickness change, as also confirmed by the AFM analysis in Figure 5-11.

The results in this work suggest that the low dc plasma polymers consist of highly mobile chains, and a significant proportion of which may be lost to aqueous surroundings. However, the modified SiO_2 layer was implemented which covalently binds the functional polymer, thus the dissolution of the swollen films (increase in $n \cdot d$) was hindered after immersion in milliQ-H_2O

5.2.4 Conclusion

The adhesion of plasma polymerized films to the substrate surface can vary depending on the chemical and physical nature of the substrate. Moreover, in solution, the deposited plasma film can lift off from the surface due to swelling by the solvent and insufficient adhesion. In order to improve the adhesion properties of maleic anhydride plasma polymers on diverse substrates in aqueous media, plasma polymerized multilayer were implemented.

The synthesis of SiO_2–like films from plasma polymerized HMDSO in excess oxygen intended for adhesion improvement of functional plasma polymerized maleic anhydride has been presented. For optimization of the SiO_2-like layer different gas ratios of HMDSO and O_2 as well as different RF input powers were investigated. High quality SiO_2–like films with a typical stoichiometry of $Si_1O_{1.9}C_{0.1}$ were

obtained. The adhesion of pp-MA on top of the SiO_2 –like films was compared to that on a SAM of dodecanethiol on Au and on bare Au layers using in situ surface plasmon resonance studies. Optimum stability of the pp-MA films was obtained only after a surface modification of the SiO_2-like layers using a short O_2 plasma treatment, which is believed to form reactive sites on the SiO_2-like film that participate in subsequent plasma polymerization steps using reactive precursors such as maleic anhydride. The stability of the films was also characterized using electrochemical impedance spectroscopy, which showed constant impedances for over 24 hour of measurement.

5.3   References

1.   D'Agostino, R.; Cramarossa, F.; Fracassi, F.; Illuzzi, F., *Plasma Deposition, Treatment, and Etching of Polymers*. Academic Press, San Diego, CA,: 1990.

2.   Förch, R.; Zhang, Z. H.; Knoll, W., Soft plasma treated surfaces: Tailoring of structure and properties for biomaterial applications [Review]. *Plasma Processes & Polymers* **2005,** 2, (5), 351-372.

3.   Zhang, Z.; Chen, Q.; Knoll, W.; Forch, R., Effect of aqueous solution on functional plasma polymerized films. *Surface & Coatings Technology* **2003,** 174, 588-590.

4.   Williams, T. L.; Vareiro, M. M. L. M.; Jenkins, A. T. A., Fluorophore-encapsulated solid-supported bilayer vesicles: A method for studying membrane permeation processes. *Langmuir* **2006,** 22, (15), 6473-6476.

5.   Yasuda, H., *Plasma Polymerization*. Academic Press: 1985.

6.   Bastos, A. C.; Ostwald, C.; Engl, L.; Grundmeier, G.; Simoes, A. M., Formability of organic coatings - an electrochemical approach. *Electrochimica Acta* **2004,** 49, (22-23), 3947-3955.

7.   D'Agostino, R.; Fracassi, F.; Palumbo, F., *Plasma Process. Polym.* **2005,** 2.

8.   Ryan, M. E.; Hynes, A. M.; Badyal, J. P. S., Pulsed Plasma Polymerization of Maleic Anhydride. *Chemistry of Materials* **1996,** 8, (1), 37-42.

9.   Schiller, S.; Hu, J.; Jenkins, A. T. A.; Timmons, R. B.; Sanchez-Estrada, F. S.; Knoll, W.; Forch, R., Chemical structure and properties of plasma-polymerized maleic anhydride films. *Chemistry of Materials* **2002,** 14, (1), 235-242.

10.   Jenkins, A. T. A.; Hu, J.; Wang, Y. Z.; Schiller, S.; Foerch, R.; Knoll, W., Pulsed plasma deposited maleic anhydride thin films as supports for lipid bilayers. *Langmuir* **2000,** 16, (16), 6381-6384.

11.   Förch, R.; Chifen, A. N., .; Bousquet, A.; Khor, H.-L.; Jungblut, M.; Chu, L.-Q.; Zhang, Z.; Osey-Mensah, I.; Sinner, E.-K.; Knoll, W., Recent and expected roles of plasma polymerized films for biomedical applications. *Chemical Vapor Deposition* **2006 (submitted)**.

12.   Harsch, A.; Calderon, J.; Timmons, R. B.; Gross, G. W., Pulsed plasma deposition of allylamine on polysiloxane: a stable surface for neuronal cell adhesion. *Journal of Neuroscience Methods* **2000,** 98, (2), 135-144.

13.   Badyal, J. P.; Cameron, A. M.; Cameron, N. R.; Coe, D. M.; Cox, R.; Davis, B. G.; Oates, L. J.; Oye, G.; Spanos, C.; Steel, P. G., Plasmachemical surface functionalised beads: versatile tailored supports for polymer assisted organic synthesis. *Chemical Communications* **2004**, (12), 1402-1403.

14.   Bender, K., *Entwicklung und Charakterisierung verschiedener biomimetischer Lipidmembransysteme zur Untersuchung von Membranproteinen*. Cullivier: 2004.

15.   Kasemo, B., Biological surface science. *Surface Science* **2002,** 500, (1-3), 656-677.

16.   Larrieu, J.; Held, B.; Martinez, H.; Tison, Y., Ageing of atactic and isotactic polystyrene thin films treated by oxygen DC pulsed plasma. *Surface & Coatings Technology* **2005,** 200, (7), 2310-2316.

17.   Ray, M. A.; Greene, J. E.; Polack, A. J.; Welsh, L. B., Rf-Sputter-Deposited Multilayer Thin-Film Oxygen Sensors. *Journal of Vacuum Science & Technology a-Vacuum Surfaces and Films* **1983,** 1, (2), 322-322.

18.   Greenwood, O., *Journal of Adhesion Science and Technology* **1995,** 9, (3), 311-326.

19.   Pompe, T.; Zschoche, S.; Herold, N.; Salchert, K.; Gouzy, M.-F.; Sperling, C.; Werner, C., Maleic Anhydride CopolymerssA Versatile Platform for Molecular Biosurface Engineering. *Biomacromolecules* **2003,** 4, (1), 1072-1079.

20. Oran, U.; Swaraj, S.; Lilpitz, A.; Unger, W. E. S., Surface analysis of plasma deposited polymer films, 7 - "In situ" characterization of plasma deposited allylamine films by ToF-SSIMS, XPS and NEXAFS spectroscopy. *Plasma Processes and Polymers* **2006,** 3, (3), 288-298.

21. Oran, U.; Swaraj, S.; Friedrich, J. F.; Unger, W. E. S., Surface analysis of plasma-deposited polymer films, 3 - In situ characterization of plasma-deposited ethylene films by ToF-SSIMS. *Plasma Processes and Polymers* **2004,** 1, (2), 141-152.

22. Lejeune, M., *Surf. Coat. Technol.* **2006,** 200.

23. Wixom, M. R., *J. Am. Ceram. Soc.* **1990,** 73.

24. van Os, M. T.; Menges, B.; Foerch, R.; Vancso, G. J.; Knoll, W., Characterization of plasma-polymerized allylamine using waveguide mode spectroscopy. *Chemistry of Materials* **1999,** 11, (11), 3252-3257.

25. Beck, A. J.; Whittle, J. D.; Bullett, N. A.; Eves, P.; Mac Neil, S.; McArthur, S. L.; Shard, A. G., Plasma co-polymerisation of two strongly interacting monomers: Acrylic acid and allylamine. *Plasma Processes and Polymers* **2005,** 2, (8), 641-649.

26. Oran, U.; Swaraj, S.; Friedrich, J. F.; Unger, W. E. S., Surface analysis of plasma-deposited polymer films, 1 - ToF-SSIMS of plasma polystyrene before and after exposure to ambient air. *Plasma Processes and Polymers* **2004,** 1, (2), 123-133.

27. Kim, J.-T., *Surface Coatings Technol.* **2004,** 182, 1-6.

28. Chen, M., *J. Polym. Sci. A,* **1999,** 37, (325).

29. Prohaska, G. W.; Evans, J. F., Styrene and Vinyldimethylethoxysilane plasma polymerization and plasma copolymerization. *J. Vac. Sci. Technol. A* **1984,** 2, (2 (April-June 1984)).

30. Liu, S.; Vareiro, M. L. M.; Fraser, S.; Jenkins, A. T. A., *Langmuir* **2005,** 21, 8572-8575.

31. Macdonald, J. R., *Impedance spectroscopy*. Wiley: New York, 1987.

32. Kahanda, G. L. M. K. S.; Tomkiewicz, M., *J. Electrochem. Soc* **1990,** 137.

33. Newman, J., Electrochemical Systems. In Wiley Inter-science: NJ, 2004.

34. Bard, A. J.; Faulkner, L. R., *Electrochemical Methods - Fundamentals and Applications*. John Wiley & sons: New York, 1994.

<div align="right">

Chapter 6

</div>

6   Attachment of Stable Phospholipid Bilayer Vesicles to Plasma Polymerized Maleic Anhydride / SiO₂ multilayers

(*This work is in press Langmuir – Feb. 2007.*)

Abstract

A method of multilayer fabrication will be described in this chapter, which will be implemented as a platform to bind vesicles chemically. The multilayer composes of both plasma polymerized maleic anhydride films bonded on silicon oxide like films on Au substrates. Surface Plasmon Field-Enhanced Fluorescence Spectroscopy (SPFS) combined with Surface Plasmon Resonance (SPR) was used to monitor the activation of the plasma deposited maleic anhydride (pp-MA) film with EDC / NHS and the subsequent coupling of lipid vesicles. The vesicles were formed from a mixture of phosphatidylcholine and phosphatidylethanolamine lipids, with a water soluble fluorophore encapsulated within. Vesicle attachment was measured in real time on plasma films formed under different pulse conditions (plasma duty cycle). Optimum vesicle attachment was observed on the pp-MA films containing the highest density of maleic anhydride groups. Phospholipase A_2 was used to lyse the surface-bound vesicles and to release the encapsulated fluorophore.

6.1   Introduction

This chapter focuses on the attachment and stability of lipid vesicles on plasma deposited maleic anhydride films. The pp-MA plasma film has two specific functions: to provide a soft, polymeric cushion for the support of intact lipid vesicles and to allow for the straightforward covalent coupling of vesicles using classical peptide coupling chemistry. In order to ensure optimum adhesion of the MA to the substrate, a double layer system was designed in which a plasma deposited SiO_2 layer was deposited on the gold substrate prior to MA-deposition. This SiO_2 layer also had two functions: to act as an adhesion layer and to spatially distance fluorophores contained within the vesicles from the gold substrate to minimize quenching effects by the Au. The overall aim of this work was to construct stable, surface bound lipid bilayer vesicles which would retain many of the characteristics of biological cellular membranes such as fluidity, protein incorporation, and the compartmentalization of ions.

Much of the research on biomimetic lipid films has focused on creating planar bilayer membranes; where the lipid membrane is either suspended across a small diameter aperture (a black lipid membrane) or supported on a solid surface. A comprehensive review of advances in this area is

given elsewhere.[1] Unilamellar lipid vesicles are lipid spheres consisting of two leaflets of lipid monolayer. In aqueous solution they arrange so that their hydrophobic tails interact. Naturally occurring lipid vesicles have critical functions in cellular biology, for example they are involved in the transport of neurotransmitters across synaptic junctions. Synthetic unilamellar vesicles, as used in this study, can be constructed easily by hydrating lipids, extrusion or sonication.[2] Vesicles have previously been studied both in bulk solution[3] and in surface bound systems. Xu and Cheng used electrochemical methods to study the effect of streptolysin, a pore forming bacterial toxin, on electrode immobilized large unilamellar vesicles filled with potassium ferrocyanide.[4] Jung *et al.* investigated the binding of phospholipase A_2 (PLA$_2$) to surface immobilized vesicles using SPR. The vesicle contained ether linked lipids which were not susceptible to PLA$_2$ action as PLA$_2$ catalyses the hydrolysis of the 2-acyl group in the glycerol linkage between the fatty acid chains and the phospholipid head group of lipids such as 1,2-Dimyristoyl-sn-Glycero-3-Phosphocholine. The biotin tagged vesicles were supported on a structured biotin – streptavidin self-assembled monolayer on to which streptavidin had been attached. They determined the equilibrium dissociation constant for PLA$_2$ interacting with the vesicles to be 6 x 10^{-7} mol dm^{-3}.[5] Separate studies by Boxer and Städler have extended the tethered vesicles concept by attaching oligonucleotides to vesicles and measuring hybridization with complementary surface immobilized oligonucleotides attached to a solid supported lipid bilayer.[6, 7] Sanchez and co-workers have studied real time lysis of giant unilamellar vesicles by fluorescently tagged PLA$_2$, which has given valuable real-time information on the kinetics of vesicle lysis by PLA$_2$.[8] Experiments on phospholipid bilayer – streptavidin supported vesicles by Williams *et al.* have initiated the utilization of combined SPR and SPR enhanced Fluorescence for studying vesicle lysis by PLA$_2$.[9]

If unilamellar lipid vesicles are introduced to surfaces they can rupture and fuse with the surface, adsorb as intact vesicles or both fuse and adsorb. The fate of the vesicle depends on the surface free energy and is influenced by the lipid composition of the vesicle, the vesicle size, the lipid phase transition temperature and the system temperature. Surfaces that can lower their free energy as a result of vesicle fusion will tend to induce vesicle fusion. For example, very hydrophobic surfaces such as octadecanethiol Self-Assembled Monolayers (SAMs) induce vesicle fusion and the formation of lipid monolayers, since the alignment of hydrophilic head groups away from the adsorbed lipid monolayer on the SAM is energetically favored.[10, 11] On non-homogenous or patterned surfaces, containing domains of both hydrophobic and hydrophilic surface bound molecules, it is believed that contact with hydrophobic domains can induce vesicle rupture subsequent to initial adsorption.[12] Tawa and Morigaki have shown that when egg-PC vesicles are added to NH$_2$ –functionalised SAMs on SiO$_2$ substrates, it appears that metastable lipid vesicles are adsorbed, which subsequently rupture on rinsing of the surface to form a bilayer.[13] Tanaka and Sackmann discuss the adsorption of lipids onto polymer and other tether systems.[14, 15]

The process and analysis of plasma deposition of hexamethyldisiloxane (HMDSO) was explained in chapter 4. XPS analysis showed that silicon and oxygen containing films can be deposited with a number of Si:O stoichiometries, with relative proportions depending on input power and oxygen flow rate in the reactor. Maleic anhydride (MA) films have properties which make them of particular interest for surface modification; they can be formed in a way that anhydride group functionality is retained. They can be prepared using plasma polymerization, and the functional groups can be tuned by pulsing the input power. Ryan *et al*. described the first detailed study of the radio frequency (plasma) induced polymerization of maleic anhydride in 1996.[16] They showed that variations in applied power and duty cycle could be used to vary the chemical functionality of plasma polymerized maleic anhydride films with excellent retention of the maleic anhydride ring in the film. Maleic anhydride films have been used as substrates for the attachment of amino functionalized alkyl chains[17] the polymerization of styrene[18] and protein attachment.[19]

Jenkins *et al.* have shown previously that lipid vesicles can undergo fusion when introduced to pp-MA films, forming a continuous lipid bilayer.[20] They used calcium ions to chelate negatively charged phosphatidylglycerol lipids to hydrolysed pp-MA films containing carboxylic acid functional groups. They concluded that that the presence of calcium at relatively high concentrations likely enhanced the vesicle fusion / rupture process.
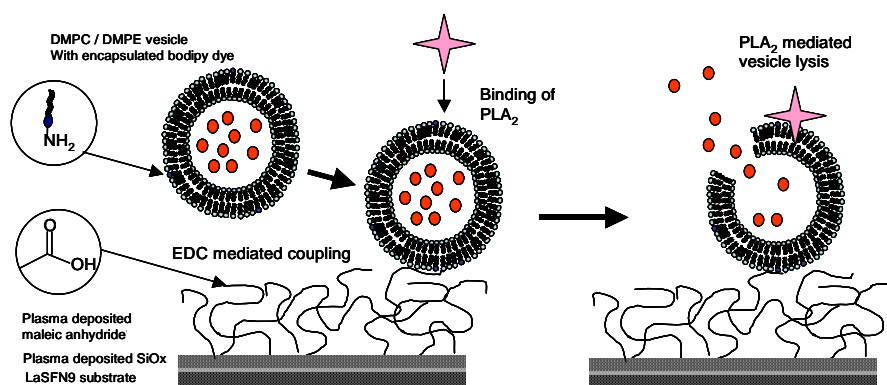

Figure 6-1: Schematic of the attachment of DMPC / DMPE vesicles to pp-MA-SiO$_2$ after immersion for 30 min in buffer, followed by lysis using PLA$_2$.

In this chapter of this work, an alternative method of attaching lipids to a pp-MA-SiO$_2$ multilayer will be presented. The aim is to immobilize whole vesicles rather than a bilayer or bilayer fragments to the surface of SiO$_2$ / pp-MA multilayer. The field enhancement of SPR was used to selectively enhance fluorophores contained within whole vesicles situated within the evanescent field close to the gold surface (< 250 nm). The vesicles were attached by coupling free amino groups on the phosphatidylethanolamine head groups in the bilayer with carboxylic acids groups in the hydrated pp-MA film using standard peptide coupling protocols. The technique of SPFS is has been explained in

chapter 3 of this work. A schematic of the system, showing the vesicle binding and lysis by PLA$_2$ is shown in Figure 6-1.

6.1.1 Preparation of DMPC-DMPE Vesicles and Encapsulation of Fluorophore

Lipid vesicles containing 95 mol% dimyristolyl phosphatidylcholine (DMPC) (Avanti, Alabster, USA) and 5 mol% dimyristoyl ethanolamine (DMPE) (Avanti, Alabster, AL) were prepared by mixing the dry lipid in chloroform, evaporation of solvent under vacuum and hydration in HEPES buffer at pH. 5.5 containing 1 μmol$\cdot$dm^{-3} bodipy dye (Invitrogen, U.K. (excitation $\lambda = 647$ nm). The mixture was extruded 11 times through 100 nm diameter pores in a polycarbonate membrane, before being cooled to 5° C and centrifuged at 500 rpm for 5 min. The lipid component pelleted at the bottom of the centrifuge tube, allowing removal of the supernatant containing excess fluorophore dye not contained within the vesicles. The lipid pellet was re-suspended in buffer containing no fluorophore dye.

6.1.2 Vesicle Attachment

The first measurements investigated the effect of plasma duty cycle on the degree of vesicle attachment onto the plasma films. Prior to vesicle attachment, films were immersed in HEPES coupling buffer for 30 min to ensure film swelling and hydrolysis of the MA groups to give carboxylic acid functionality. Vesicles were attached to the surfaces using EDC-NHS peptide coupling chemistry (Figure 6-1),[21] where the amino-functionalized PE lipid was conjugated to the carboxylic acid groups on the swollen pp-MA film. The pp-MA films were immersed in a freshly made solution of 0.1 mol$\cdot$dm^{-3} N-hydroxy succinamide (NHS) and 0.4 mol$\cdot$dm^{-3} ethylenedicarboimide (EDC) for 5 min in pH 5.5 HEPES buffer, prior to introduction of vesicles. Vesicles were coupled for up to 70 min, before rinsing. The coupling process was followed in real time by SPR. Measurements of vesicle lysis were all carried out on 1/41 duty cycle MA films, with fluorophore encapsulated within the vesicles. SPFS was used to determine the stability of the vesicles before and during lysis. Lysis of the vesicles was induced by the addition of phospholipase A$_2$ (PLA$_2$), (Worthington Biochemical, U.K.), which was added to the circulating buffer without stopping the continuous flow.

6.2 Results and Discussion

This section comprises of three sub-sections: formation of the SiO$_2$ / MA films by plasma deposition; an investigation into the optimum film plasma deposition conditions for vesicle attachment and finally, studying the effect of lysing the attached vesicles using PLA$_2$.

6.2.1 Plasma Film Fabrication and Characterization

HMDSO was plasma polymerized in the presence of oxygen using a gas ratio of 1:10 ($HMDSO:O_2$) at a process pressure of 0.2 mbar and an input power (cw) of 150 W. The final SiO_2 film thickness was 22 +/- 2 nm. XPS analysis of the SiO_x layer gave a stoichiometry of $SiO_{1.8}C_{0.2}$. In order to improve adhesion between the SiO_2 and the pp-MA film for subsequent measurements in aqueous medium, a short oxygen plasma pre-treatment (5 sec, 10 sccm 50 W) of the SiO_2 layer was used to activate the surface. Maleic anhydride was deposited using either low power cw (5W), or two different duty cycles (1/41 and 10/50) at 100 W input power. The process pressure during MA-deposition was 0.06 mbar and films were deposited with a thickness of 30 nm ± 3 nm.

The IRRAS spectra of films made from plasma polymerization of HMDSO / O_2 and MA films have been explained explicitly in chapter 5 of this work. For clarifications, Figure 5-4 shows the IR-bands typical of the pp-MA film on the SiO_2 –like film for the films fabricated under dc 1/41 at 100 W. Under this condition, the films show a high retention of the anhydride group, which can be hydrolyzed to carboxyl groups.[22]
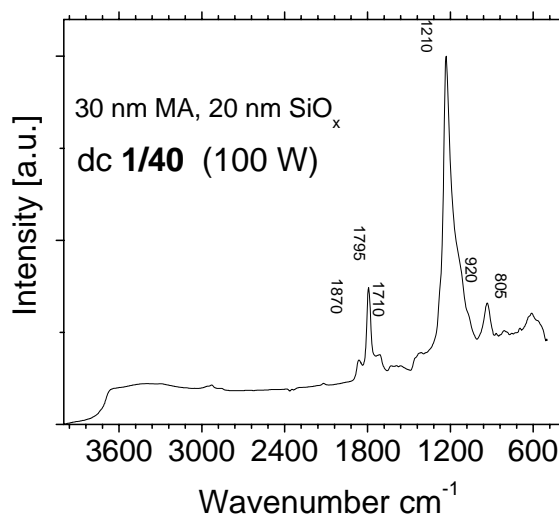

Figure 6-2: IRRAS measurements of SiO_2–MA films showing the retention of MA functionality of the pp-MA films. The pp-MA films on SiO_2-like surfaces were deposited at low duty cycle, dc 1/41 at 100 W input power.

6.2.2 Investigation into Vesicle Binding as a Function of Duty Cycle

Initially, it was necessary to determine whether the functional group density of the deposited films could be correlated to the relative degree of vesicle binding on the hydrolyzed pp-SiO_2-MA films. All films were immersed in HEPES buffer for 30 min prior to the surface activation with EDC / NHS. The process of EDC / NHS activation and vesicle attachment was followed in real-time using SPR, Figure 6-3. The initial increase in resonance angle seen between 10 and 20 min upon addition of the EDC / NHS coupling reagent may be related to chemical composition of the modified films. 1/41

films showed a greater initial change in resonance angle, probably due to a larger refractive index change on EDC activation compared to 10/50 and cw films. Vesicle binding was carried out following rinsing of the system with excess buffer after approximately 40 min. A clear increase in reflectivity is seen for the duty cycle films, but not for the film deposited under cw conditions. Since the change in SPR reflectivity is proportional to the change in surface mass density, it can be reasonably concluded that there is a decreasing degree of vesicle attachment on the 1/41, 10/50 relative to the cw film. This result correlates to a higher density of carboxylic acid groups in low duty cycle films and therefore suggests vesicles are being chemically attached via EDC / NHS coupling rather than simply adsorbing on the surface. A control experiment under identical conditions, but without EDC / NHS coupling, showed initial non-specific adsorption of vesicles as depicted in Figure 6-3, but these were rapidly removed on rinsing the flow cell with buffer.
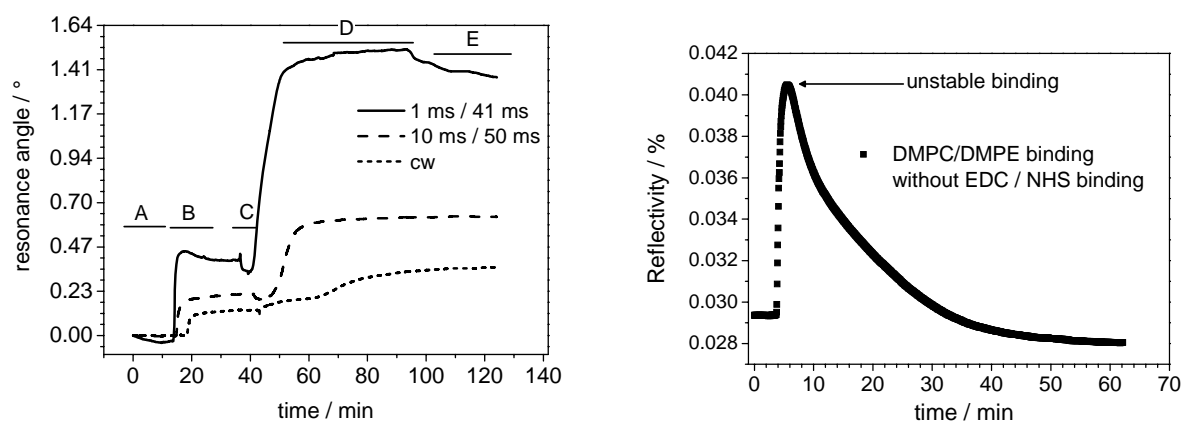

Figure 6-3: on the right: change in SPR resonance angle with time showing real-time attachment of DMPC – DMPE vesicles via EDC-NHS coupling as a function of plasma duty cycle. The PLA_2 caused rapid lysis of the adsorbed vesicles, clearly depicted as a decrease in both SPR resonance angle and loss of fluorescence. **A**: Equilibration in HEPES buffer, **B**: NHS/EDC surface activation, **C**: rinsed with HEPES buffer, **D**: DMPE/DMPC binding, **E**: rinsed with HEPES buffer. On the left: effect of binding DMPC - DMPE vesicles without EDC – NHS coupling on duty-cycle film measured as a change in reflectivity. The non – EDC / NHS bound vesicles do not bind irreversibly to the surface.

6.2.3 Lysis of Attached Vesicles by PLA_2 Enzyme

The next section of the study looked at vesicle attachment and lysis using combined SPR / SPFS. Vesicles were attached via EDC coupling to a hydrolyzed pp-SiO_2-MA film formed in a pulse 1/41 duty cycle plasma, with 2.5 W equivalent power. The increase in fluorescence and SPR angular shift on binding was measured and is shown in Figure 6-4. Once vesicles containing bodipy dye were attached, they appeared to be very stable, with no measurable leakage of dye prior to PLA_2 induced lysis. This compares favourably to SAM / streptavidin vesicle binding systems, where a significant loss of dye from immobilized vesicles can be observed.[21] After 320 minutes, phospholipase A_2 at a final concentration in the running buffer of 35 µg ml^{-1}, was added. A rapid decrease in both reflectance

and fluorescence was observed, indicating that material was being lost from the surface due to the action of the enzyme. The discontinuity in the graph, seen both in the SPR and fluorescence at about 420 minutes is not understood, but similar fluctuations have been observed on other measurements on these pp-MA supported vesicles. Measurements were running overnight without operator interference. This may be related to loss of poorly adhered polymer from the surface, possibly due to the continuous flow environment. The subsequent recovery in fluorescence could be due to re-adsorption of fluorophore into the polymer matrix.
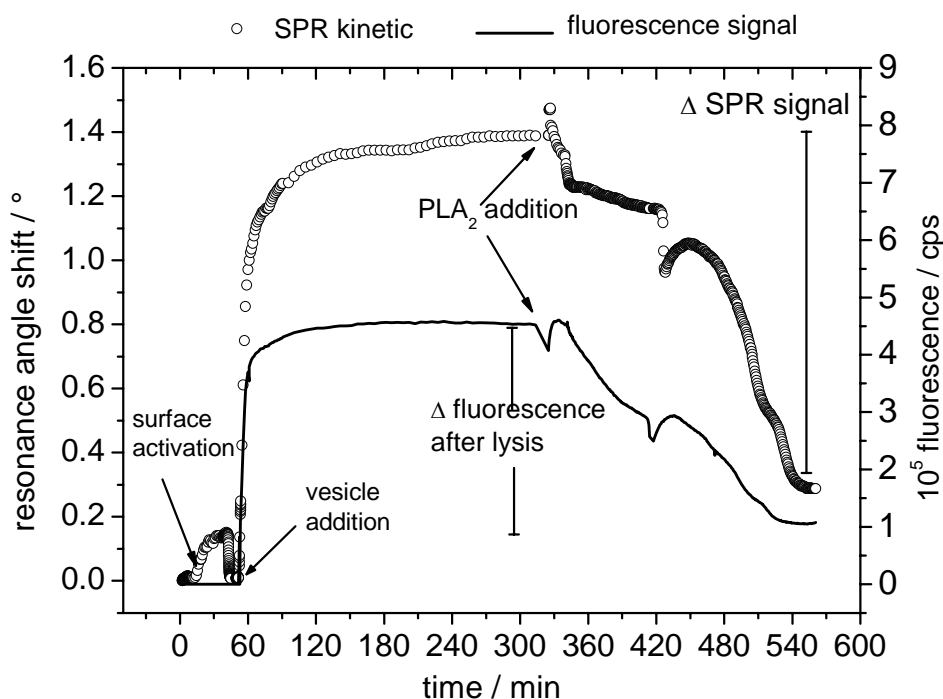

Figure 6-4: Combined SPFS / SPR measurements of the attachment of vesicles containing bodipy dye on a 1/41 pp-MA film and subsequent lysis by 35 μg ml^{-1} PLA$_2$. The change is calculated from the loss in fluorescence after and before adding PLA$_2$ enzyme.

The final part of this study examined whether there was a dose response effect on adding various concentrations of PLA$_2$ to the immobilized vesicles. The effect of adding different concentrations of PLA$_2$ on the loss of adsorbed vesicles expressed as a percentage decrease in resonance angle and fluorescence response of the adsorbed vesicle layer is shown in figure 6. An almost linear correlation between the change in SPR resonance angle and fluorescence response with PLA$_2$ concentration is observed, up to 55 μg ml^{-1} PLA$_2$, after which it appeared that all (or almost all) the vesicles were lysed. Although PLA$_2$ behaves catalytically when interacting with a membrane or vesicles (i.e. one enzyme can lyse many lipids); on the solid supported vesicle system studied here it is possible that a dose dependent (non-catalytic) response was observed. This would happen if the PLA$_2$ became

deactivated after vesicle lysis, either by irreversible interactions with the maleic anhydride substrate or because it was removed from the surface with departing vesicle fragments.

The change in SPR and fluorescence intensity was calculated as follows;

$$100 - \left[\frac{X \text{ intensity (after PLA}_2)}{X \text{ intensity (before PLA}_2)} \right] \cdot 100 \quad ;$$

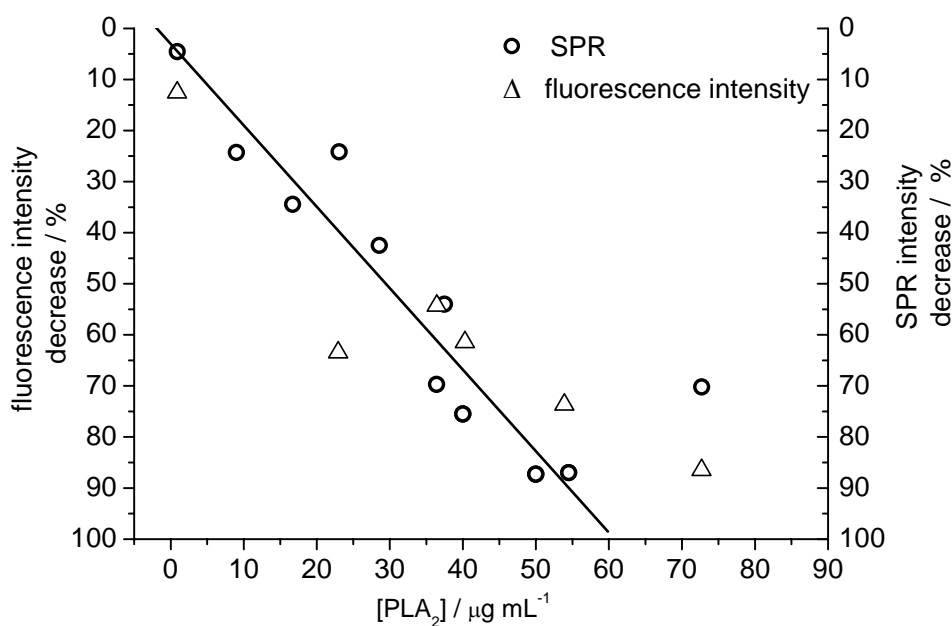whereby X represents SPR or fluorescence respectively.

Figure 6-5: The change in the fluorescence intensity and SPR intensity as function of the concentration of PLA2 added to the solid supported vesicle system. The vesicle lysis is dose dependent.

6.2.4 Conclusions[*]

In this chapter, it has been demonstrated that intact lipid vesicles containing a fluorescent dye could be covalently bound to pulsed plasma polymerized maleic anhydride – SiO_2 multilayers attached to gold substrates. It was shown that the degree of immobilization is dependent on the plasma duty cycle, which correlates the film chemical composition, as shown in chapter 5. SPFS and SPR measurements showed that vesicles appeared stable for over 600 minutes of measurement. Upon addition of the enzyme, PLA_2, which caused the attached vesicles to lyse, releasing the fluorescent dye encapsulated within them.

Such crude PLA_2 sensor could easily be adapted for the study of a range of membrane lysing toxins or for drug delivery purposes.

6.3   Reference

1.   Tien, H. T.; Ottova-Leitmannova, A., *Planar lipid bilayers and their applications,.* Elsevier: 2003.

2.   Berger, N.; Sachse, A.; Benderb, J.; Schubert, R.; Brandl, M., Int. J. Pharmaceutics. **2001,** 223.

3.   Jenkins, A. T. A.; Olds, J. A., *Chem. Comm.* **2004**.

4.   Xu, D.; Cheng, Q., *J. Amer. Chem. Soc.* **2002**, (124).

5.   Jung, L. S.; Shumaker-Parry, J. S.; Campbell, C. T.; Yee, S. S.; Gelb, M. H., Quantification of tight binding to surface-immobilized phospholipid vesicles using surface plasmon resonance: Binding constant of phospholipase A(2). *Journal of the American Chemical Society* **2000,** 122, (17), 4177-4184.

6.   Yoshina-Ishii, C.; Miller, G. P.; Kraft, M. L.; Kool, E. T.; Boxer, S. G., *J. Am. Chem. Soc.* **2005,** 127.

7.   Städler, B.; Falconnet, D.; Pfeiffer, I.; Höök, H.; Vörös, J., *Langmuir* **2004,** 20.

8.   Sanchez, S. A.; Bagatolli, L. A.; Gratton, E.; Hazlett, T. L., *Biophysical Journal* **2002,** 82.

9.   Williams, T. L.; Vareiro, M. M. L. M.; Jenkins, A. T. A., Fluorophore-encapsulated solid-supported bilayer vesicles: A method for studying membrane permeation processes. *Langmuir* **2006,** 22, (15), 6473-6476.

10. Rädler, J.; Strey, H.; Sackmann, E., *Langmuir* **1995,** 11.

11. Plant, A. L., *Langmuir* **1999,** 15.

12. Jenkins, A. T. A.; Bushby, R. J.; Evans, S. D.; Knoll, W.; Offenhäusser, A.; Ogier, S. D., *Langmuir* **2002,** 18, 3176-3180.

13. Tawa, K.; Morigaki, K., *Biophysical Journal* **2005,** 89, 2750-2758.

14. Tanaka, M.; Sackmann, E., *Nature* **2005,** 437, 656-66.

15. Sackmann, E.; Tanaka, M., *Trends Biotechnol.* **2000,** 18, 58-64.

16. Ryan, M. E.; Hynes, A. M.; Badyal, J. P. S., Pulsed plasma polymerization of maleic anhydride. *Chemistry of Materials* **1996,** 8, (1), 37-42.

17. Jacobsen, V.; Menges, B.; Forch, R.; Mittler, S.; Knoll, W., In-situ thin film diagnostics using waveguide mode spectroscopy. *Thin Solid Films* **2002,** 409, (2), 185-193.

18. Teare, D. O. H.; Schofield, W. C. E.; Roucoules, V.; Badyal, J. P. S., *Langmuir* **2003,** 19, 2398-2403.

19. Liu, S.; Vareiro, M. L. M.; Fraser, S.; Jenkins, A. T. A., *Langmuir* **2005,** 21, 8572-8575.

20. Jenkins, A. T. A.; Hu, J.; Wang, Y. Z.; Schiller, S.; Foerch, R.; Knoll, W., Pulsed plasma deposited maleic anhydride thin films as supports for lipid bilayers. *Langmuir* **2000,** 16, (16), 6381-6384.

21. Grabarek, Z.; Gergely, J., *J. Anal. Biochem.* **1990,** 185, 131-135.

22. Schiller, S.; Hu, J.; Jenkins, A. T. A.; Timmons, R. B.; Sanchez-Estrada, F. S.; Knoll, W.; Forch, R., Chemical structure and properties of plasma-polymerized maleic anhydride films. *Chemistry of Materials* **2002,** 14, (1), 235-242.

Chapter 7

7 Fabrication of nano-porous silicon-oxide films

*(This work has been published in Materials Letters 61 (**2007**) 1722 -1724.)*

Abstract

In this chapter, the well-known plasma assisted deposition of a silicon oxide layer from hexamethyl disiloxane (HMDSO) and oxygen with simple polymer colloid assembly on surfaces to obtain porous quartz like coating (SiO_x) is combined. The SiO_2 layers are deposited onto one or more sacrificial layers of poly methylmethacrylate (PMMA) colloids. Subsequent annealing of the films to high temperature (500°C) leads to the pyrolysis of the polymeric particles resulting in a 3D nano porosity in the SiO_2 film.

The morphology and thickness of the samples were analyzed by Scanning Electron Microscope (SEM, Leo Gemini) and Tencor Alpha Step 200 profilometer respectively. X-ray Photoelectron Spectroscopy (XPS) and Fourier Transformed InfraRed (FT-IR) spectroscopy were used to determine the chemical composition of the films. Ellipsometry was used to determine the refractive index.

7.1 Introduction

The demand for novel materials with unconventional properties have received great attention over the past decades.[1] While micro-porous membranes in the past have revolutionized sensor-, separation-, and biomedical technologies, the new trend has been towards nano-porous membranes, films and scaffolds in these same areas. The three dimensional structure of nano-porous films is particularly attractive for sensing and bio-material applications, since they do not only offer a larger sensing surface area, but also follow the need for continuously decreasing dimensions of sensing devices. Different technologies for the synthesis of these highly specialized materials have included methods based on sol-gel,[2, 3] spin coating, free radical aqueous polymerisation,[4] electrochemical anodic etching,[5-8] photochemical etching methods[9, 10] and laser ablation[11], but not much has so far been reported using plasma enhanced chemical vapour deposition methods to fabricate nano-porous layers.[12]

Nanoporous SiO_2 materials are used as anti-reflective coatings in optics and in electronics as low k-materials whereby relatively thin films are deposited on different kind of substrates.[4] These materials are also used as separation membranes for purification of fluids.[13] However, the use of these materials in the biological sector is still under development.[14] The application of inter-connected porous layers as bio-substrates would favor the control of cell growth and proliferation.[15]

This chapter concentrates basically on the fabrication of nano-porous SiO_2 films, which could be a potential material for bio-applications. Films were fabricated using Hexamethyl disiloxane as the monomer and poly(methylmethacrylate) colloids as the pore directing material. Plasma polymerization of the SiO_2 films was under excess oxygen plasma, and the removal of the colloids was carried out by pyrolysis.

The films characterized by SEM, FT-IR and Ellipsometry showed highly porous silicon oxide films generated from single and double layer of the colloids, which is solely responsible for the pore sizes and direction.

7.2   Sample Preparation

The samples were prepared by creating a sacrificial template of poly(methylmethacrylate) (PMMA) nano-particles (Postnova Analytics, Germany) on a substrate (Au on glass or Si-wafer) by spin coating an aqueous suspension of the polymeric nano-particles to obtain a single or double layer. The single layered PMMA nano-particles were obtained by dropping 0.5 µl of the aqueous suspension on a Si-wafer at 400 rpm, while the double layer was achieved with the same volume of suspension at 240 rpm. These templates were dried at ambient conditions and then were introduced into a 13.56 MHz low pressure plasma reactor, which has been described in chapter 4.[16] A mixture of HMDSO and O_2 (gas ratio of 1:10) was introduced into the reaction chamber and SiO_x layer was deposited at a pressure of 0.2 mbar, under input power of 140 W for either 30 seconds or 60 seconds. The 30 second deposition led to a 50 ($\pm$ 4) nm thick film and was applied to a single layer of nano-spheres on the surface, while the 60 second deposition, which led to a 100 ($\pm$ 6) nm thick film was used for the double layer of nano-spheres. The deposition parameters for the SiO_2 film deposition have been explained in details in chapter 4.

After the plasma polymerisation step the samples were placed in an oven under dry nitrogen and heated to 150°C within 1 hour and were kept at 150°C for 1 hour. After this time the temperature was increased at a rate of 50 °C/hour to 300 °C, then at a rate of 50 °C/hour up to 460 °C. The samples were tempered at both 300 °C and 460°C for 1 hour. The 100 nm thick samples, containing a double layer of PMMA nano-spheres, was subjected to a further temperature increase at a rate of 50 °C/ hour to 500 °C. Finally, it was kept at 500°C for 1 hour and then cooled to room temperature at a rate of 50 °C/ hour.

The film thickness was determined using a surface profiler (P-10, KLA Tencor, U.S.A.) on reference Si-wafers, which was used to acquire the optical data using the variable angle spectroellipsometer. This spectroellipsometer was operated at 5 different wavelengths (range ~ 611 – 650 nm) at 60° angle of incidence to determine the refractive index.

7.3   Results and Discussion

Figure 7-1 shows the SEM image of the assembled layer of a mono-dispersed nano-spheres. The magnified view (a) reveals a single layer closed packing of PMMA nano-spheres, which covers the substrate. The template material must fulfill several criteria in order to successfully create a porous material, e.g. melting temperature should be lower than the SiO_2-like film. The SiO_2 film deposited must be mechanically stable, to avoid collapse when the template is thermally removed.
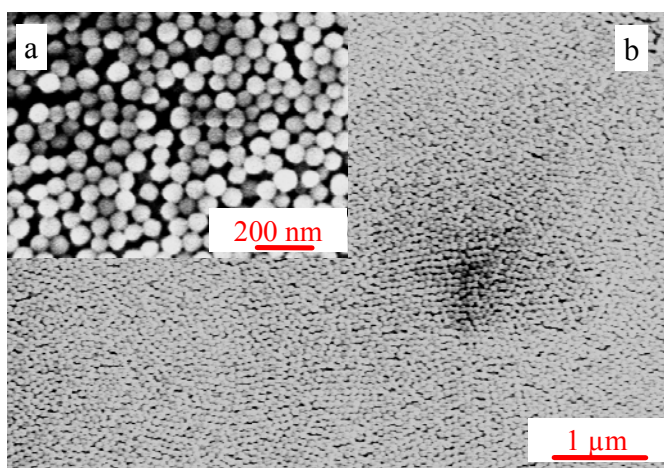

Figure 7-1: SEM images of a mono-layer PMMA template assembled on Si-wafer from a 50 nm PMMA nanosphere.

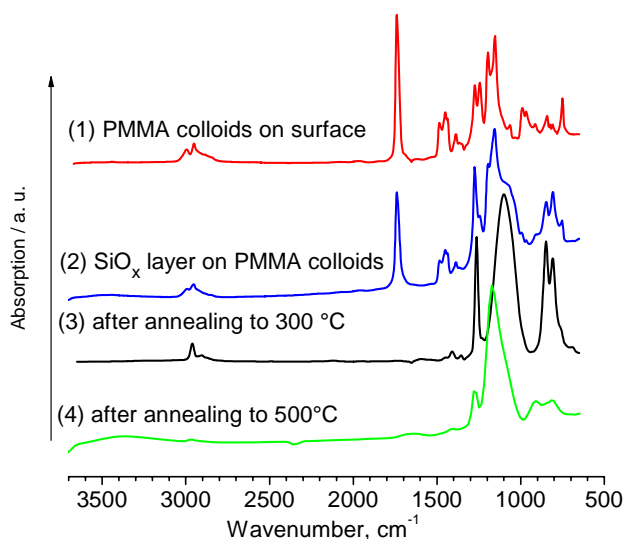## 7.3.1 Chemical Analysis of the Colloidal Template and SiO_x Film.

Figure 7-2: Infra-Red Absorption Spectra showing the film chemistry after each processing step

XPS analysis of the plasma deposited films only at these conditions gave a typical stoichiometry of $Si_1O_{1.89}$. as explained in chapter 4. To elucidate the chemical structure and composition of the porous films, FT-IR analysis was carried out in the transmission mode.

The FT-IR spectra of the films after the various preparation steps are shown in Figure 7-2. The PMMA nano-spheres on the surface of the Si-wafer gave the typical absorption bands for the polymer, denoted as spectra (1). The regions mainly characterized the PMMA material, between $1150 - 1300$ cm^{-1}, where the carboxylic group occurs, and around $1450 - 1600$ cm^{-1} the in-plane C-H stretches appear, additionally the acrylate band appears around 1745 cm^{-1} and the -CH$_3$ stretch region can be seen between $2850 - 3035$ cm^{-1}. After plasma deposition of a SiO$_x$ layer the spectrum is a mixture of the PMMA and a SiO$_2$ spectrum. Furthermore, the characteristic Si-O peak appeared at 1100 cm^{-1}, and Si-CH$_3$ absorption band at 1275 cm^{-1} as a result of the HMDSO fragmentation. Compared to IRRAS measurements (measured on Au substrates), the shift of the Si-O-Si to lower wavenumber in the transmission mode is related to the incidence of the IR light, which has been explained in chapter 4.

After annealing to 300 °C, spectra (3), the peak at 1740 cm^{-1}, originating from the acrylate groups in the PMMA, disappeared indicating that the polymer colloids were already undergoing pyrolysis at this temperature. The presence of low intensity peaks around 3000 cm^{-1} and the relatively high intensity bands between 800 and 900 cm^{-1} still indicate the presence of some hydrocarbon character. A further temperature increase to 460 °C and to 500 °C, spectra (4) led to a complete removal of the typical PMMA fingerprint bands as shown in spectra (1). The obtained spectra after annealing demonstrates complete removal of the PMMA nano-spheres, thus a spectrum typical of plasma deposited SiO$_x$ layers from HMDSO/O$_2$ was achieved. The residual Si-CH$_3$ absorption band observed at 1275 cm^{-1} is probably due to residual carbon within the SiO$_x$ deposit, which was unable to diffuse out of the nano-porous film.

7.3.2 Film Morphology Characterized using SEM

Scanning electron microscopy (SEM) images of the surface of the single layer of PMMA nano-sphere embedded in SiO$_x$ and annealed at 460 °C showed a ripple structure on the surface at low magnification, which may suggest subsurface nano-channels left behind by the PMMA nano-spheres, as shown in Figure 7-3 (a). A 10 and 20 fold increase in the magnification shows the surface to have many holes of circular and elongated shape and the outlines of mostly spherical structures below the surfaces can be observed, Figure 7-3 (b) and (c) respectively. A side view of the film, Figure 7-3 (d) confirms that pores left behind by the PMMA nano-spheres, are inter-connected and others appear to be isolated.
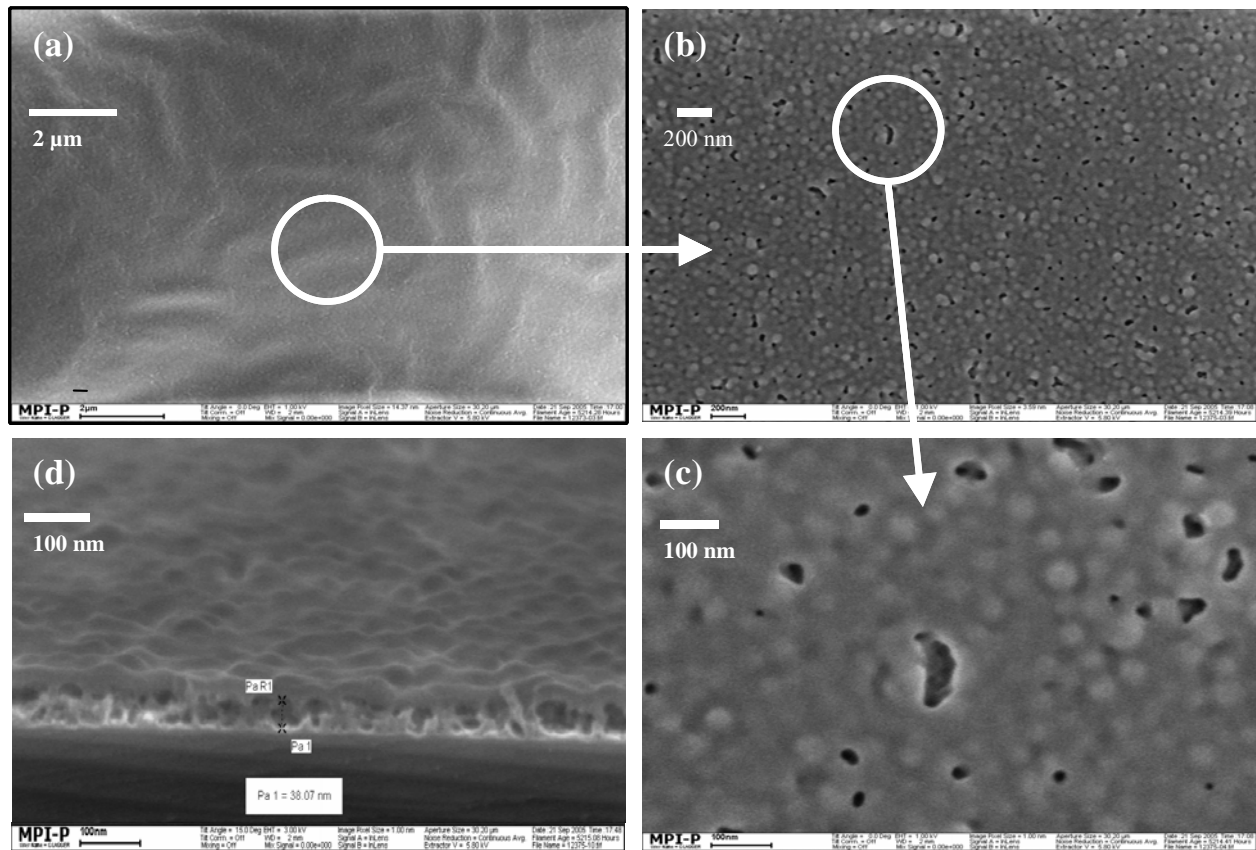
Figure 7-3: SEM micrographs under different magnification of (a) a plasma deposited SiO$_x$ layer with embedded single layer of PMMA nano-spheres, (b) after annealing to temperatures of 460°C to obtain nano-porous films, (c) magnified top-view of micrograph "b", (d) cross-sectional view nano-porous film.

The refractive index of the single layer annealed to 500 °C was found to be 1.242, which lies well between typical refractive indices of PMMA (n $_{PMMA}$ ≈ 1.5), quartz (n $_{SiO_2}$ = 1.42) and interstitial air in the cavities (n $_{air}$ ≈ 1).
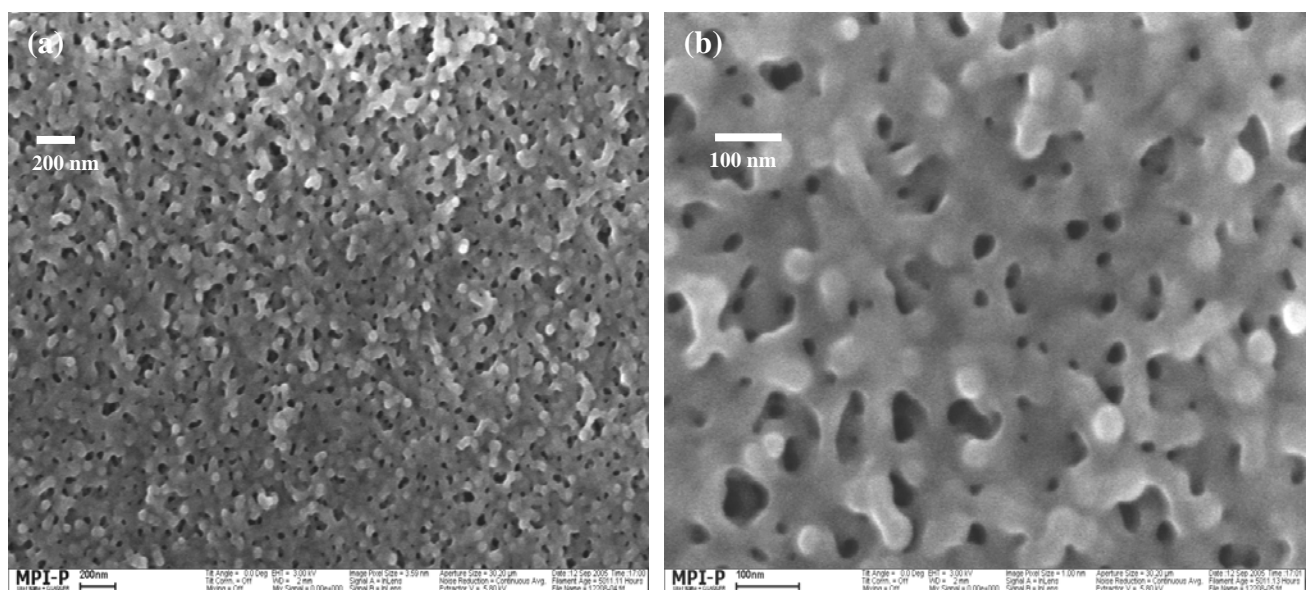

Figure 7-4: SEM micrographs of a plasma deposited SiOx film with two layers of embedded PMMA nano-nano-spheres after annealing to temperatures of 500 °C.

Figure 7-4 depicts the samples fabricated using two layers of PMMA nano-spheres covered by the SiO_2 –like layer, then followed by annealing to a temperature of 500 °C. The micrographs indicate that the porosity of the SiO_x layer has been enhanced due to the pyrolysis treatment, whereby a fairly irregular 3 dimensional nano-porosity is formed.

7.4   Conclusions

In this chapter of this thesis, a relatively easy method to synthesise nano-porous films with a high surface area-to-volume ratio has been presented. This was done by the pyrolysis of organic nano-spheres inclusions within a plasma deposited silicon oxide layer. By careful choice of deposition conditions, it was possible to deposit a single and double template layer. This is required to fabricate nano-porous films with different degrees of porosity.

Due to the pyrolysis of the PMMA nano-spheres beneath the SiO_x –like layer plasma polymerised from HMDSO and O_2, nano-porous SiO_x films or scaffolds with different pore sizes were achieved.

Bearing in mind that these SiO_2 –like nano-porous films are mechanically stable and can be post-treated with oxygen plasma to yield hydrophilic surfaces, makes them a potential substrate in the biological sensor sector, for example a support for lipid bilayers, or vesicles, and cell growth, which will improve their lateral stability due to the defined pore sizes.[15] The application of such nano-porous films is also favored by its environmental and economical advantages.

7.5   References

1.   Kresge, C. T.; Leonowicz, M. E.; Roth, W. J.; Vartuli, J. C.; Beck, J. S., Ordered Mesoporous Molecular-Sieves Synthesized by a Liquid-Crystal Template Mechanism. *Nature* 1992, 359, (6397), 710-712.

2.   Zhong, S. H.; Li, C. F.; Li, Q.; Xiao, X. F., Supported mesoporous SiO_2 membrane synthesized by sol-gel-template technology. *Separation & Purification Technology* 2003, 32, (1-3), 17-22.

3.   Zhang, J.; Palaniappan, A.; Su, X. D.; Tay, F. E. H., Mesoporous silica thin films prepared by argon plasma treatment of sol-gel-derived precursor. *Applied Surface Science* 2005, 245, (1-4), 304-309.

4.   Zhao, Q. C.; Chen, W. M.; Zhu, Q. R., Preparation of nanoporous SiO_x materials via interpenetrating polymer network method. *Materials Letters* 2003, 57, (22-23), 3606-3608.

5.   kim, D. A.; Kwon, Y. J., *Appl. Surf. Sci.* 2004, 239, (124).

6.   Ohl, A.; Schroder, K.; Keller, D.; Meyer-Plath, A.; Bienert, H.; Husen, B.; Rune, G. M., Chemical micropatterning of polymeric cell culture substrates using low-pressure hydrogen gas discharge plasmas. *Journal of Materials Science-Materials in Medicine* 1999, 10, (12), 747-754.

7.   Ohl, A.; Schleinitz, W.; Meyer-Sievers, A.; Becker, A.; Keller, D.; Schroder, K.; Conrads, J., Design of an UHV reactor system for plasma surface treatment of polymer materials. *Surface & Coatings Technology* 1999, 119, 1006-1010.

8.   Kim, D. A.; Im, S. I.; Whang, C. M.; Cho, W. S.; Yoo, Y. C.; Cho, N. H.; Kim, J. G.; Kwon, Y. J., Structural and optical features of nanoporous silicon prepared by electrochemical anodic etching. *Applied Surface Science* 2004, 230, (1-4), 125-130.

9.   Canham, L.; Slinger, C., Porous silicon lights up micro-optics. *Physics World* 1997, 10, (10), 24-24.

10. Cullis, A. G.; Canham, L. T.; Calcott, P. D. J., The structural and luminescence properties of porous silicon. *Journal of Applied Physics* 1997, 82, (3), 909-965.

11. Yang, D. Q.; Meunier, M.; Sacher, E., The surface modification of nanoporous SiO_x thin films with a monofunctional organosilane. *Applied Surface Science* 2005, 252, (5), 1197-1201.

12. Wu, Q. G.; Ross, A. D.; Gleason, K. K., Nanoporous organosilicate glass films via chemical vapor deposition onto colloidal crystal templates. *Plasma Processes & Polymers* 2005, 2, (5), 401-406.

13. Bao, X. Y.; Zhao, X. S.; Li, X.; Li, J., Pore structure characterization of large-pore periodic mesoporous organosilicas synthesized with varying SiO2/template ratios. *Applied Surface Science* 2004, 237, (1-4), 380-386.

14. Stylios, G. K.; Giannoudis, P. V.; Wan, T., Applications of nanotechnologies in medical practice. *Injury, Int. J. Care Injured* 2005, 36S, 8.

15. Baker, S. M.; Kolthammer, W. S.; Tan, J. B.; Smith, G. S., Nanoporous thin films and porous inorganic substrates for lipid bilayer support materials. *Zeitschrift Fur Kristallographie* 2004, 219, (3), 179-185.

16. van Os, M. T.; Menges, B.; Foerch, R.; Vancso, G. J.; Knoll, W., Characterization of plasma-polymerized allylamine using waveguide mode spectroscopy. *Chemistry of Materials* 1999, 11, (11), 3252-3257.

<div align="right">

Chapter 8

</div>

8 Investigating the Aging and Stability of Plasma Polymerized SiO$_x$C$_y$ films fabricated using Industrial Processes

(in collaboration with Leybold-Optics, Alzenau, Germany)

Abstract:

A comparative study with respect to the aging and stability of plasma polymerized films fabricated using laboratory and industrial processes will be presented in this chapter.

Three different industrial reactors and the laboratory reactor presented in chapter 3 were used for the fabrication of SiO$_2$-like films. The films fabricated using industrial reactors (L400, D1V and PylonMet) were carried out at Leybold Optics, Alzenau, Germany. Both Hexamethyl disiloxane (HMDSO) and tetramethyl disiloxane (TMDSO) monomers in the presence of excess oxygen were used separately for the film deposition.

The ageing and stability in air of all the films were monitored during storage in air using Fourier Transformed InfraRed (FT-IR) spectroscopy, Scanning Electron Microscope (SEM), and X-ray Photoelectron Spectroscopy (XPS).

The results showed that the morphology of the plasma polymerized films ranged from porous to pore-free films, rough to smooth films and some changes in their chemical composition. These discrepancies could be related to the difference in chemical structure of both monomers, the different deposition conditions implemented and the deposition volume for each reactor. Also, the different chemical compositions of the films obtained from the industrial reactors were monitored upon aging in air, and their stability ranged from stable to less stable for the period measured.

8.1   Introduction

When a plasma polymer is exposed to atmospheric conditions, the free radicals trapped in the polymer can react with oxygen and water vapor, and to some extent the radicals may also recombine. The oxygen reaction follows the same fundamental mechanism described by Bolland and Gee in the late 1940's,[1-4] which is based on the fact that any active sites remaining on the surface are prone to undergo oxidation reactions.[5] Such reactions might lead to the restructuring of the surface due to the tendency of the polymer to achieve an energetically favorable state by oxidative diffusion processes.

It is therefore important to study the aging and stability of plasma deposited organosilicon films, which are presently used in many domains, e.g. protective coatings, optical devices, integrated optics, semiconductor devices, transducer coatings and biomedical applications.

From the few investigations on the long-term stability of organosilicon addressed, the aging of a plasma polymer depends on the structure of the monomer and the conditions of the plasma polymerization, which include the design of the plasma reactor.[6-8] A. Wroebel used attenuated total reflection infrared (ATR-IR) spectroscopy to monitor structural changes in coatings deposited from three monomers: hexamethyl disilane (HMDS), hexamethyl disiloxane (HMDSO) and hexamethyl disilazane (HMDSA). The IR data revealed the formation of –OH, > C=O, Si–O–Si and Si–O–C groups and the decay of Si-H groups to be general trends in the aging of the three materials polymerized. The aging of the films was related to reactions of atmospheric oxygen and water with alkyl and silyl radicals as well as with other reactive bonds present in the plasma polymers after deposition.[6, 9]

Other authors have investigated the oxidative aging or oxygen uptake of polymers by characterizing the surface properties. The effects of any chemical change on surface properties were followed by contact angle measurements, and were found to consist of an increase in the polar component over storage time.[10, 11]

Both precursors used here are advantageous over other organosilicon precursors because of the non-toxic nature and low vapor pressures. The organosilicon monomers provide long-term stability due to the presence of the siloxane (Si-O-Si) bond, whereby the side groups on the siloxane unit determines the film network structure, when plasma poymerized.

Upon subjecting both monomers to plasma conditions, the abstraction of methyl groups is the major activation mechanisms to form a cross-linked siloxane network. Thus, the stable Si-H group might be retained in pp TMDSO film. The occurrence of a Si-H group within the polymer network would lead to the so-called "network-breakers", because H-atoms are unable to form more than one covalent bond within the network and the ability to react with water molecules upon exposure to atmosphere to form –OH groups. The effects of H-atoms within siloxane networks have been explained by Wertheimer and other authors.[12, 13]

The chemical structures of the monomers used for the film deposition in this chapter are shown in Figure 8-1.
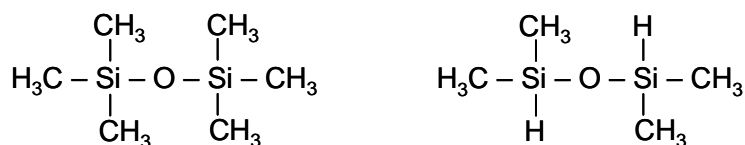

Figure 8-1: chemical structures of HMDSO (left) and TMDSO (right). The main difference is the presence of Si–H bonds in the TMDSO molecule.

A theoretical representation of the plasma polymerization of both monomers is shown in Figure 8-2, whereby the network breaker is denoted by the presence of H-atom for the pp TMDSO film. The

presences of trapped oxygen radicals within both networks are prone to further reactions during storage.
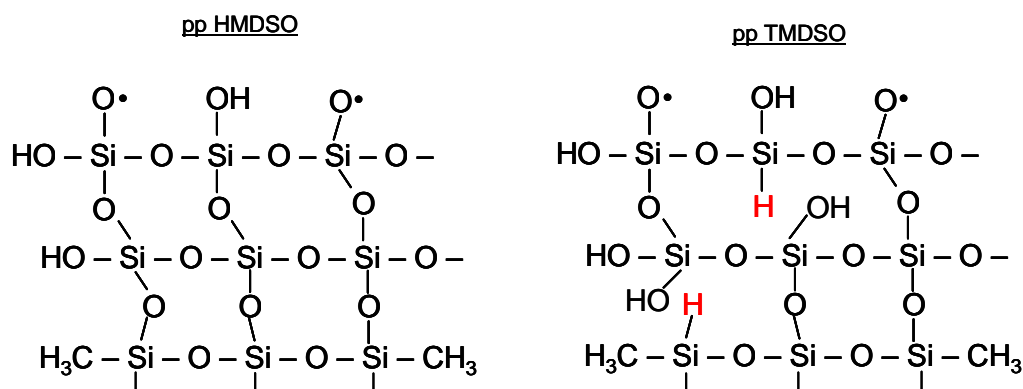

Figure 8-2: theoretical representation of the plasma polymerized HMDSO and TMDSO monomer. The TMDSO network shows presence of H-atoms (network-breaker), thus defects within the siloxane network.

The films investigated here were fabricated at Leybold Optics using the industrial reactors, which are currently used in diverse applications in the packaging, automobile, and optical industries. A concrete investigation of the chemical and structural properties of the films synthesized at Leybold Optics has so far not been carried out to understand any possible aging during storage.

Therefore, this chapter presents the aging and stability in air of some of the films fabricated using the different reactors, whereby a correlation between the process parameters and the chemical properties will be explained in this study.

In this comparative study, the films were deposited from HMDSO and TMDSO monomers under the conditions stated in Table 8-1. It is well known that high plasma power leads to extensive monomer fragmentation in the glow discharge, and consequently, to films of a more or less inorganic nature.[7, 14] The films were characterized using FT-IR, supported by XPS which provides quantitative information on the amounts of chemical groups present in the film. Furthermore, the film morphology was examined by SEM, which showed the surface and cross-sectional views of the deposited films. The experiments are divided into different processes, which will be treated separately.

"Process 1" was designed for the fabrication of SiO_2-like films in the lab, which has been optimized by numerous experiments as explained in chapter 4. The aging and stability of these films were monitored up to 300 days storage in air.

The industrial fabrication ("Process 2") gave valuable information regarding the influence of the process parameters on the morphology, which showed porous siloxane films fabricated from TMDSO / O_2. The films showed instability upon storage as compared to "Process 1". Likewise the laboratory process, HMDSO monomer was plasma polymerized in excess oxygen in "Process 3". The SiO_2 –like films obtained were stable with reference to all the other films deposited using the industrial process.

In "Process 4", the deposited SiO_2 –like coatings from HMDSO / O_2 were stable for the period monitored. This was also confirmed by IR spectra and SEM micrographs, no signs of aging was observed during the storage period.

8.1.1 Sample Preparation

All the samples were kept in open sample boxes in the laboratory, at an average room temperature (22 ± 2 °C), with an average relative humidity value of about 40 ± 8 %.

	Laboratory process	Industrial processes		
	Process 1	Process 2	Process 3	Process 4
Reactor name	MPIP 2	L 400	D1V	PylonMet 1V
Monomer: gas ratio	HMDSO: O_2 1: 10	TMDSO: O_2 180: 900	HMDSO: O_2 200: 10000	HMDSO: O_2 150:750
Input power	100 W	4 x 1.1 kW	4 x 3 kW	5 kW
Frequency	RF (13.56 MHz)	MW (4 transmitter x 2 kW)	MW (4 transmitter x 3 kW)	Mid-frequency 40kHz (1 transmitter x 5 kW Plate electrode
Deposition rate /nm sec^{-1}	1.32	40	7.2	1.17
pre-treatment	5 sec (O_2 plasma)	30 sec (TMDSO)	60 sec (Ar + HMDSO)	30 sec (Ar plasma)
Monomer pressure / mbar	0.2	0.5	0.5	0.05
Thickness	40-45 nm	600	1300	920

Table 8-1: summary of process parameters implemented for fabrication processes.

The substrates used for the plasma deposition were Si(100)-wafer and Polycarbonat (Makrolon, Bayer), whereby both substrates were used for the XPS and SEM analysis, and only Si-wafer was used for the FT-IR characterization due to its optical properties.

The plasma deposition conditions are stated in Table 8-1. In the laboratory process, the radio frequency (RF) 13.56 MHz plasma reactor described in chapter 3 was used. Industrial plasma microwave (MW) reactors, L 400 and D1V and the PylonMet 1V which was operated at a mid-frequency of 40 kHz were used at Leybold Optics for the film deposition in Process 2, Process 3 and Process 4 respectively.[15]

L 400 is equipped with 8 Duo-Plasma lines, which consist of 4 MW transmitters powered by 2 kW each. The distance between the plasma tubes and the substrate is 30 cm and the total deposition area is about 300 mm x 300 mm.

The D 1V reactor is similar to L 400, whereby the transmitters in D 1V are powered by 3 kW each, which has a larger deposition area of about 400 mm x 800 mm. The plasma tubes and the substrate are built 20 cm apart. The commercial reactor, PylonMet 1V has 2 plate electrodes in a cylindrical rotary cage, which is operated with one transmitter at a mid-frequency at 40 kHz, and has a deposition area of about 1.5 m^2. A summary of the process parameters are stated in Table 8-1.

8.2   Results and Discussion

First, the data of the films fabricated using the laboratory process conditions will be presented, and secondly the results from the industrial processes will explained.

8.2.1 Laboratory Fabrication (process 1)

X-ray Photoelectron Spectroscopy (XPS)

The detail scan surveys from the XPS analysis of the deposited film contain C, O, Si, i.e. the constituent elements of the HMDSO monomer, enabled the comparison of their composition. A minor change of the atomic concentration of silicon was observed over the period measured (32.1 % $\pm$ 0.7). The atomic ratio of the carbon/silicon (C/Si) and the oxygen/silicon (O/Si) was 0.3 and 1.75 respectively after deposition as seen in Figure 8-4. Both ratios show a minor increase, which can not be related to the phenomena proposed by H. Yasuda, B. Muir and T. Gegenbach, which states an increase in the oxygen content in plasma polymer during storage can be attributed to reactions between trapped, carbon-centered radicals in the plasma polymer with O_2 diffusing into the material.[7, 16, 17] For over 300 days of storage, the C/Si atomic ratio showed an increase of 0.04, which is far below the experimental error. The peak shapes and widths of the O 1s and C 1s photoelectron peaks remained unchanged, indicating insignificant change in the chemical environment over the storage period occurred.

The C 1s, O 1s and Si 2p high resolution XPS spectra were studied in detail to identify the chemical binding states for pp HMDSO films. Usually, the C 1s binding energy (BE) of aliphatic hydrocarbons (285.0 eV) is used in the surface analysis of polymers as an internal reference value.[18] For organosilicon polymers, the C 1s BE for CH_3-Si is lowered due to the adjacent silicon to 284.4 eV.[19, 20] This binding energy was used for the analysis of the C 1s spectra in the SiO_2 –like films in this work. The O 1s species in the chemical environment of the pp HMDSO film was identified at a BE of 533.9 eV ($\pm$ 0.23 eV) as shown in Figure 8-3. These species were observed during the storage period up to 300 days, which showed minimal decrease in intensity, which lies within the experimental error

range. Similarly, the mean BE of Si 2p in the chemical species of the pp-HMDSO was measured at 103.2 eV ($\pm$ 0.25 eV), which represents the $Si(-O)_3C_1$ chemical configuration.[20, 21]

Figure 8-4 shows the atomic ratio change over storage time of the pp HMDSO films, at the conditions stated in Table 8-1. The C/ Si and O /Si ratios show insignificant changes, which are within the experimental error range. This further confirms the stability of the films fabricated by "Process 1" for over the storage time measured.
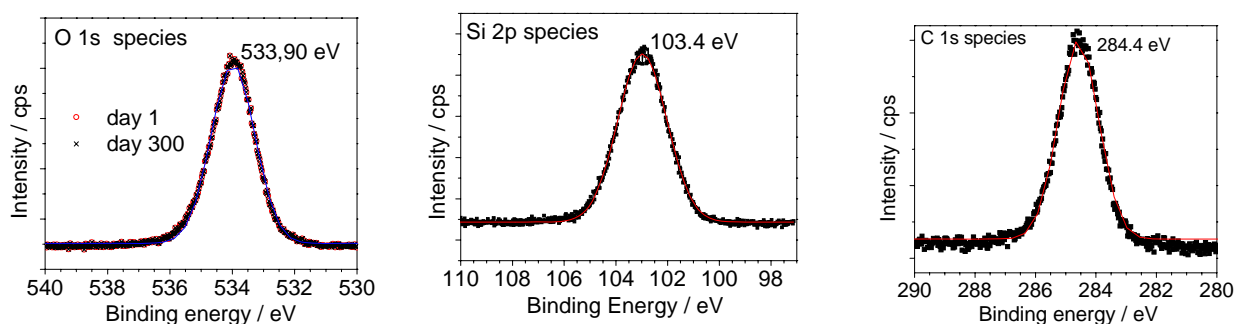

Figure 8-3: O 1s, C 1s and Si 2p high–resolution XPS spectra of pp HMDSO /O_2 (1:10) films at 100 W and were treated with O_2 plasma for 5 sec under 50 W. Films were stored for over 300 days under ambient conditions in the laboratory.
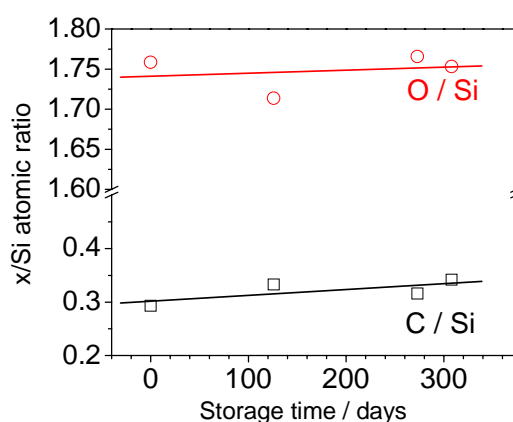

Figure 8-4: XPS C /Si and O /Si atomic ratios as a function of storage time under ambient conditions for pp HMDSO /O_2 (1:10) films at 100 W and were treated with O_2 plasma for 5 sec under 50 W.

Chemical Composition Analyzed using FT-IR

From the previous experiments carried out using HMDSO/O_2, it was observed that less than 10 % atomic C was present in the films fabricated above 100 W input power (see chapter 4). Aging has been reported to occur for films with less than 10 % atomic C. [4, 22, 23] Thus, 100 W input power was chosen to ensure retention of some % atomic C and the monomer structure in the resulting polymeric film, which may be available for any possible aging reactions, i.e. if the film is not stable.

Figure 8-5 shows the spectra of the pp HMDSO films after 300 days of storage. The main peaks detected by the IR in the films are the Si–O–Si stretching vibration and the absorption associated

114

$Si(CH_3)_x$ species at 1223 cm^{-1} and 931 cm^{-1} respectively. These groups were stable for over 300 days of storage.

Furthermore, Figure 8-6 shows SEM micrographs of pore free films fabricated by the laboratory procedure, did not reveal any differences of the surface and bulk structures between the freshly deposited film (day 0) and after about 305 days of storage.
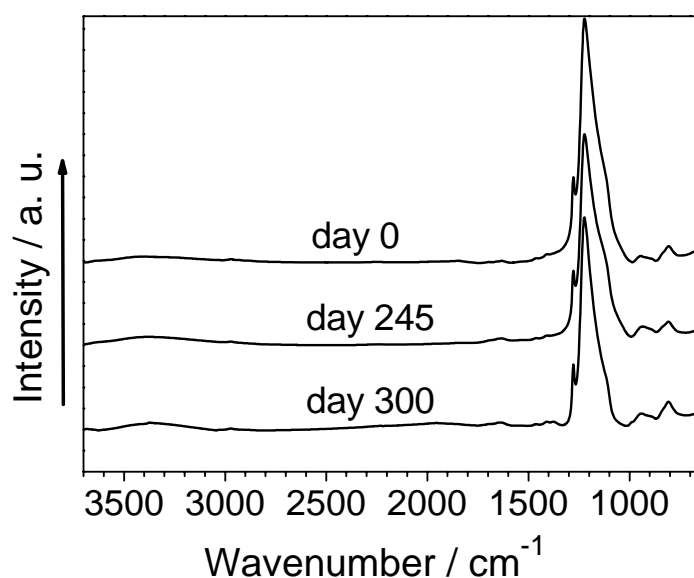

Figure 8-5: plasma polymerized HMDSO/O$_2$, (1:10) under 100 W, and surface treated with oxygen plasma for 5 sec, under 50 W input power.
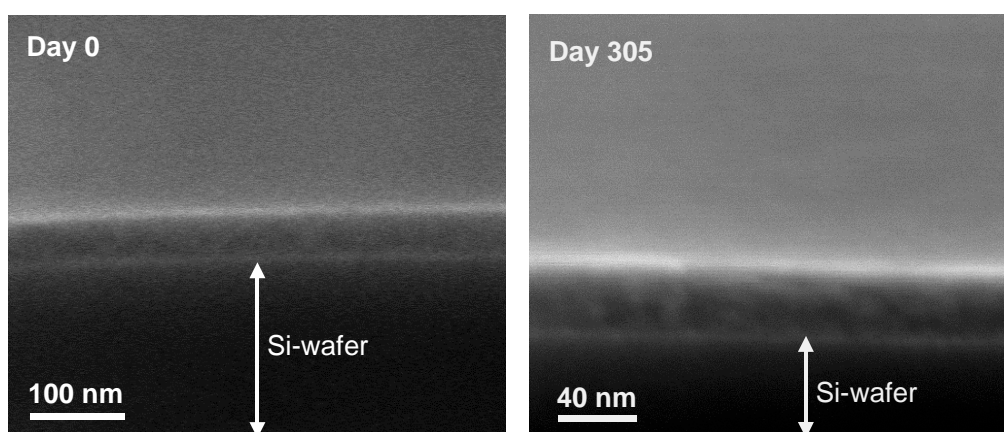

Figure 8-6: SEM micrographs of cross-sectional view of SiO$_2$-like film (100 W, 1:10)

8.3   Industrial Fabrication Processes

In this section, the plasma films fabricated using process 2 (L 400 reactor), process 3 (D 1V reactor) and process 4 (PylonMet 1V) will be presented.

8.3.1 Process 2 (L 400)

Figure 8-7 shows the SEM micrographs of the pp TMDSO/O_2 films. The top view shows a rough surface morphology with few defects such as pinholes. Close to the substrate, an adhesion layer (pinhole free) can be seen of about 40 nm that was first deposited in a pre-treatment step, (30 sec, TMDSO plasma, "gradient layer"). The structural morphology of the films may be related to the high deposition pressure implemented because of the high TMDSO /O_2 ratio for a small deposition area of about 0.9 m^2.

The side views of these micrographs show a thin film of the TMDSO formed during the pre-treatment step (30 sec TMDSO), whereafter the process destabilizes for a while and a porous structure could be seen. This porous section of the film was also noticed after 21 days of storage. The film starts to delaminate from the substrate deposited, as seen in Figure 8-8. However, it is difficult to analyse quantitatively the change in porosity upon storage. The FT-IR method was used for the quantitative chemical analysis of these films, as shown in Figure 8-9.
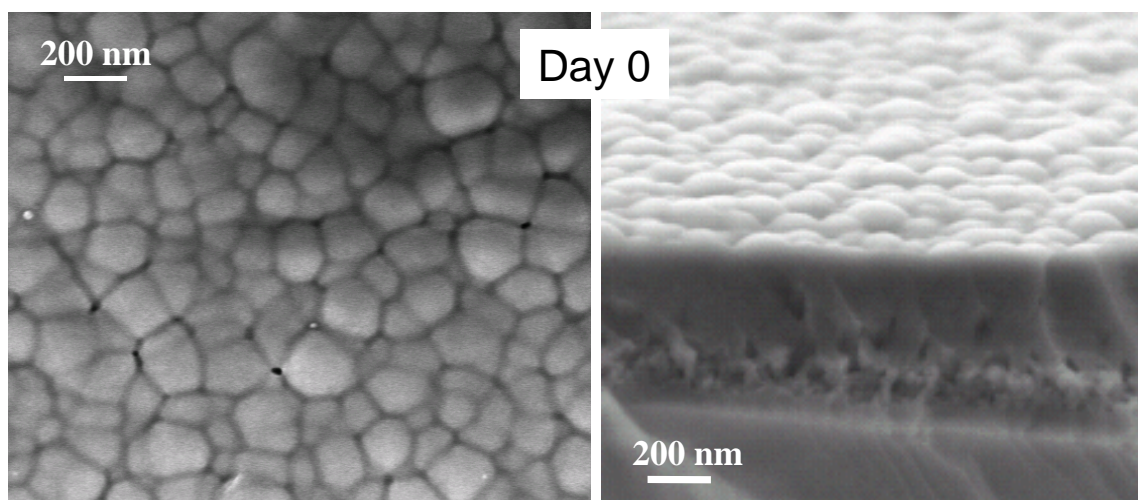

Figure 8-7: top and cross sectional views of freshly deposited pp TMDSO/O_2 by the process 2, showing the adhesion layer and pores formed at the early stage of film deposition.
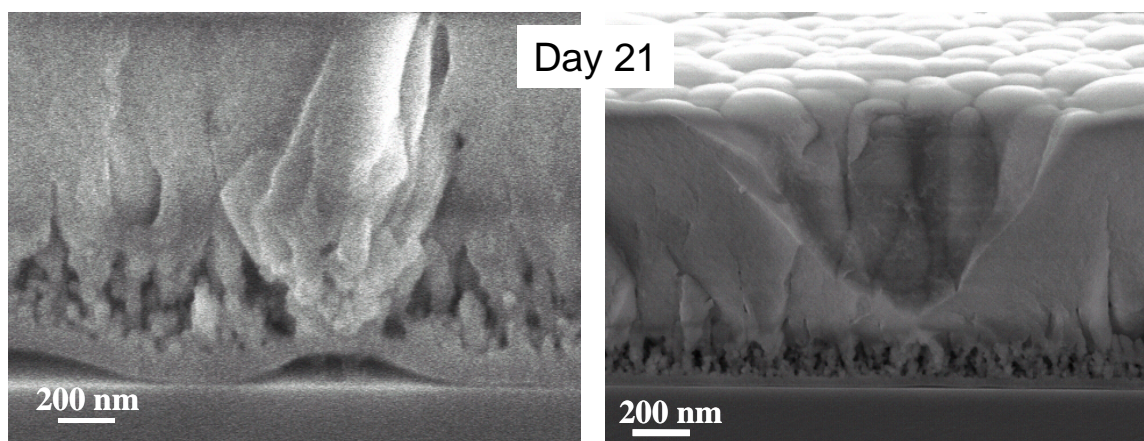

Figure 8-8: micrographs of pp TMDSO films after 21 days of storage in air, the delamination from the substrate occurred after 21 days of storage.
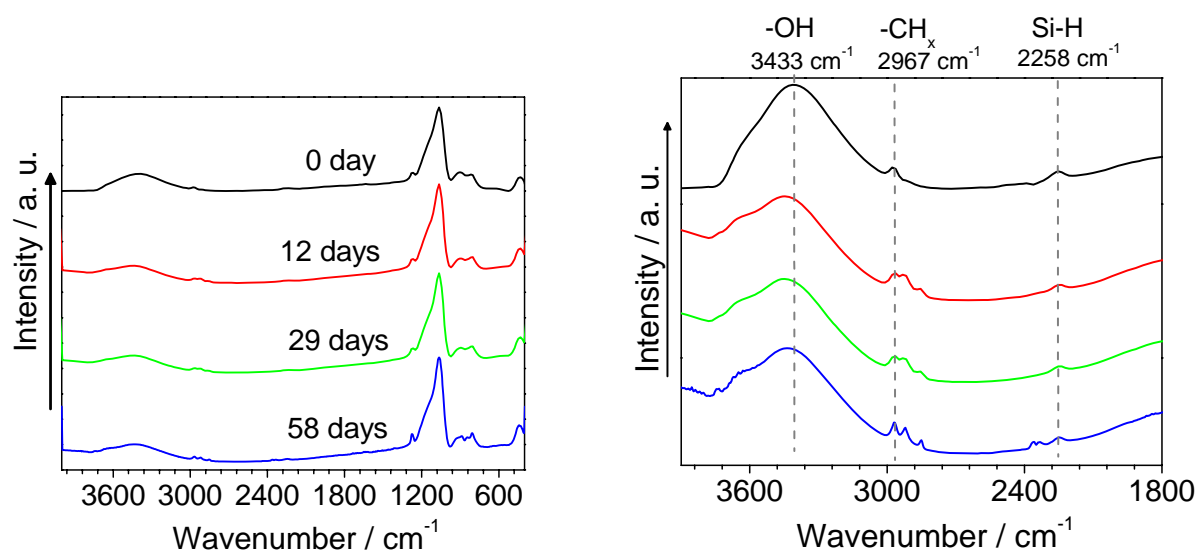
116

Chemical Characterization

Figure 8-9: FT-IR spectra of TMDSO recorded at different storage time as indicated. The spectrum of the freshly deposited film (0 day) is included for comparison.

The compositional changes observed during storage of the pp TMDSO film by FT-IR are presented in Figure 8-9. A broad absorption band between 1202 cm^{-1} and 987 cm^{-1} due to the Si-O-Si stretching vibration and a group of absorption band between 940 cm^{-1} and 430 cm^{-1} originating from various vibrational modes of the $Si(CH_3)_x$ structure and the Si–OH (907 cm^{-1}) absorption could be seen from spectra. The –OH band intensity (3430 cm^{-1}) decreased over the time measured, and the $Si(CH_x)_x$ absorption band (1260 cm^{-1}) was relatively constant. The Si-H absorption spectra seen around 2258 cm^{-1} decrease gradually upon storage while the -CH$_x$ (2967 cm^{-1}) peak increases. The presence of the Si-H groups indicates the insufficient oxidation reaction of the TMDSO monomer which would yield Si-O-Si bonds. Furthermore, Si-H is susceptible to react with water molecules in air to form reactive Si-OH groups. Thus, during storage a condensation reaction may occur due to the reactive Si-OH groups present the film, thus

$$Si\text{-}OH + Si\text{-}OH \rightarrow Si\text{-}O\text{-}Si + H_2O \uparrow.$$
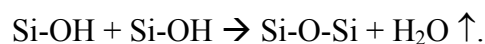
It can be concluded that the aging of these films depends upon the presence of Si-H and Si-OH groups in the films, which is responsible for the changes in the chemical environment.

8.3.2 Process 3 (D 1V)

Figure 8-10 shows the SEM micrographs of the deposited films of HMDSO/O$_2$ by implementing the process 3 parameters. The low deposition rates implemented at high input power may be attributed to the homogeneous surface of the films fabricated from pp HMDSO:O$_2$ (1:50). Furthermore, the micrographs of the the side view depicts a homogeneous pinhole-free film deposited, which might be related to the longer post-treatment time (60 sec) than in "Process 2". Therefore, the stability of the

117

process during deposition was improved. The films fabricated under "Process 2" conditions, may have been affected upon storage to air, this was examined quantitatively using the FT-IR spectra as shown in Figure 8-11.
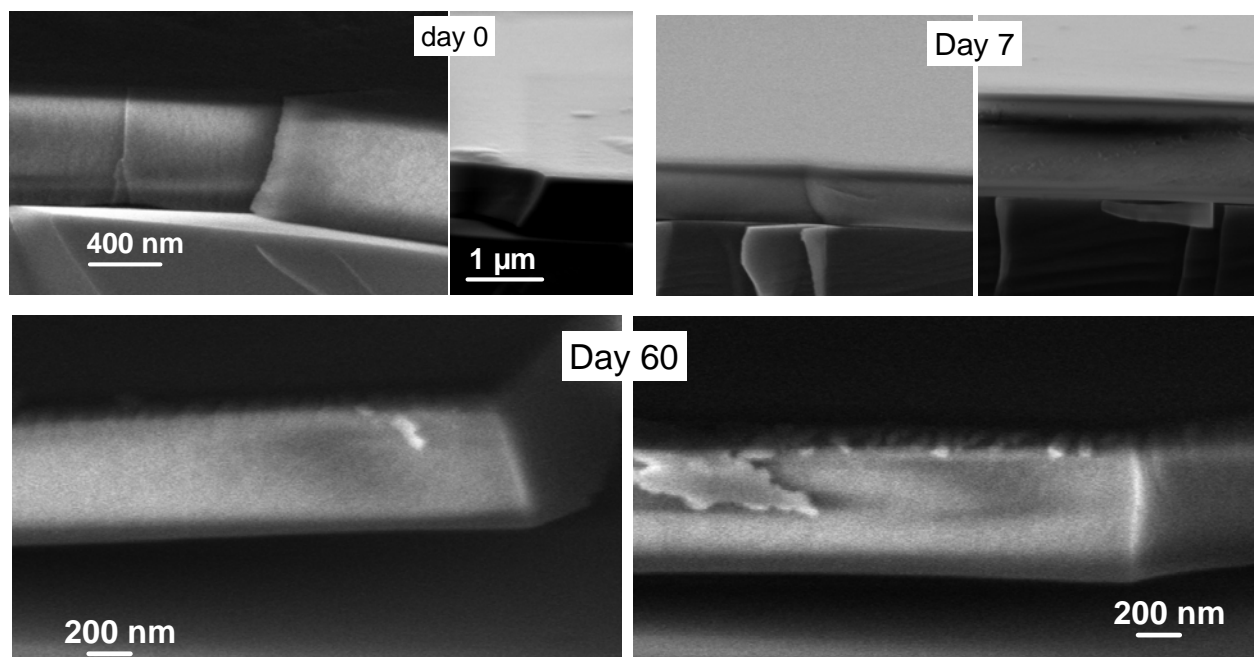

Figure 8-10: SEM micrographs of the pp HMDSO imaged during storage. (Process 3)
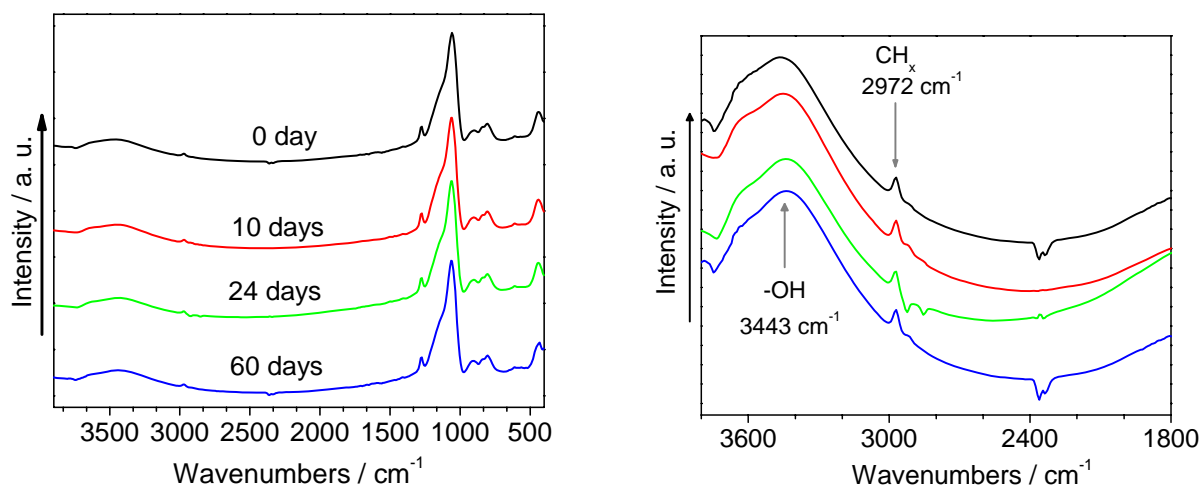

Figure 8-11: FT-IR spectra of HMDSO recorded at different time storage as indicated, selected spectra showing intermediate times. The spectrum of freshly deposited film (0 day) is included for comparison.

Figure 8-11 shows the compositional changes from the IR spectra of pp HMDSO in excess oxygen recorded during storage, whereas these specific absorption bands were also seen for the laboratory "Process 1", and have been explained in details in chapter 4. The appearance of the CH_x band absorption at 2972 cm^{-1} and –OH band absorption at 3443 cm^{-1} in absorption spectra was noticed, which showed constant intensity after 60 days of storage in air. These films were deposited at

relatively higher input power and excess oxygen flow, which may be responsible for the stability in the Si-O-Si network formed.
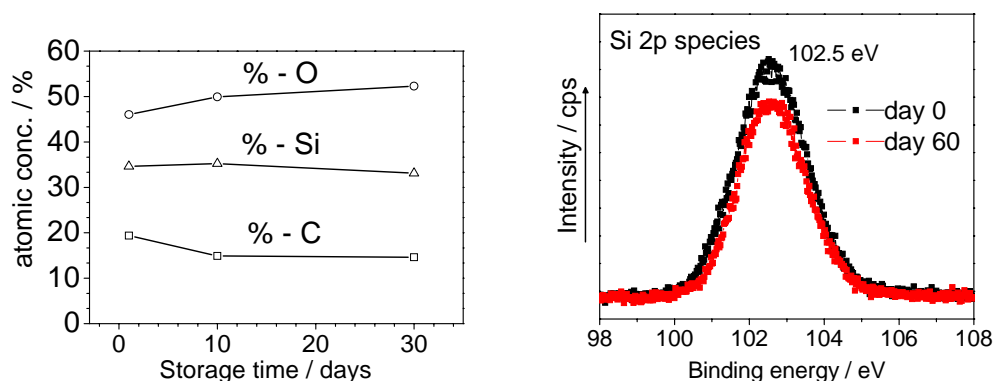

Figure 8-12: atomic concentration of pp HMDSO films upon storage (left), binding energy Si 2p spectra obtained after 30 days of storage.

Figure 8-12 shows the chemical composition of all the pp HMDSO film examined using XPS after 30 days of storage in air. The chemical composition of the surface film stoichiometry obtained after 10 days of storage was $Si:O_{1.6}:C_{0.4}$ as compared to $Si:O_{1.3}:C_{0.6}$ (day 0). This minor change in C/O ratio was constant after 30 days of storage, whereby this change was limited to the film surface. However, the stoichiometry was stable after 30 days of measurement, which confirms its stability. In a separate analysis of plasma polymerized $TMDSO:O_2$ films (200:500), the chemical composition obtained showed a higher amount carbon atoms $Si:O_{1.3}:C_{0.7}$ (day 0), which was almost constant after 30 days ($Si:O_{1.2}:C_{0.8}$) of storage in air as compared to HMDSO monomer. This may be related to the difference in chemical structures, particurlary the attached groups on the siloxane molecule.

The binding energy of the Si 2p peak (Figure 8-12, left) was determined at 102.5 eV, which corresponds to the $Si(-O)_2$- chemical environment, as described earlier in chapter 4. The binding energies of both O 1s and Si 2p peaks did not shift upon 30 days storage.
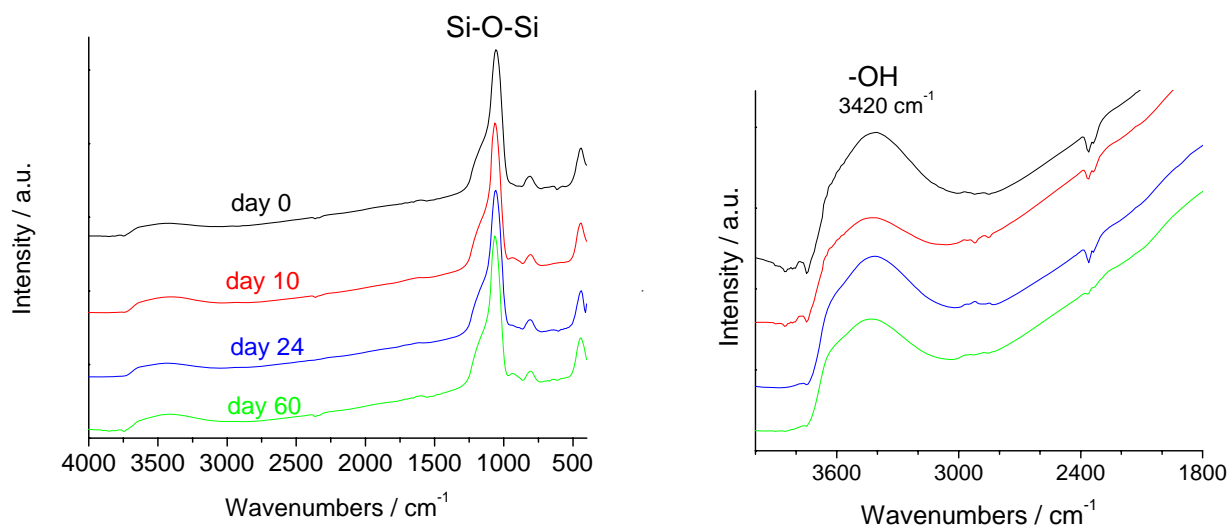
8.3.3 Process 4 (Pylonmet 1V)

Figure 8-13: FT-IR spectra of HMDSO films fabricated using PylonMet 1V. Spectra recorded at different time storage as indicated. The –OH absorption band shows a constant intensity over storage period.

Figure 8-13 shows the FT-IR spectra of pp HMDSO films measured for over 60 days of storage. The Si-O-Si and –OH absorption bands at 1060 cm^{-1} and 3420 cm^{-1} respectively show very minor changes upon storage up to 60 days. These changes were relatively smaller as compared to the films fabricated in "Processes 2 & 3", this might be related to the low deposition rate of 1.17 nm/sec, and excess O_2 flow which favors the deposition of stable SiO_2-like films. Also, the small amount of hydrocarbon seen on the absorption spectra around 3000 cm^{-1} was stable for over the storage period.

Figure 8-14 shows the SEM micrographs of the deposited HMDSO films in the PylonMet 1V reactor which have been monitored for over 60 days of storage. The deposition pressure was kept at 0.05 mbar, which was the lower than the pressures used in D 1V and L400 reactors. This deposition pressure might have influenced the film properties achieved. The micrographs depict a homogeneous morphology achieved, whereby no delamination was seen as in the case of the films produced using the L400 reactor.
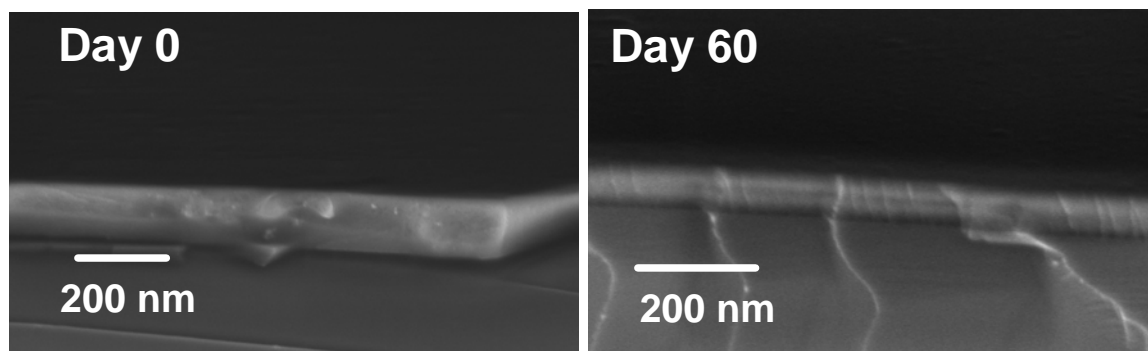

Figure 8-14: SEM micrographs of pp HMDSO films using the PylonMet 1V reactor. Films were store under ambient conditions for 60 days.

8.4   Conclusion

The properties of the plasma polymerized films presented in this chapter were dependent upon the process conditions employed.

The films fabricated in the laboratory were stable for over 300 days of storage in air. These films were characterized using FT-IR and SEM, which showed no major changes in both chemical and structural properties.

In the L400 reactor, the films were mostly rough and grains were formed, which were instable over the period of storage in air. The roughness of the films fabricated in the (microwave) D1V and (mid-frequency) PylonMet 1V reactors was absolutely less, as compared to the films fabricated in L400 reactor.

The SEM micrographs showed that porous films were achieved from the L400 reactor, which delaminated during the storage period in air. The chemical composition data obtained from the XPS data showed the presence of C-atom in the films, which is probably limited to the surface, because the FT-IR spectra showed only a minor carbon content.

Some variations in IR intensity of the Si-O-Si and –OH absorption bands were measured for the films fabricated using the TMDSO and HMDSO monomer. Due to the structural difference of both monomers, the TMDSO films showed minor changes in the Si-H and Si-$(CH_x)_x$ absorption bands, which may have reacted with the water molecules in the atmosphere, thus favoring aging. However, the films fabricated from TMDSO monomer in the PylonMet 1V reactor showed a major improvement with respect to porosity, adhesion and stability for over 60 days storage.

Comparatively, the films fabricated from the HMDSO monomer were more stable than the pp TMDSO films. The presence of low $–CH_x$ absorption band intensity in the IR spectra of the pp HMDSO did not change upon storage. Additionally, the SEM micrographs of all the pp HMDSO films showed homogeneous, smooth surfaces and pore-free films that were stable after 60 days of storage in air.

8.5   Reference

1.   Theil, J. A.; Brace, J. G.; Knoll, R. W., Carbon Content of Silicon-Oxide Films Deposited by Room-Temperature Plasma-Enhanced Chemical-Vapor-Deposition of Hexamethyldisiloxane and Oxygen. *Journal of Vacuum Science & Technology a-Vacuum Surfaces and Films* **1994,** 12, (4), 1365-1370.

2.   Bolland, J. L., *Quart. Rev. Chem. Soc.* **1949,** 3, (1).

3.   Garbassi, F.; Morra, M.; Occhiello, E.; Barino, L.; Scordamaglia, R., *surface interface analysis* **1989,** 14.

4.   Mittal, K. L., *Polymer Surface Modification: Relevance to Adhesion*. VSP BV, The Netherlands, : Utrecht, 1996.

5.   Nakamatsu, J.; Delgado-Aparicio, L. F.; Da Silva, R.; Soberón, F., *J. Adhsion Sci. Technol.* **1999,** 13.

6.   Wrobel, A. M., Aging Process in Plasma-Polymerized Organo-Silicon Thin-Films. *Journal of Macromolecular Science-Chemistry* **1985,** A22, (8), 1089-1100.

7.   Yasuda, H., New insights into aging phenomena from plasma chemistry. Nuclear Instruments & Methods in Physics Research Section a-Accelerators Spectrometers Detectors and Associated Equipment **2003,** 515, (1-2), 15-30.

8.   Wertheimer, M. R.; Thomas, H. R.; Perri, M. J.; KlembergSapieha, J. E.; Martinu, L., Plasmas and polymers: From laboratory to large scale commercialization. *Pure and Applied Chemistry* **1996,** 68, (5), 1047-1053.

9.   Vasile, M. J.; Smolinsk.G, Organosilicon Films Formed by an Rf Plasma Polymerization Process. *Journal of the Electrochemical Society* **1972,** 119, (4), 451-&.

10.   Canal, C.; Molina, R.; Bertran, E.; Erra, P., Wettability, ageing and recovery process of plasma-treated polyamide 6. *J. Adhesion Sci. Technol.* **2004,** 18, (9), 1077-1089.

11.   Zaharescu, T., Oxygen uptake: A procedure for evaluating oxidative stability and performances of polymers. *Mat Res Innovat.* **2001,** 5, 35-39.

12.   Dennler, G.; Houdayer, A.; Segui, Y.; Wertheimer, M. R., Growth and structure of hyperthin SiO2 coatings on polymers. *Journal of Vacuum Science & Technology a-Vacuum Surfaces and Films* **2001,** 19, (5), 2320-2327.

13.   Sacher, E.; Klembergsapieha, J. E.; Schreiber, H. P.; Wertheimer, M. R., Moisture Barrier Properties of Plasma-Polymerized Hexamethyldisiloxane. *Applied Polymer Symposia* **1984**, (38), 163-171.

14.   Yasuda, H., *Plasma Polymerization*. Academic Press: 1985.

15.   Leybold Optics; Siemensstraße 88, *D-63755 Alzenau*.

16.   Gegenbach, T. R.; Griesser, H. J., Post-deposition ageing reactions differ markedly between plasma polymers deposited from siloxane and silazane monomers. *Polymer* **1999,** 40, (18), 5079-5094.

17.   Muir, B. W.; Thissen, H.; Simon, G. P.; Murphy, P. J.; Griesser, H. J., Factors affecting the adhesion of microwave plasma deposited siloxane films on polycarbonate. *Thin Solid Films* **2006,** 500, (1-2), 34-40.

18.   Balazs, D. J.; Triandafillu, K.; Chevolot, Y.; Aronsson, B. O.; Harms, H.; Descouts, P.; Mathieu, H. J., Surface modification of PVC endotracheal tubes by oxygen glow discharge to reduce bacterial adhesion. *Surface and Interface Analysis* **2003,** 35, (3), 301-309.

19. Beamson, G.; Briggs, S., *High-Resolution XPS of Organic Polymers. The Science ESCA Database*. John Wiley and Sons: New York, 1992.

20. Alexander, M. R.; Short, R. D.; Jones, F. R.; Michaeli, W.; Blomfield, C. J., A study of HMDSO/O_2 plasma deposits using a high-sensitivity and -energy resolution XPS instrument: curve fitting of the Si 2p core level. *Applied Surface Science* **1999,** 137, (1-4), 179-183.

21. Alexander, M. R.; Short, R. D.; Jones, F. R.; Stollenwerk, M.; Zabold, J.; Michaeli, W., An X-ray photoelectron spectroscopic investigation into the chemical structure of deposits formed from hexamethyldisiloxane/ oxygen plasmas. *Journal of Materials Science* **1995**.

22. Clergereaux, R.; Escaich, D.; Martin, S.; Gaillard, F.; Raynaud, P., Aging of plasma-deposited carbon layers: effect of their thickness and material structure. *Thin Solid Films* **2005,** 482, (1-2), 216-220.

23. Creatore, M.; Palumbo, F.; d'Agostino, R., Deposition of SiOx films from hexamethyldisiloxane/oxygen radiofrequency glow discharges: Process optimization by plasma diagnostics. *Plasmas and Polymers* **2002,** 7, (3), 291-310.

Conclusions

Recent developments in materials technology, fuelled by the growing hype surrounding thin film technology have given rise to the application of functionalized thin films. There are numerous methods presently available for the fabrication of such films. Amongst these methods, plasma polymerized thin functionalized films are receiving more attention as supports for biological molecules. The concept of this thin film polymerization method is based on the elemental reactions occurring in the plasma state which leads to the fragmentation of monomer molecules, the formation of active sites (radicals) from the monomer and recombination of the activated fragments to form a polymer film. This well known method of thin film deposition is typically a one-step solvent free process and therefore offers an attractive alternative to wet chemical processes.

Generally, plasma polymers show a high degree of adhesion on various substrates, and stability in air. However, the behavior of such films in aqueous media must be understood to ensure successful implementations and exploitation of their unique properties. Specifically, in the domain of biosensors, the reactivity of surface bio-functionalized thin films needs to be optimized so as to obtain efficient sensitivity. Despite the various plasma polymerized bio-films available, their instability or poor adhesion in natural extra-cellular environment is one of the greatest drawbacks which hinders possible implementations in device designing.

From this point of view, it would be important to design a stable bio-material platform that will address some of these drawbacks, so as to improve the efficiency of the surface bio-functionalized films, when incorporated on a device, such as a biosensor.

In this work, it was possible to design functional multilayers using plasma enhanced chemical vapor deposition (PECVD) for the films presented here. Thin SiO_2 –like films were deposited from hexamethyl disiloxane and excess oxygen gas. The adhesion properties of the SiO_2 –like layer was optimized via oxygen plasma modification process, for the subsequent plasma polymerization of a functional bio-film. The obtained SiO_2 –like films served as an adhesion interlayer between the functional bio-film and an electrical substrate.

The fabrication of SiO_2 –films using PECVD has been earlier carried out, but for the purpose of improving biomaterial implementations, this is still a new field, which could improve the adhesion and stability of many unstable bio-films on a transducer (the electrical component of a biosensor). All biosensor devices consist of three main components, namely; bio-material, transducer (connects both components) and detector element. Thus, the crucial step for

developing a stable biomaterial in aqueous medium, is to optimize the adhesion between the electrical surface and the functional bio-material.

Multilayer systems have been presented in this work, whereby functional plasma polymerized allylamine, styrene, and maleic anhydride films were deposited on top of optimized SiO_2 –like films. The different process conditions implemented for the functional films deposition showed different chemical composition. Furthermore, the stability of the functional films on the SiO_2 –like film (multilayer) was characterized in aqueous medium using electrochemical impedance spectroscopy and surface plasmon resonance (SPR) spectroscopy. The electrochemical analysis of these multilayers showed an improved stability in the aqueous electrolyte for over 24 hours achieved, which might be related to the thin activated SiO_2 –like film beneath the functional films. This was also confirmed by kinetic measurements using surface plasmon resonance spectroscopy. Plasma polymerized maleic anhydride (pp-MA) was deposited on three different surfaces, namely; the activated SiO_2 adhesion promoting film, a 1-dodecanthiol self assembled monolayer (SAM), and directly on gold substrate. The multilayers with the adhesion promoting SiO_2 film was more stable, whereas pp-MA film dissolution of the Au and SAM layers were pronounced. More so, the chemical reactivity of the SiO_2-MA multilayer was retained, which was necessary for the binding of bio-molecules.

Principally, the application of these multilayers for biosensor applications requires the combined stability, adhesion, and surface biofunctional properties, which have been achieved in the SiO_2-MA multilayer. For the development of a biosensor, a method by which intact vesicles have been chemically attached to the multilayer was presented, i.e. hydrolyzed maleic anhydride films covalently bound to plasma polymerized SiO_2 on Au substrates. Surface Plasmon Field-Enhanced Fluorescence Spectroscopy (SPFS) combined with SPR was used to monitor the activation of plasma deposited maleic anhydride (pp-MA) film with EDC / NHS and the subsequent coupling of lipid vesicles. The vesicles were formed from a mixture of phosphatidylcholine and phosphatidylethanolamine lipids, with a water-soluble fluorophore encapsulated within. Vesicle attachment was measured in real time on plasma films formed under different pulse conditions (plasma duty cycle). Optimum vesicle attachment was observed on the pp-MA films containing the highest density of maleic anhydride groups. Phospholipase A_2 was used to lyse the surface-bound vesicles and to release the encapsulated fluorophore. The release of the fluorophores enzymatically can be associated to drug release procedures, which can be likewise achieved by using bio-functional multilayer supports presented in this work.

Additionally, the applications of thin SiO_2 –like films have drawn more attention in the industry due to its tunable properties. This instigated the comparative laboratory research and

industrial (Leybold Optics) processes presented in this work, whereby the ageing and stability of the SiO_2 –like films upon storage in air after storage were monitored for over 300 days. The chemical and film morphology of both processes underwent insignificant changes, due to the optimized deposition conditions implemented. This implies the films may be used after several months of fabrication due to their long term stability.

This work has shown that the stability of plasma polymerized films such as maleic anhydride in aqueous medium has been improved, which was used to bound stable vesicles for over 10 hours. The perspective of using multilayer seems so far to be stable and promising. However, to improve the lateral stability of supported bilayers, vesicles, and cell growth in the field of material research, the application of nano-porous materials would improve this property. A major challenge of fabricating such nanoporous materials may be related to the pore size reproducibility and pores interconnection, whereby the latter property is important for such specific application. The fabrication of such materials has been presented in this work. PECVD techniques was used to create the SiO_2 –like films on top of sacrificial polymethyl methacrylate colloids. Coupled with the fact that these nanoporous materials can be activated by oxygen plasma to yield hydrophilic surfaces, and are mechanically stable, the nano-porous material presented here would serve in the field of bioengineering or bioelectronics in the nearest future.

List of Publication

Published / in Press

   i.   **Anye Ngu Chifen**, Wolfgang Knoll, Renate Förch
"Fabrication of nano-porous silicon oxide layers by plasma polymerisation methods"

      Materials Letters 61 **(2007)** 1722 -1724

  ii.   **Anye N. Chifen**, Renate Förch, Wolfgang Knoll, Petra J. Cameron, Thomas L. Williams, A. Toby A. Jenkins
"Attachment and Phospholipase A_2 Induced Lysis of Phospholipid Bilayer Vesicles to Plasma Polymerized Maleic Anhydride / SiO_2 multilayers"

      Langmuir, **in press** Feb. **2007**

 iii.   **Anye N. Chifen**, A. Toby A. Jenkins, Wolfgang Knoll, Renate Förch
"Adhesion improvement of plasma polymerized maleic anhydride films on gold using $HMDSO/O_2$ adhesion layers"

      Plasma Processes and Polymers, submitted Jan. **2007**

  iv.   Renate Förch, **Anye N. Chifen**, Angelique Bousquet, Hwei Ling Khor, Melanie Jungblut, Li-Qiang Chu, Zhihong Zhang, Ivy Osey-Mensah, Eva-Katrin Sinner, Wolfgang Knoll
"Recent and expected roles of plasma polymerized films for biomedical applications"

      Advanced Materials - CVD Journal – special edition, in accepted March **2007**

   v.   Shinichi Igarashi, Akiko N Itakura, **Anye N. Chifen**, Renate Förch, Rüdiger Berger
"Surface stress control using ultraviolet light irradiation of plasma-polymerized thin films"

      Applied Phys. Letters 88 (14) **2006**

  vi.   Shinichi Igarashi, Akiko N Itakura, Masaya Toda, Masahiro Kitajima, Liqiang Chu, **Anye N. Chifen**, Renate Förch, Rüdiger Berger
"Swelling signals of polymer films measured by a combination of micromechanical cantilever sensor and surface plasmon resonance spectroscopy"

      Sensors & Actuators: B. Chemical, Vol. 117 (1) Sep. **2006**

Conferences

17th International Symposium on Plasma Chemistry (ISPC-17), Toronto, Canada
17-12.08.2005

"*Investigating the optical and electrical characteristics of plasma polymerised thin gradient films before/after thermal treatment*"

Anye N. Chifen, Wolfgang Knoll, Renate Förch

"*Investigating the properties of plasma polymerised films (Polystyrene and Allylamine) on organosiloxane polymer films.*"

Anye N. Chifen, Wolfgang Knoll, Renate Förch

Plasma Processing Science, Boston, USA
16-21.07.2006

"*Embedded inorganic nano-particles in/on plasma polymerized multilayers,,*

Anye N. Chifen, Jun Fu, Wolfgang Knoll, Renate Förch

Acknowledgement

It goes without saying that the research presented in this thesis, performed over the last three years, is the result of some team work and not only the efforts of a single person.
I wish then to thank all those who have contributed, in whatever way, to the realization of this manuscript.

I would first like to thank my supervisor, Dr. Renate Förch for her guidance for the last 3 years, inexhaustible energy and enthusiasm, for introducing me into Plasma world. Also thank you for the collaborating the projects and proof-reading this thesis.

I am grateful to Prof. W. Knoll for offering me a position at this great institute to improve my knowledge in science and also for your constant interest about my work. Thank you to Prof. J. Rühe for the scientific advices and also offering me a position at your institute to defend my PhD.

Dear Toby, it was my pleasure to work with you during the rainy months in Bath. Thank you so much for making use of my multilayers. Your research group is a great one, I enjoyed the three months with your colleagues and students, although we didn't have time to go shooting "elephants". (I must say: the nitrogen stuff, it was not my fault, it could have been dangerous, if I was locked up in that room ☹).
Also – I never felt homesick, if I could define "home". Also thanks for reading/correcting the Electrochemistry section in this work.

Vielen Vielen Dank Daniela Mössner für deine Zeit und Hingabe meine XPS Proben zu messen. Bei Dr. R. Berger, U. Rietzler (AFM), und G. Glasser (REM) möchte ich mich für die ständige Diskussionsbereitschaft und die Hilfe bei der Durchführung von AFM und SEM Messungen bedanken.

Many thanks also to the members of the AK-Knoll group, esp. the Plasma Group for sharing your work and life experience with me, it has been a nice time to know all of you, both past and present. A big thanks to Nathalie for introducing me to the SPR technique and also to Walter Scholdei for spending your time constructing the FT-IR to fit my "funny" samples.
Danke Danica for doing the final corrections, - I appreciate it.

I would like to express my gratitude to Dr. S. Küper and Dr. T. Schmauder of Leybold Optics, Alzenau for the industry project collaboration. Also, thanks to Dr. R. Förch for her supervision and the tough scientific questions concerning the ageing of SiO_2 film. I must say the collaboration increased my interest how to relate research and industrial processes.

To my office mates both past and present; Hwei Ling, Ed, Carmen, Per, Melanie, Mark and the others... (I decided to keep your names in my mind) I will miss you all, I hope it is reciprocal!
Den Mitarbeitern der Elektronik- und Mechanikwerkstatt danke ich für die vielfältigen Anregungen sowie für die Anfertigung von vielen Teilen und Vorrichtungen.

LEBENSLAUF

Persönliche Daten:

Name:	Anye Ngu Chifen
Geburtsdatum:	27. Februar 1979
Geburtsort:	Bamenda, Kamerun
Anschrift:	Kardinal-von-Galen-Str. 19
	55127 Mainz
Familienstand:	ledig

Ausbildung

1984 – 1989	Grundschule, Bamenda, Kamerun
1989 – 1994	Secondary school, General certificate of Examination London: Ordinary Level
1994 – 1996	Gymnasium: High school, General certificate of Examination London: Advanced Level (Abitur)
01/98 – 08/98	Deutschkurs, Zertifikat Deutsch als Fremdsprache, TU Clausthal- Zellerfeld
10/98 – 01/ 2004	Diplom-Ingenieur (Chemietechnik) „Struktur-/Eigenschaftsbeziehungen von Polymeren nach kryogener Zerkleinerung." Lehrstuhl für Werkstoffkunde, Universität Dortmund
Seit 03/2004	Doktorand, Max-Planck Institut für Polymerforschung, Mainz